University of Alberta

NEW INTERPOLATORY SUBDIVISION SCHEMES IN COMPUTER GRAPHICS

by

Robert Junli Liao

A thesis submitted to the Faculty of Graduate Studies and Research
in partial fulfillment of the requirements for the degree of
Master of Science

in

Applied Mathematics

Department of Mathematical and Statistical Sciences
Edmonton, Alberta
Fall, 2004

Library and Archives Canada
Bibliothèque et Archives Canada

Published Heritage Branch
Direction du Patrimoine de l'édition

395 Wellington Street
Ottawa ON K1A 0N4
Canada

395, rue Wellington
Ottawa ON K1A 0N4
Canada

Your file Votre référence
ISBN: 0-612-95799-3
Our file Notre référence
ISBN: 0-612-95799-3

The author has granted a non-exclusive license allowing the Library and Archives Canada to reproduce, loan, distribute or sell copies of this thesis in microform, paper or electronic formats.

L'auteur a accordé une licence non exclusive permettant à la Bibliothèque et Archives Canada de reproduire, prêter, distribuer ou vendre des copies de cette thèse sous la forme de microfiche/film, de reproduction sur papier ou sur format électronique.

The author retains ownership of the copyright in this thesis. Neither the thesis nor substantial extracts from it may be printed or otherwise reproduced without the author's permission.

L'auteur conserve la propriété du droit d'auteur qui protège cette thèse. Ni la thèse ni des extraits substantiels de celle-ci ne doivent être imprimés ou aturement reproduits sans son autorisation.

In compliance with the Canadian Privacy Act some supporting forms may have been removed from this thesis.

Conformément à la loi canadienne sur la protection de la vie privée, quelques formulaires secondaires ont été enlevés de cette thèse.

While these forms may be included in the document page count, their removal does not represent any loss of content from the thesis.

Bien que ces formulaires aient inclus dans la pagination, il n'y aura aucun contenu manquant.

Canada

To my wife Li Zhu,

and to my parents.

ACKNOWLEDGEMENT

First I would like to sincerely thank my supervisor Dr. B. Han for suggesting the research topics and his warmhearted guidance.

Secondly, I would like to thank other members in our group: Dr. R. Q. Jia, Dr. W. Chen and Dr. Q. Mo. I have learned a lot from them.

Also I would like to thank all the members in my final oral defense committee, Dr. B. Han, Dr. R.Q. Jia and Dr. X. Li, for carefully reading my thesis and their helpful suggestions to improve the presentation of my thesis.

Finally, I would like to thank the University of Alberta and the Department of Mathematical and Statistical Sciences in the University of Alberta for their financial support and other support during my study.

Table of Contents

1 Introduction and Motivation **1**

1.1 Introduction of Subdivision Schemes 1

1.1.1 A Short Survey of Subdivision Surfaces 1

1.1.2 Some Notations 3

1.1.3 Properties of Subdivision Surfaces 5

1.2 Examples of Classical Subdivision Schemes 7

1.2.1 Classification of Subdivision Schemes 7

1.2.2 Some Known Subdivision Schemes 8

1.3 Motivation 9

1.4 Analysis of Subdivision Triplets 11

1.4.1 Definition of Subdivision Triplets 11

1.4.2 Convergence and Smoothness Properties 14

2 One-dimensional Interpolatory Subdivision Schemes with Dilation Factor 4 **19**

2.1 Optimal One-dimensional Interpolatory Subdivision Schemes . 19

2.1.1 The Optimal Subdivision Scheme 20

2.1.2 Smoothness of 4-adic Interpolatory Subdivision Schemes 26

2.1.3 Associated Subdivision Stencils 28

2.2 Projection Method for Multi-dimensional Subdivision Triplets 29

3 Two-dimensional Interpolatory Four-adic Subdivision Schemes with Two-ring Stencils 32

3.1 Subdivision Schemes for the Regular Triangular Mesh 32

3.1.1 Computing the b Sequence 33

3.1.2 Computing the Quantity $\nu_\infty(a, 4I_2)$ 35

3.1.3 Interpolatory Subdivision Stencils for the Triangular Meshes 40

3.2 Subdivision Schemes for the Regular Quadrilateral Mesh . 47

3.2.1 Masks of the Two-dimensional Interpolatory Four-adic Subdivision Schemes for the Quadrilateral Meshes . . . 47

3.2.2 Computing the Smoothness $\nu_\infty(a, 4I_2)$ 49

3.2.3 Subdivision Stencils for the Quadrilateral Meshes . . . 52

4 Smoothness Analysis at Extraordinary Vertices 60

4.1 Subdivision Matrix and Characteristic Map 60

4.1.1 Parameterization of Subdivision Surfaces 61

4.1.2 Subdivision Matrix and Eigenvalue Analysis 63

4.1.3 Characteristic Map 65

4.1.4 Diagonalizing the Subdivision Matrix 68

4.2 Special Subdivision Rules for Ternary Subdivision Schemes . . 69

4.2.1 Stencils of Ternary Subdivision Scheme for Regular Meshes 69

4.2.2 Subdivision Rule for $k = 3$ case 70

4.2.3 Subdivision Rule for $k = 4$ case 76

4.3 Four-adic Subdivision Rule for $k = 3$ case 80

Bibliography **85**

List of Figures

1.1 Refinement of the subdivision surface. 5

2.1 Find out the optimal parameter of "t". 24

2.2 The calculation of free parameter "t". 25

2.3 Graph of $|2t + 3/32|, |4t + 1/16|$ and $|3t + 1/16| + |t|$. 27

2.4 Associated subdivision stencils for the best interpolatory 4-adic subdivision scheme. By the symbol "$\triangle$" we denote the new inserted vertex, and the symbol "$\circ$" denotes vertices at the previous level. 28

3.1 The interpolatory 4-adic subdivision scheme for the triangular mesh. By adding 3 new vertices on an edge and 3 new vertices for each face, one edge is split into 4 new edges and one face is split into 16 new faces. "$\diamond$" denotes the old vertices and "$\circ$" denotes the new inserted vertices. 41

3.2 Associated subdivision stencils for the best two-dimensional interpolatory 4-adic subdivision scheme for the interior new inserted vertex. By the symbol "$\triangle$" we denote the new inserted vertex, and the symbol "$\bigcirc$" denotes vertex of the previous level, the numbers inside the circles, which are named $u1,\ u2,\ \ldots, u7$, are the weights of the corresponding vertices. 42

3.3 The interpolatory subdivision stencil for new inserted *interior vertex* inside a face, with $t_1 = 10/3,\ t_2 = 0,\ t_3 = -5/3$ and $t_4 = 0$. All the numbers in the above stencil should be divided by 576. 42

3.4 Associated subdivision stencils for "1/4 vertex" on an edge. . 43

3.5 The interpolatory subdivision stencil for "1/4 vertex" on an edge, with $t_1 = 10/3,\ t_2 = 0,\ t_3 = -5/3$ and $t_4 = 0$. All the numbers in the above stencil should be divided by 576. 44

3.6 Associated subdivision stencil for "1/2 vertex" on an edge. . . 44

3.7 The interpolatory subdivision stencil for "1/2 vertex" on an edge, with $t_1 = 10/3,\ t_2 = 0,\ t_3 = -5/3$ and $t_4 = 0$. All the numbers in the above stencil should be divided by 288. 45

3.8 The graph of the basis function ϕ for the subdivision triplet in the Theorem 3.1 with $t_1 = 10/3,\ t_2 = 0,\ t_3 = -5/3$ and $t_4 = 0$. 45

3.9 The graph of the contour value of the basis function ϕ for the subdivision triplet in the Theorem 3.1 with $t_1 = 10/3,\ t_2 = 0,\ t_3 = -5/3$ and $t_4 = 0$. 46

3.10 An example of subdivision surfaces by applying interpolatory 4-adic subdivision scheme on the regular triangular mesh. They are the initial mesh, the first step subdivision surface and the second step subdivision surface, respectively. 46

3.11 The interpolatory 4-adic subdivision scheme for the quadrilateral mesh. By adding 3 new vertices on an edge and 4 new vertices for each face, one edge is split into 4 new edges and one face is split into 16 new faces. "◇" denotes the old vertices and "○" denotes the new inserted vertices. 52

3.12 Associated subdivision stencils for new inserted vertices on an edge. Up triangle denote the "1/4 vertex" and down triangle denotes the "1/2 vertex". 53

3.13 Associated subdivision stencils for new inserted interior vertices inside a face. The upper triangle symbol denotes the "(1/4, 1/4) vertex", down triangle symbol denotes the "(1/2, 1/4) vertex" and small circle symbol denotes the "(1/2, 1/2) vertex". . . . 54

3.14 Associated subdivision stencils for new inserted vertices on an edge at the "1/4 vertex". All the numbers in the above stencil should be divided by 384. 56

3.15 Associated subdivision stencils for new inserted vertices on an edge at the "1/2 vertex". This coincides with the stencil of the univariate 4-point interpolatory scheme. 57

3.16 Associated subdivision stencils for new inserted vertices interior of a face at the "(1/2, 1/2) vertex". All the numbers in the above stencils should be divided by 32. 57

3.17 Associated subdivision stencils for new inserted vertices interior of a face at the "(1/4, 1/4) vertex" and at "(1/2, 1/4) vertex". All the weights are divided by 768. 58

3.18 The graph of the basis function ϕ for the subdivision triplet in Theorem 3.2, when $t_6 = t_8 = t_9 = t_{10} = t_{12} = t_{13} = t_{14} = t_{15} = 0$ and $t_5 = -1/384$. 59

3.19 The graph of the contour of the basis function ϕ for the subdivision triplet in Theorem 3.2, when $t_6 = t_8 = t_9 = t_{10} = t_{12} = t_{13} = t_{14} = t_{15} = 0$ and $t_5 = -1/384$. 59

4.1 Parameterization of the subdivision surface (see [1]). 62

4.2 The k-gon without origin extraordinary vertex can be decomposed into similar rings. Taking dyadic subdivision schemes into account, each two times smaller than the previous ring. The size of the ring is chosen in such a way that the control set of any ring does not contain the extraordinary vertex. In this figure the control set is assumed to consist of the vertices of the triangles of the ring itself, and of a single layer of vertices outside the ring. 67

4.3 The stencils of the ternary subdivision schemes for regular meshes. The numbers at left shall be divided by 99; the numbers at right shall be divided by 891 [19]. 70

4.4 Numbering of the k-gon for the order as in the subdivision matrix. 70

4.5 The stencil at left is for a new inserted "1/3 vertex", and at right is for a new inserted "2/3 vertex" on an edge associated with a $k = 3$ extraordinary vertex. 71

4.6 The stencil for a new inserted interior vertex inside a face which contains an extraordinary vertex with the valence $k = 3$. . . . 71

4.7 Identify a section around extraordinary vertex with a sector in the regular triangular mesh. All the vertices inside this bold area can be computed by the vertices within two rings outside this bold area. 74

4.8 Applying the special interpolatory ternary subdivision scheme on an example mesh with an unique extraordinary vertex ($k = 3$). From left to right are the initial, first level and second level subdivision surfaces, respectively. 75

4.9 The stencils for the new inserted "1/3 vertex" and "2/3 vertex" on an edge associated with a $k = 4$ extraordinary vertex. . . . 76

4.10 The stencil for a new inserted interior vertex inside a face which contains a $k = 4$ extraordinary vertex. 76

4.11 Applying the special interpolatory ternary subdivision scheme on an example mesh with an unique extraordinary vertex ($k = 4$). From left to right are the initial, first level and second level subdivision surfaces, respectively. 80

4.12 Numbering of the k-gon for the order as subdivision matrix . . 80

4.13 The stencil for a new inserted "1/4 vertex" and "1/2 vertex" on an edge associated with a $k = 4$ extraordinary vertex. . . . 81

4.14 The stencil for a new inserted "3/4 vertex" on an edge associated with a $k = 3$ extraordinary vertex. 81

4.15 The stencil at left is for a new inserted interior "(1/4,1/4)" vertex, and at right is for a new inserted interior "(1/2, 1/4)" vertex inside a face which contains a $k = 3$ extraordinary vertex. 82

4.16 Applying the special interpolatory 4-adic subdivision scheme on an example mesh with an unique extraordinary vertex ($k = 3$). From left to right are the initial, first level and second level subdivision surfaces, respectively. 84

Chapter 1

Introduction and Motivation

1.1 Introduction of Subdivision Schemes

1.1.1 A Short Survey of Subdivision Surfaces

Subdivision is a method for generating smooth surfaces, which first appeared as an extension of splines to control nets with arbitrary topology. It has been studied for more than 20 years for representing complex surfaces, since two well-known schemes were given by Catmull and Clark [4] (Catmull-Clark) and Doo and Sabin [7] (Doo-Sabin) in 1978. During the period from 1978 to 1995, some new interesting subdivision schemes, such as Loop, Butterfly, Modified Butterfly, Kobbelt and Midedge schemes, were proposed. Recently, in order to have a better smoothness, many people are starting investigating subdivision schemes such as ternary and quincunx schemes, with the hope that the smoothness of the corresponding basis functions with other refinements instead of the traditional dyadic refinement can achieve C^2 continuity.

Actually, the basic ideas behind subdivision are very old, and it can be traced back as far as the late 40's and early 50's when G. de Rham used "corner

cutting" to describe smooth curves. In recent years, subdivision schemes have found their way into many applications in computer graphics and computer aided geometric design (CAGD). One milestone has occurred when subdivision hit the big screen in Pixar's short "Geri's Game." At Siggraph '98, Pixar unveiled a short animated film: Christened Geri's Game, it was, to quote its academy award press release, the "endearing tale of an aging codger who likes to play chess in the park against himself." Not only was it artistically stunning, but it was also a technological powerhouse. In the last few years these techniques have received more interest in the computer graphics literature because of many potential benefits of subdivision. Subdivision scheme deserves further research, since it has a good prospect in many applications.

Subdivision surfaces are an efficient way of describing a surface using a polygonal model. Like the polygonal model, the surface can be of any shape and any size, that is of arbitrary topology. Unlike that polygonal model, the surface itself is perfectly smooth. From the point of view of implementation, starting with a base mesh U_0, subdivision [22] is the process of obtaining a smooth surface F as a limit of a sequence of successive refinement operation $S_{a,M}$, where a is the mask and M is the dilation matrix. Subdivision schemes are similar to spline-based schemes [11] but are more general than spline-based schemes because subdivision schemes can be defined for functions with arbitrary topology. The iterative transform $S_{a,M}$ is used to obtain a finer level mesh representation U_{j+1} of the surface from a coarse level mesh U_j and is expressed as $U_{j+1} = S_{a,M}(U_j)$. Subdivision schemes allow one to take the original polygonal model and produce an approximation of the surface by adding new vertices and faces by subdividing the existing polygons. The subdivision mesh can be as coarse or as detailed as your needs allow because of the property of arbitrary topology.

1.1.2 Some Notations

Mesh Type For an arbitrary initial mesh, if we keep applying subdivision schemes on it, we will get the refined subdivision surfaces. However, the faces of the mesh can be formed in different ways. For a regular mesh, in order to have a symmetric property, it is natural to use faces that are identical. If, in addition, we assume that the faces are regular polygons, it turns out that there are only three ways to choose the face polygons: squares, equilateral triangles and regular hexagons. In applications of computer graphics and CAGD, hexagonal meshes are seldom used, because it is difficult to implement; meanwhile triangular meshes and quadrilateral meshes are the most convenient and widely used ones for practical purposes.

Regular and Extraordinary Each triangular mesh is made up of a sequence of faces. There are altogether 3 vertices and 3 edges per face. An edge has two vertices, but a vertex may have various valences. In terms of the number of valences, there are two types of vertices: regular vertices and extraordinary vertices. For triangular meshes, a vertex is a regular one if it has 6 valences, otherwise it is an extraordinary vertex; for quadrilateral meshes, a vertex with 4 valences is a regular one. Here we have to determine whether a vertex is a regular one or an extraordinary one, because we can apply regular subdivision schemes on regular meshes, but we shall employ special subdivision rules for extraordinary vertices, which will be discussed in detail in Chapter 4.

Vertex Insertion and Corner Cutting In CAGD there are two main approaches that are used to generate a refined mesh: one is vertex insertion and another is corner cutting. The schemes using the first method are often called primal, and the schemes using the second method are called dual. Considering the dyadic subdivision schemes, in the first case, each edge of a triangular or quadrilateral mesh is split into two. Old vertices of the mesh are retained, and new vertices inserted on edges are connected. For quadrilaterals, an additional vertex is inserted for each face. In the second case of dual schemes, for each

old face, a new similar face is created inside of it and the newly created faces are connected. As a result, we get four new vertices for each old edge, and a new face for each edge and each vertex. The old vertices are discarded. Geometrically, one can think about this process as first cutting off the vertices, and then cutting off the edges of a polyhedron. For quadrilateral meshes, this can be done in such a way that the refined tiling has only quadrilateral faces. For triangles, we can get only a hexagonal tiling. Thus, a regular corner-cutting algorithm for triangles would have to alternate between triangular and hexagonal meshes.

Odd and Even For vertex insertion (primal) schemes, the vertices of the coarser mesh are also vertices of the refined mesh. For any subdivision level, we call all new vertices that are created at that level, odd vertices. This term comes from the one-dimensional case, while vertices of the control polygons can be enumerated sequentially and on any level the newly inserted vertices are assigned odd numbers. The vertices inherited from the previous level are called even.

Interpolating and Approximating Any subdivision scheme can be classified as interpolating subdivision or approximating subdivision. In approximating subdivision, the vertices at the current level are updated after the new vertices are added at each new level, whereas in interpolating subdivision, the existing vertices do not change as we introduce new vertices at each new level. The new vertices introduced at each step are usually referred to as the odd vertices and the old vertices are usually referred to as the even vertices. The Loop subdivision scheme [26] and the butterfly subdivision scheme [28] are two classical examples of approximating and interpolating subdivision schemes, respectively. The modified butterfly subdivision scheme [31] is an improvement over the original butterfly scheme.

Intuitively, the refined polygon meshes are obtained by adding new vertices to the mesh and connecting them with old vertices, but the rules of connectivity

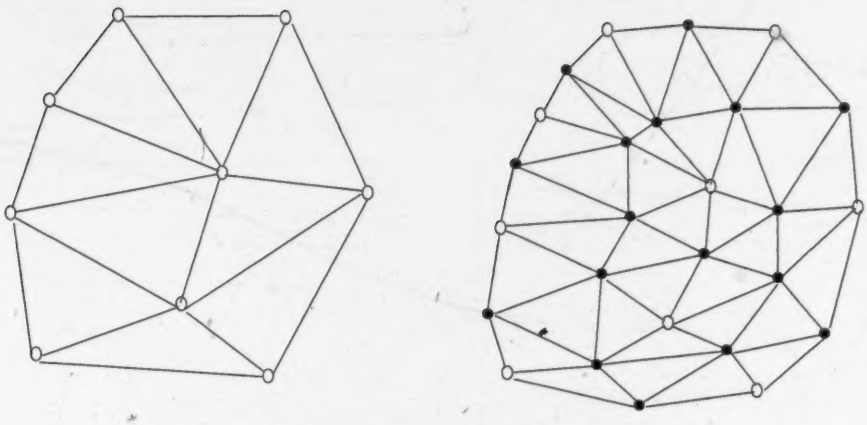

Figure 1.1: Refinement of the subdivision surface.

are different for different schemes. The positions of new vertices are computed as functions of positions of the old vertices; the positions of old vertices in the refined mesh can be modified or fixed. Figure 1.1 shows a very simple example of a subdivision surface for a triangular mesh, where the linear interpolating subdivision scheme is used on a simple 2-dimensional mesh.

More complex subdivision schemes (rules) are often used to obtain a smoother surface, for example, a subdivision surface with C^2 continuity. These rules are based on more complicated principles such as compact support, efficient algorithms and affine invariance. We shall discuss them in details in the following chapters.

1.1.3 Properties of Subdivision Surfaces

Before delving into the details of how a subdivision scheme works, let's have a look at its properties by comparing it with other possible modelling approaches for smooth surfaces: traditional splines, implicit surfaces, and variational surfaces [1].

Efficiency: In applications, computational cost is an important aspect of a modelling method. Subdivision is easy to implement and is computationally

efficient, since only a small number of neighboring old points (i.e. those with a short support size) are used in the computation of the new points. On the other hand, implicit surfaces, for example, are much more costly. An algorithm such as marching cubes is required to generate the polygonal approximation needed for rendering. Variational surfaces can be even worse: a global optimization problem has to be solved each time the surface is changed.

Arbitrary topology: It is desirable to build surfaces of arbitrary topology. Here, "arbitrary topology" means the topological genus of the mesh and the associated surface can be arbitrary, and the structure of the graph formed by the edges and vertices of the mesh can be arbitrary too. Specifically, each vertex may be of an arbitrary degree. Classic spline approaches have great difficulty with control meshes of arbitrary topology. When rectangular spline patches are used in arbitrary control meshes, enforcing higher order continuity at extraordinary vertices becomes difficult and considerably increases the complexity of the representation. Although implicit surfaces can be of arbitrary topological genus, the genus, precise location, and connectivity of a surface are typically difficult to control. Variational surfaces can handle arbitrary topology better than any other representation, but the computational cost can be high. Subdivision on the other hand can handle arbitrary topology quite well without losing efficiency; this is one of its key advantages over other modelling approaches. Historically subdivision was brought forth when researchers were looking for ways to address the arbitrary topology modelling challenge for splines.

Surface features: Often it is desirable to control the shape and size of features such as creases, grooves, or sharp edges. Variational surfaces provide the most flexibility and exact control for creating features. Implicit surfaces, on the other hand, are very difficult to control, since all modelling is performed indirectly and there is much potential for undesirable interaction between different parts of the surface. Spline surfaces allow very precise control, but it is computationally expensive and awkward to incorporate features, in particular

if one wants to do so in arbitrary locations. Subdivision allows more flexible control than is possible with splines. In addition to choosing locations of control points, one can manipulate the coefficients of subdivision to achieve effects such as sharp creases or control the behavior of the boundary curves.

Complex geometry: For interactive applications, efficiency is of primary importance. Because subdivision is based on repeated refinement it is quite straightforward to incorporate ideas such as level-of-detail rendering and compression for the Internet. During interactive editing locally adaptive subdivision can generate just enough refinement based on geometric criteria, for example. For applications that only require the visualization of fixed geometry, other representations, such as progressive meshes, are likely to be more suitable.

1.2 Examples of Classical Subdivision Schemes

In order to well understand the basic ideas of subdivision schemes, we shall briefly review some classical schemes in this section.

1.2.1 Classification of Subdivision Schemes

Based on three criteria, we can classify most of the regular subdivision schemes as follows:

- The type of refinement rule (vertex insertion or corner-cutting);
- The type of generated mesh (triangular or quadrilateral);
- Whether the scheme is approximating or interpolating.

Two well-known corner-cutting schemes are: Doo-Sabin and Midedge.

The following table shows refined classification of vertex insertion schemes:

-	Triangular Meshes	Quadrilateral Meshes
Approximating	Loop	Catmull-Clark
Interpolating	Modified Butterfly, ternary	Kobbelt, ternary

The above classification and examples of subdivision schemes are only suitable for regular vertices. Additional special rules have to be specified for extraordinary vertices.

1.2.2 Some Known Subdivision Schemes

Loop Scheme The Loop scheme is a simple approximating vertex insertion scheme for triangular meshes proposed by Charles Loop [26]. The scheme is based on the three-directional box spline, which produces C^2-continuous surfaces on the regular meshes. The Loop scheme produces surfaces that are C^2-continuous everywhere except at extraordinary vertices. Hoppe, DeRose, Duchamp et al. [22] tried a piecewise C^1-continuous extension of the Loop scheme, with special rules defined for edges. Therefore the scheme can be applied to arbitrary polygonal meshes, after the mesh is converted to a triangular mesh, for example, by triangulating each polygonal face.

Modified Butterfly Scheme The Butterfly scheme was proposed by Dyn, Gregory and Levin in [10]. However, although the original Butterfly scheme is defined on arbitrary triangular meshes, the limit surface is not C^1-continuous at extraordinary points of valence $k = 3$ and $k > 7$ [33]. It is C^1 on regular meshes.

Unlike approximating schemes based on splines, this scheme does not produce piecewise polynomial surfaces in the limiting case. In [35] a modification of the Butterfly scheme was proposed, which guarantees that the scheme produces C^1-continuous surfaces for arbitrary meshes (for a proof see [33]). The

scheme is known to be C^1 but not C^2 on regular meshes.

Catmull-Clark Scheme The Catmull-Clark scheme was described in [4]. It is based on the tensor product bicubic spline. The scheme produces surfaces that are C^2 everywhere except at extraordinary vertices, where they are C^1. The tangent plane continuity of the scheme was analyzed by Ball and Storry [2], and C^1-continuity by Peters and Reif [31].

The rules of Catmull-Clark scheme are defined for meshes with quadrilateral faces. Arbitrary polygonal meshes can be reduced to quadrilateral meshes using a more general form of Catmull-Clark rules [4].

Kobbelt Scheme This is an interpolating scheme and was described by Kobbelt in [11]. For regular meshes, it reduces to the tensor product of the four point scheme. C^1-continuity of this scheme for interior vertices for all valences is proven in [34]. Crucial for the construction of this scheme is the observation (valid for any tensor-product scheme) that the face control points can be computed in two steps: first, all edge control points are computed. Next, face vertices are computed using the "edge rule" applied to a sequence of edge control points at the same level.

1.3 Motivation

For evaluating a subdivision scheme, one criterion is to see whether or not the refined surfaces have good smoothness, which is determined by the continuity of the surfaces. In general, the basis functions of subdivision schemes are required to be at least C^2, otherwise the curvature of the generated subdivision surfaces which are refined from the initial mesh would be discontinuous.

It is well known that in order to have a smoother subdivision surface, it is necessary for a basis function in a subdivision scheme to enlarge the support of its associated mask. This is almost equivalent to saying that lager support

size of the mask implies a smoother surface. On the other hand, once the stencil contains one or more extraordinary vertices the subdivision scheme will be totally different, since the topology is different. Therefore, from the point of view of implementation and computation (especially the computational cost), we have to reduce the probability of using special subdivision rules for extraordinary vertices. Thus in the application of CAGD, it is strongly suggested that the associated subdivision stencils should be restricted within no more than two-ring neighboring vertices, which is almost equivalent to saying that its mask should have a very short support. Consequently we can say that high smoothness of a basis function in a subdivision scheme and the shortness of the support size of its mask are two mutually conflicting requirements. For example, it was proved in [12] that there is no C^2 interpolatory dyadic subdivision scheme whose mask can be supported on $[-3, 3]^s$ (that is, it has two-ring stencils). As a consequence, the butterfly scheme [10], which is an interpolatory dyadic subdivision scheme with two-ring stencils, cannot be a C^2 scheme.

Since the support size of the mask is suggested to be no more than two rings, it is worthwhile to analyze some properties of subdivision schemes in order to achieve continuity of the curvature in a subdivision surface. Hence, in recent years, quite a few researchers have been actively tackling issues in the area of interpolatory ternary subdivision surfaces, and several works have been done on these corresponding subdivision schemes due to the expected at least C^2 continuity. For example, in the one-dimensional case, C^2 interpolatory ternary subdivision scheme with two-ring stencils have been studied and obtained in [21]. Some examples of two-dimensional interpolatory ternary subdivision schemes have been proposed in [19, 6, 17]. In particular, several examples of two-dimensional C^2 interpolatory ternary subdivision schemes have been obtained in [19]. The goal of this thesis is to generalize the results in [19] on ternary interpolatory subdivision schemes, and to investigate the smoothest optimal interpolatory dilation 4 subdivision schemes with two-ring stencils in one and two dimensions for both triangular meshes and quadrilateral meshes.

Although the smoothness of the basis function of our new interpolatory subdivision scheme can achieve $\log_4 24 (\approx 2.29248$, which is better than 2), the scheme is only for regular meshes. In order to apply these schemes to an initial mesh with an arbitrary topology, we shall attempt to find reasonable special rules for extraordinary vertices to have a C^1 continuity around extraordinary vertices, otherwise they will lead to a coarse visual quality on the local surface around extraordinary vertices. By analyzing the subdivision matrix and its eigenvalues, we can figure out suitable subdivision stencils for extraordinary vertices. Therefore we have at least C^1-continuity around extraordinary vertices.

1.4 Analysis of Subdivision Triplets

In this section, we shall discuss the idea of subdivision triplets which can completely determine a subdivision scheme in any dimension. We shall also discuss two important quantities which will be used in estimating the smoothness of the basis function of a subdivision triplet.

1.4.1 Definition of Subdivision Triplets

The notion of subdivision triplets has been introduced in [17]. In this section, let us recall the definition of subdivision triplets here. We say that G is a *symmetry group* on $\mathbb{Z}^s$ if each element $E \in G$ is an isomorphism on $\mathbb{Z}^s$ (i.e. E is an integer matrix with $|\det E| = 1$) and G forms a group under matrix multiplication.

Definition 1.1. ϕ is a refinable function if ϕ satisfies the following refinement equation

$$\phi = \sum_{\alpha \in \mathbb{Z}^s} a(\alpha)\phi(M \cdot -\alpha), \tag{1.1}$$

where $\{a(\alpha)\}_{\alpha\in\mathbb{Z}^s}$ is a finitely supported sequence on $\mathbb{Z}^s$ such that $\sum_{\alpha\in\mathbb{Z}^s} a(\alpha) = |detM|$. Such a sequence a is called a *mask* for the refinable function ϕ.

Any subdivision scheme can be completely determined by a unique triplet (a, M, G), where a is a mask giving all the subdivision stencils, M is a dilation matrix determining the refinement of the mesh, and G is a symmetry group on $\mathbb{Z}^s$ distinguishing the mesh type (see [17]). The two commonly used meshes: quadrilateral meshes and triangular meshes are invariant under the symmetry groups D_4 and D_6, respectively, which are defined to be

$$D_4 := \left\{ \pm \begin{bmatrix} 1 & 0 \\ 0 & 1 \end{bmatrix}, \pm \begin{bmatrix} 1 & 0 \\ 0 & -1 \end{bmatrix}, \pm \begin{bmatrix} 0 & 1 \\ 1 & 0 \end{bmatrix}, \pm \begin{bmatrix} 0 & 1 \\ -1 & 0 \end{bmatrix} \right\}$$

and

$$D_6 := \left\{ \pm \begin{bmatrix} 1 & 0 \\ 0 & 1 \end{bmatrix}, \pm \begin{bmatrix} 0 & -1 \\ 1 & -1 \end{bmatrix}, \pm \begin{bmatrix} -1 & 1 \\ -1 & 0 \end{bmatrix}, \pm \begin{bmatrix} 0 & 1 \\ -1 & 0 \end{bmatrix}, \pm \begin{bmatrix} 1 & -1 \\ 0 & -1 \end{bmatrix}, \pm \begin{bmatrix} -1 & 0 \\ -1 & 1 \end{bmatrix} \right\}.$$

A $\sqrt{2}$ subdivision scheme is given by a triplet $(a, M_{\sqrt{2}}, D_4)$, a $\sqrt{3}$ subdivision scheme is given by $(a, M_{\sqrt{3}}, D_6)$, a ternary subdivision scheme is either $(a, 3I_2, D_4)$ or $(a, 3I_2, D_6)$, and a dilation-4 subdivision scheme is either $(a, 4I_2, D_4)$ or $(a, 4I_2, D_6)$ for the quadrilateral mesh and the triangular mesh, respectively, where a is a mask and

$$M_{\sqrt{2}} := \begin{bmatrix} 1 & 1 \\ 1 & -1 \end{bmatrix}, \quad M_{\sqrt{3}} := \begin{bmatrix} 1 & -2 \\ 2 & -1 \end{bmatrix}, \quad I_2 := \begin{bmatrix} 1 & 0 \\ 0 & 1 \end{bmatrix}.$$

In this thesis, for simplicity, we only consider the dilation matrices $M = mI_s$ case, where m is an integer such that $m > 1$. In the setting of CAGD, this kind of subdivision schemes are also called m-adic subdivision schemes.

It is difficult to have a global coordinate system on a general mesh because there are corresponding connectivities between certain vertices, which are also called edges. Clearly, different edge has different direction, therefore it is much

complicated to identify the directions in $\mathbb{R}^3$ in implementation. In order to overcome such difficulty, we require that the stencils satisfy a symmetric property in a subdivision scheme. This is equivalent to saying that a subdivision scheme is a *subdivision triplet* (a, M, G) (see [17]) that satisfies the following two conditions:

1. The mask a is *G-symmetric*:

$$a(E\beta) = a(\beta) \qquad \forall\, \beta \in \mathbb{Z}^s \quad \text{and} \quad E \in G; \tag{1.2}$$

2. G is a symmetry group with respect to the dilation matrix M (see [14]); that is, G is a symmetry group on $\mathbb{Z}^s$ such that

$$MEM^{-1} \in G \qquad \text{for all} \quad E \in G. \tag{1.3}$$

When $M = mI_s$, the condition in (1.3) is automatically satisfied. The basis function ϕ of a subdivision triplet (a, mI_s, G) is a unique solution to the refinement equation:

$$\phi = \sum_{\beta \in \mathbb{Z}^s} a(\beta)\phi(m \cdot -\beta) \qquad \text{with} \qquad \hat{\phi}(0) = 1, \tag{1.4}$$

where the Fourier transform is defined to be $\hat{f}(\xi) := \int_{\mathbb{R}^s} f(x)e^{-ix\xi}\, dx, \xi \in \mathbb{R}^s$. Since (a, mI_s, G) is a subdivision triplet, it is easy to see that $\phi(E\cdot) = \phi$ for all $E \in G$. In fact, ϕ is given by $\hat{\phi}(\xi) = \prod_{j=1}^{\infty}[m^{-1}\hat{a}(m^{-j}\xi)]$, where $\hat{a}$ is the Fourier series of the sequence a and is defined to be

$$\hat{a}(\xi) := \sum_{\beta \in \mathbb{Z}^s} a(\beta)e^{-i\beta\cdot\xi}, \qquad \xi \in \mathbb{R}^s. \tag{1.5}$$

By $\ell_0(\mathbb{Z}^s)$ we denote the space of all finitely supported sequences on $\mathbb{Z}^s$. For a subdivision triplet (a, mI_s, G), the *subdivision operator* $S_{a,mI_s} : \ell_0(\mathbb{Z}^s) \mapsto \ell_0(\mathbb{Z}^s)$ is defined to be

$$[S_{a,mI_s}u](\alpha) := \sum_{\beta \in \mathbb{Z}^s} a(\alpha - m\beta)u(\beta), \qquad \alpha \in \mathbb{Z}^s,\ u \in \ell_0(\mathbb{Z}^s). \tag{1.6}$$

Since (a, mI_s, G) is a subdivision triplet, it is easy to check that if $u \in \ell_0(\mathbb{Z}^s)$ is G-symmetric, then $S_{a,mI_s}u$ is also G-symmetric. The subdivision operator S_{a,mI_s} plays an important role in CAGD. Let Π_k denote the space of all polynomials of total degree at most k. In general, one requires that a subdivision scheme can reproduce some polynomial space Π_k for some integer k; in other words, the mask a satisfies the *sum rules* of order $k+1$ ([24]) with respect to the lattice $m\mathbb{Z}^s$, that is,

$$\sum_{\beta \in m\mathbb{Z}^s} a(\alpha+\beta)p(\alpha+\beta) = \sum_{\beta \in m\mathbb{Z}^s} a(\beta)p(\beta) \qquad \forall\, \alpha \in \mathbb{Z}^s, p \in \Pi_k. \tag{1.7}$$

We say that (a, mI_s, G) is an *interpolatory subdivision triplet* if (a, mI_s, G) is a subdivision triplet and a is an *interpolatory mask* with respect to the lattice $m\mathbb{Z}^s$, that is,

$$a(0) = 1 \quad \text{and} \quad a(m\beta) = 0 \qquad \forall\, \beta \in \mathbb{Z}^s \backslash \{0\}. \tag{1.8}$$

It is easy to see that if (a, mI_s, G) is an interpolatory subdivision triplet, then $[S_{a,mI_s}u](m\beta) = u(\beta)$ for all $\beta \in \mathbb{Z}^s$ and $u \in \ell_0(\mathbb{Z}^s)$.

Now we see that in order to compute the value of f^1 at the point $m^{-1}\gamma$, the stencil is given by $(a(\gamma - m\beta))_{\beta \in \mathbb{Z}^s}$; that is, the stencil is given by $(a_*(\beta - m^{-1}\gamma))_{\beta \in \mathbb{Z}^s}$, where $a_*(\beta) = a(-m\beta), \beta \in m^{-1}\mathbb{Z}^s$.

1.4.2 Convergence and Smoothness Properties

In this subsection, we shall discuss convergence and smoothness properties of subdivision triplets, in particular, of interpolatory subdivision triplets. In order to do so, let us first introduce some notation and recall some results from the literature, in particular, from Han and Jia [18].

We denote by $\ell_p(\mathbb{Z}^s)$ the linear space of all sequences u on $\mathbb{Z}^s$ such that

$$\|u\|_{\ell_p(\mathbb{Z}^s)} := \Big(\sum_{\beta \in \mathbb{Z}^s} |u(\beta)|^p \Big)^{1/p} < \infty.$$

For any $\alpha \in \mathbb{Z}^s$, we denote by δ_α the sequence on $\mathbb{Z}^s$ such that $\delta_\alpha(\alpha) = 1$ and $\delta_\alpha(\beta) = 0$ for all $\beta \in \mathbb{Z}^s \backslash \{\alpha\}$. In particular, $\delta := \delta_0$. The convolution of two sequences is defined to be

$$[u * v](\alpha) := \sum_{\beta \in \mathbb{Z}^s} u(\beta) v(\alpha - \beta), \qquad u, v \in \ell_0(\mathbb{Z}^s).$$

Clearly, $\widehat{u * v} = \hat{u}\hat{v}$. For a finitely supported sequence a on $\mathbb{Z}^s$, we define the following quantity:

$$(1.9) \quad \rho(a, mI_s, p, u) := \lim_{n \to \infty} \|u * [S^n_{a, mI_s} \delta]\|^{1/n}_{\ell_p(\mathbb{Z}^s)}, \qquad 1 \leqslant p \leqslant \infty, u \in \ell_0(\mathbb{Z}^s).$$

For $\alpha \in \mathbb{Z}^s$ and $t \in \mathbb{R}^s$, we define

$$(1.10) \quad \nabla_\alpha v := v - v(\cdot - \alpha), \quad \nabla_t f := f - f(\cdot - t), \qquad v \in \ell_0(\mathbb{Z}^s), f \in L_p(\mathbb{R}^s).$$

Denote $\mathbb{N}_0 := \mathbb{N} \cup \{0\}$. For $\mu = (\mu_1, \ldots, \mu_s) \in \mathbb{N}_0^s$, $|\mu| = |\mu_1| + \cdots + |\mu_s|$ and $\nabla^\mu := \nabla^{\mu_1}_{e_1} \cdots \nabla^{\mu_s}_{e_s}$, where e_j is the jth coordinate unit vector in $\mathbb{R}^s$.

Note that

$$\nabla^\mu v = [\nabla^\mu \delta] * v,$$

and

$$\nabla^\mu f = [\nabla^\mu \delta] * f = \sum_{\beta \in \mathbb{Z}^s} [\nabla^\mu \delta](\beta) f(\cdot - \beta).$$

The partial derivative of a differentiable function f with respect to the jth coordinate is denoted by $\partial_j f$. For $\mu = (\mu_1, \ldots, \mu_s)$, we denote $\partial^\mu := \partial_1^{\mu_1} \cdots \partial_s^{\mu_s}$.

If a mask a satisfies the sum rules of order k but not $k + 1$, then for $1 \leqslant p \leqslant \infty$, we define (see [14, 16]) the following quantity:

$$\nu_p(a, mI_s) := s/p - \log_m \max\{\rho(a, mI_s, p, \nabla^\mu \delta) \ : \ |\mu| = k\}.$$

The following result has been established in [19]:

Theorem 1.1. *([19, Theorem 2.1]) Let (a, mI_s, G) be a subdivision triplet and let ϕ denote its basis function. Then for any nonnegative integer k, the following statements are equivalent:*

1. $\nu_\infty(a, mI_s) > k$;

2. *For every compactly supported function $f \in C^k(\mathbb{R}^s)$ such that*

$$\hat{f}(0) = 1 \quad \text{and} \quad \partial^\mu \hat{f}(2\pi\beta) = 0 \qquad \forall\, |\mu| \leqslant k, \beta \in \mathbb{Z}^s \backslash \{0\}, \tag{1.11}$$

the cascade sequence $Q^n_{a,mI_s} f$ is a Cauchy sequence in $C^k(\mathbb{R}^s)$ (in fact, $\lim_{n\to\infty} \|Q^n_{a,mI_s} f - \phi\|_{C^k(\mathbb{R}^s)} = 0$), where the cascade operator $Q_{a,mI_s} : C(\mathbb{R}^s) \mapsto C(\mathbb{R}^s)$ is defined to be

$$Q_{a,mI_s} f := \sum_{\beta\in\mathbb{Z}^s} a(\beta) f(m\cdot - \beta), \qquad f \in C(\mathbb{R}^s); \tag{1.12}$$

3. *The basis function $\phi \in C^k(\mathbb{R}^s)$ and*

$$\lim_{n\to\infty} \|m^{kn} \nabla^\mu [S^n_{a,mI_s}\delta](\cdot) - [\partial^\mu \phi](m^{-n}\cdot)\|_{\ell_\infty(\mathbb{Z}^s)} = 0 \qquad \forall\, |\mu| = k; \tag{1.13}$$

4. *For every sequence $u \in \ell_\infty(\mathbb{Z}^s)$, there exists a function $g \in C^k(\mathbb{R}^s)$ such that*

$$\lim_{n\to\infty} \|m^{n|\mu|} [\nabla^\mu S^n_{a,mI_s} u](\cdot) - [\partial^\mu g](m^{-n}\cdot)\|_{\ell_\infty(\mathbb{Z}^s)} = 0 \forall\, |\mu| \leqslant k. \tag{1.14}$$

For any $0 < \nu \leqslant 1$ and a function $f \in L_p(\mathbb{R}^s)$, we say that f belongs to the *Lipschitz space* $\mathrm{Lip}(\nu, L_p(\mathbb{R}^s))$ if there exists a positive constant C such that

$$\|f - f(\cdot - t)\|_{L_p(\mathbb{R}^s)} \leqslant C\|t\|^\nu \qquad \forall\, t \in \mathbb{R}^s.$$

The L_p smoothness of a function $f \in L_p(\mathbb{R}^s)$ is measured by its L_p *critical smoothness exponent* $\nu_p(f)$ which is defined by

$$\nu_p(f) := \sup\{n + \nu \quad : \quad \partial^\mu f \in \mathrm{Lip}(\nu, L_p(\mathbb{R}^s)) \quad \forall\, |\mu| = n\}.$$

For the basis function ϕ of any subdivision triplet (a, mI_s, G), one always has $\nu_p(\phi) \geqslant \nu_p(a, mI_s)$. A function f is an *interpolatory function* if f is a continuous function such that $f(\beta) = \delta(\beta)$ for all $\beta \in \mathbb{Z}^s$.

The following result is known in the literature (e.g., see [14, 16, 18]).

Theorem 1.2. *([14, Theorem 3.1]) Let (a, mI_s, G) be an interpolatory subdivision triplet and ϕ denote its basis function. Then ϕ is an interpolatory function if and only if $\nu_\infty(a, mI_s) > 0$. Moreover, if $\nu_\infty(a, mI_s) > 0$, then $\nu_p(\phi) = \nu_p(a, mI_s)$ for all $1 \leqslant p \leqslant \infty$.*

The ℓ_p-norm joint spectral radius has been introduced in Jia [23]. The quantity $\rho(a, mI_s, p, u)$ in (1.9) can be rewritten using the ℓ_p-norm joint spectral radius. Let $\mathcal{T}$ be a finite collection of linear operators acting on a finite-dimensional normed vector space V. For a positive integer n, we denote $\mathcal{T}^n = \{(T_1, \ldots, T_n) \,:\, T_1, \ldots, T_n \in \mathcal{T}\}$ and we define

$$\|\mathcal{T}^n\|_p^p := \sum_{(T_1,\ldots,T_n)\in\mathcal{T}^n} \|T_1 \cdots T_n\|^p, \qquad 1 \leqslant p < \infty$$

and

$$\|\mathcal{T}^n\|_\infty := \max\{\|T_1 \cdots T_n\| \,:\, (T_1, \ldots, T_n) \in \mathcal{T}^n\},$$

where $\|\cdot\|$ denotes some operator norm.

For $1 \leqslant p \leqslant \infty$, the *$\ell_p$-norm joint spectral radius* of $\mathcal{T}$ (see [18, 23]) is defined to be

$$\rho_p(\mathcal{T}) := \lim_{n\to\infty} \|\mathcal{T}^n\|_p^{1/n} = \inf_{n\geqslant 1} \|\mathcal{T}^n\|_p^{1/n}. \tag{1.15}$$

Let $\Gamma := [0, m-1]^s \cap \mathbb{Z}^s$. To relate the quantity $\rho(a, mI_s, p, u)$ to the ℓ_p-norm joint spectral radius, we introduce $T_{a,\gamma}, \gamma \in \Gamma$ on $\ell_0(\mathbb{Z}^s)$ by

$$T_{a,\gamma} v(\alpha) := \sum_{\beta\in\mathbb{Z}^s} a(m\alpha - \beta + \gamma) v(\beta), \qquad v \in \ell_0(\mathbb{Z}^s), \alpha \in \mathbb{Z}^s. \tag{1.16}$$

It was proved in [18, Lemma 2.3] that if a is finitely supported, then for any finitely supported sequence u on $\mathbb{Z}^s$, there exists a finite dimensional subspace $V(u)$ of $\ell_0(\mathbb{Z}^s)$ such that $V(u)$ contains u and $V(u)$ is the smallest subspace of $\ell_0(\mathbb{Z}^s)$ which is invariant under the operators $T_{a,\gamma}$, $\gamma \in \Gamma$. We call such $V(u)$ the minimal $\{T_{a,\gamma} : \gamma \in \Gamma\}$ invariant subspace generated by u.

Let $\mathcal{T} := \{T_{a,\gamma}|_{V(u)} : \gamma \in \Gamma\}$, where $V(u)$ is the minimal $\{T_{a,\gamma} : \gamma \in \Gamma\}$ invariant subspace generated by u. Then it is known ([18]) that

$$\rho(a, mI_s, p, u) = \lim_{n\to\infty} \|u * [S^n_{a,mI_s}\delta]\|^{1/n}_{\ell_p(\mathbb{Z}^s)} = \rho_p(\mathcal{T}) = \inf_{n\geqslant 1} \|\mathcal{T}^n\|^{1/n}_p. \tag{1.17}$$

The following result is useful in calculating the quantity $\rho(a, mI_s, p, u)$ in (1.9) and is given in [19].

Theorem 1.3. *([19, Theorem 2.3]) Let a be a finitely supported mask on $\mathbb{Z}^s$. If*

$$\hat{a}(\xi) = \frac{\hat{c}(m\xi)}{\hat{c}(\xi)}\hat{b}(\xi) \quad \text{for finitely supported sequences } b \text{ and } c \text{ on } \mathbb{Z}^s, \tag{1.18}$$

such that $\hat{c}(m\xi)/\hat{c}(\xi)$ is a 2π-periodic trigonometric polynomial, then for any $1 \leqslant p \leqslant \infty$ and $u \in \ell_0(\mathbb{Z}^s)$,

$$\begin{aligned} \rho(a, mI_s, p, u * c) &:= \lim_{n\to\infty} \|u * c * [S^n_{a,mI_s}\delta]\|^{1/n}_{\ell_p(\mathbb{Z}^s)} \\ &= \lim_{n\to\infty} \|u * [S^n_{b,mI_s}\delta]\|^{1/n}_{\ell_p(\mathbb{Z}^s)} =: \rho(b, mI_s, p, u). \end{aligned} \tag{1.19}$$

Since the support of the sequence b is smaller than that of the sequence a, it is relatively simpler to compute the quantity $\rho(b, mI_s, \infty, \delta)$ than the quantity $\rho(a, mI_s, p, \delta)$. The following result provides a reasonable and convenient way for estimating the quantity $\rho(b, mI_s, \infty, \delta)$:

Theorem 1.4. *([19, Theorem 2.4]) Let b be a finitely supported sequence on $\mathbb{Z}^s$. Then*

$$\rho(b, mI_s, \infty, \delta) := \lim_{n\to\infty} \|S^n_{b,mI_s}\delta\|^{1/n}_{\ell_\infty(\mathbb{Z}^s)} = \inf_{n\in\mathbb{N}} \Big(\max_{\alpha\in\mathbb{Z}^s} \sum_{\beta\in\mathbb{Z}^s} |S^n_{b,mI_s}\delta(\alpha + m^n\beta)| \Big)^{1/n}. \tag{1.20}$$

Chapter 2

One-dimensional Interpolatory Subdivision Schemes with Dilation Factor 4

In this chapter, we shall investigate optimal one-dimensional interpolatory subdivision triplets $(a, 4, \{-1, 1\})$ with two-ring stencils. Then we discuss the smoothness property of the basis function associated with the mask a and figure out the corresponding parameters which yield the smoothest subdivision scheme. Then we shall discuss the projection method for the optimal multidimensional interpolatory subdivision schemes with two-ring stencils.

2.1 Optimal One-dimensional Interpolatory Subdivision Schemes

For the sake of convenience, in the following sections, by 4-adic subdivision schemes we denote the schemes with dilation factor 4. This new 4-adic subdivision scheme is a *primal* interpolatory subdivision scheme which adds three

new vertices on each edge, and reconnects them sequentially, that is to split one edge into four edges and make the curve smoother.

2.1.1 The Optimal Subdivision Scheme

For one-dimensional interpolatory 4-adic subdivision schemes with two-ring stencils, we have the following result.

Theorem 2.1. *Let $(a, 4, \{-1, 1\})$ be a one-dimensional interpolatory 4-adic subdivision triplet such that the mask a is supported on $[-7, 7]$ (that is, all its subdivision stencils have two-ring neighboring vertices). Then $\nu_\infty(a, 4) \leqslant \log_4 24$. Moreover, $\nu_\infty(a, 4) = \log_4 24$ if and only if a must be the unique mask a^{best} which is given by*

$$\begin{aligned}\widehat{a^{best}}(\xi) =& \frac{1}{192} e^{5i\xi}(1 + e^{-i\xi} + e^{-2i\xi} + e^{-3i\xi})^3 \\ & (-5e^{2i\xi} + 3e^{i\xi} + 8 + 8e^{-i\xi} + 3e^{-2i\xi} - 5e^{-3i\xi}),\end{aligned} \tag{2.1}$$

or equivalently, the mask a^{best} is supported on $[-7, 7]$ and is given by

$$\left[-\frac{5}{192}, -\frac{1}{16}, -\frac{13}{192}, 0, \frac{15}{64}, \frac{9}{16}, \frac{55}{64}, \mathbf{1}, \frac{55}{64}, \frac{9}{16}, \frac{15}{64}, 0, -\frac{13}{192}, -\frac{1}{16}, -\frac{5}{192}\right].$$

Proof. Since the mask a is an interpolatory mask with support $[-7, 7]$, by (1.8) we have,

$$a(0) = 1 \qquad \text{and} \qquad a(-4) = a(4) = 0.$$

Since the mask a is $\{-1, 1\}$-symmetric, it must take the following form:

$$[C_6,\ C_5,\ C_4,\ 0,\ C_3,\ C_2,\ C_1,\ \mathbf{1},\ C_1,\ C_2,\ C_3,\ 0,\ C_4,\ C_5,\ C_6].$$

Note that subdivision stencils come from the mask a. So we must have

$$\begin{aligned} C_1 + C_3 + C_4 + C_6 &= 1, \\ 2C_2 + 2C_5 &= 1. \end{aligned} \tag{2.2}$$

Moreover, suppose that $\nu_\infty(a,4) > \log_4 24 \approx 2.29248$. Then the mask a must satisfy the sum rules of order at least 3 with respect to the lattice $4\mathbb{Z}$ (see [24]). By the definition of the sum rules given by (1.7) with $k = 2$, we have the following equations, for all $\alpha \in \mathbb{Z}$,

$$\sum_{\beta\in 4\mathbb{Z}} a(\alpha+\beta) = \sum_{\beta\in 4\mathbb{Z}} a(\beta) = 1, \tag{2.3}$$

$$\sum_{\beta\in 4\mathbb{Z}} a(\alpha+\beta)(\alpha+\beta) = \sum_{\beta\in 4\mathbb{Z}} a(\beta)\beta, \tag{2.4}$$

$$\sum_{\beta\in 4\mathbb{Z}} a(\alpha+\beta)(\alpha+\beta)^2 = \sum_{\beta\in 4\mathbb{Z}} a(\beta)\beta^2. \tag{2.5}$$

By calculation, we see that (2.3) becomes (2.2). And (2.4) is equivalent to the following equation:

$$C_1 - C_3 + 5C_4 - 7C_6 = 0, \tag{2.6}$$

and (2.5) is equivalent to

$$\begin{aligned} C_2 + 9C_5 &= 0, \\ C_1 + 9C_3 + 25C_4 + 49C_6 &= 0. \end{aligned} \tag{2.7}$$

Then by solving the system of linear equations in (2.2), (2.6) and (2.7), we can figure out 5 parameters by leaving just one free parameter there. For example, we can choose C_6 as our free parameter to express all other parameters. Let $C_6 = t$, we have:

$$C_1 = 3t + \frac{15}{16},\ C_2 = \frac{9}{16},\ C_3 = -3t + \frac{5}{32},\ C_4 = -t - \frac{3}{32},\ C_5 = -\frac{1}{16}.$$

Consequently, we have

$$\begin{aligned} \hat{a}(\xi) =& (3t + \frac{15}{16})(e^{i\xi} + e^{-i\xi}) + \frac{9}{16}(e^{2i\xi} + e^{-2i\xi}) - (3t - \frac{5}{32})(e^{3i\xi} + e^{-3i\xi}) \\ & - (t + \frac{3}{32})(e^{5i\xi} + e^{-5i\xi}) - \frac{1}{16}(e^{6i\xi} + e^{-6i\xi}) + t(e^{7i\xi} + e^{-7i\xi}) + 1. \end{aligned}$$

In order to facilitate our analysis later, we rewrite $\hat{a}(\xi)$ in the following form:

$$\hat{a}(\xi) = e^{5i\xi}(1 + e^{-i\xi} + e^{-2i\xi} + e^{-3i\xi})^3\hat{b}(\xi) \tag{2.8}$$

with

$$\begin{aligned}\hat{b}(\xi) :=& t\, e^{2i\xi} - (3t + \frac{1}{16})e^{i\xi} + (2t + \frac{3}{32}) + (2t + \frac{3}{32})e^{-i\xi} \\ & - (3t + \frac{1}{16})e^{-2i\xi} + te^{-3i\xi}.\end{aligned} \tag{2.9}$$

Since the mask a satisfies the sum rules of order 3, in order to compute the quantity $\nu_\infty(a, 4)$, we have to compute $\rho(a, 4, \infty, \nabla^3\delta)$. By Theorem 1.3 we have

$$\rho(a, 4, \infty, \nabla^3\delta) = \rho(b, 4, \infty, \delta).$$

Consequently, in order to compute the quantity $\nu_\infty(a, 4)$, we have to compute $\rho(b, 4, \infty, \delta)$. In the following, we shall use ℓ_∞-norm joint spectral radius to find a lower bound for $\rho(b, 4, \infty, \delta)$ and use Theorem 1.4 to find an upper bound for $\rho(b, 4, \infty, \delta)$.

Let $T_{b,\gamma}, \gamma = -1, 0, 1, 2$ be the linear operators defined in (1.16) with $m = 4$. Since the mask a is supported on $[-7,\ 7]$, it is easy to check that the linear space $\ell([-1, 1])$ is $\{T_{b,\gamma} : \gamma = -1, 0, 1, 2\}$-invariant, for example, take $\gamma = 0$, we have

$$T_{b,0}\delta_0(\alpha) = \sum_{\beta\in\mathbb{Z}} b(4\alpha - \beta)\delta_0(\beta) = b(4\alpha) = \begin{cases} b(-4), & \text{if } \alpha = -1, \\ b(0), & \text{if } \alpha = 0, \\ b(4), & \text{if } \alpha = 1. \end{cases}$$

So

$$T_{b,0}\delta_0 = b(-4)\delta_{-1} + b(0)\delta_0 + b(4)\delta_1.$$

Similarly, we have

$$T_{b,0}\delta_{-1} = b(-3)\delta_{-1} + b(1)\delta_0 + b(5)\delta_1,$$

and

$$T_{b,0}\delta_1 = b(-5)\delta_{-1} + b(-1)\delta_0 + b(3)\delta_1.$$

All $T_{b,\gamma}\delta_\beta, \beta = -1, 0, 1$ are linear combinations of $\{\delta_{-1}, \delta_0, \delta_1\}$. So $\ell([-1,1])$ is an invariant subspace under all operators $T_{b,\gamma}; \gamma = -1,\ 0,\ 1,\ 2$.

Their matrix representations H_γ, under the standard basis $\{\delta_{-1}, \delta_0, \delta_1\}$ of $\ell([-1,1])$, are $H_\gamma = (b(4k-j+\gamma))_{-1\leqslant j,k\leqslant 1}$ for $\gamma = -1, 0, 1, 2$. So, $\rho(b, 4, \infty, \delta) = \rho_\infty(\{H_{-1}, H_0, H_1, H_2\})$, where

(2.10)

$$H_{-1} = \begin{bmatrix} 0 & 2t+3/32 & 0 \\ 0 & -3t-1/16 & t \\ 0 & t & -3t-1/16 \end{bmatrix}, \quad H_0 = \begin{bmatrix} 0 & 2t+3/32 & 0 \\ 0 & 2t+3/32 & 0 \\ 0 & -3t-1/16 & t \end{bmatrix},$$

$$H_1 = \begin{bmatrix} t & -3t-1/16 & 0 \\ 0 & 2t+3/32 & 0 \\ 0 & 2t+3/32 & 0 \end{bmatrix}, \quad H_2 = \begin{bmatrix} -3t-1/16 & t & 0 \\ t & -3t-1/16 & 0 \\ 0 & 2t+3/32 & 0 \end{bmatrix}.$$

It is easy to see that $\{0,\ -2t-1/16,\ -4t-1/16\}$, $\{0,\ t,\ 2t+3/32\}$, $\{0,\ t,\ 2t+3/32\}$ and $\{0,\ -2t-1/16,\ -4t-1/16\}$ are eigenvalues of H_{-1}, H_0, H_1 and H_2, respectively.

Consequently, we have the following inequality

$$\rho(b, 4, \infty, \delta) = \rho_\infty(\{H_{-1}, H_0, H_1, H_2\}) \geqslant \max\{\rho(H_{-1}), \rho(H_0), \rho(H_1), \rho(H_2)\}.$$

In order to find out the maximum value, we sketch the graphs of $|t|, |2t+3/32|, |2t+1/16|$ and $|4t+1/16|$, as shown in Figure 2.1.

It is easy to check that the maximum value is determined by intersection points of the line $|2t+3/32|$ and the line $|4t+1/16|$. The enlarged figure is shown in Figure 2.2. Thus

$$\rho(b, 4, \infty, \delta) \geqslant \max\{|2t+2/32|, |4t+1/16|\} \geqslant 1/24,$$

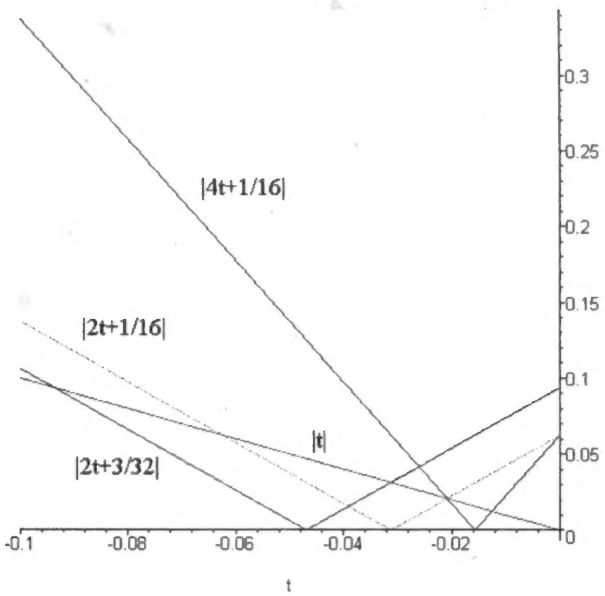

Figure 2.1: Find out the optimal parameter of "t".

where the equal sign in the last inequality holds if and only if $t = -5/192$. By Theorem 1.3, we have

$$\rho(a, 4, \infty, \nabla_{e_1}^3 \delta) = \rho(b, 4, \infty, \delta) \geqslant 1/24.$$

Therefore, we conclude that

$$\nu_\infty(a, 4) = -\log_4 \rho(a, 4, \infty, \nabla_{e_1}^3 \delta) = -\log_4 \rho(b, 4, \infty, \delta) \leqslant \log_4 24.$$

On the other hand, by (2.10), we have

$$\begin{aligned} \rho(b, 4, \infty, \delta) &\leqslant \max\{\|H_{-1}\|_{\ell_{\infty,1}}, \|H_0\|_{\ell_{\infty,1}}, \|H_1\|_{\ell_{\infty,1}}, \|H_2\|_{\ell_{\infty,1}}\} \\ &\leqslant \max\{|2t + 3/32|, |3t + 1/16| + |t|\}. \end{aligned}$$

where $\|\cdot\|_{\ell_{\infty,1}}$ is a matrix norm which is defined to be

$$\|(t_{ij})_{1\leqslant i\leqslant I,\ 1\leqslant j\leqslant J}\|_{\ell_{\infty,1}} := \max_{1\leqslant i\leqslant I} \sum_{j=1}^{J} |t_{ij}|.$$

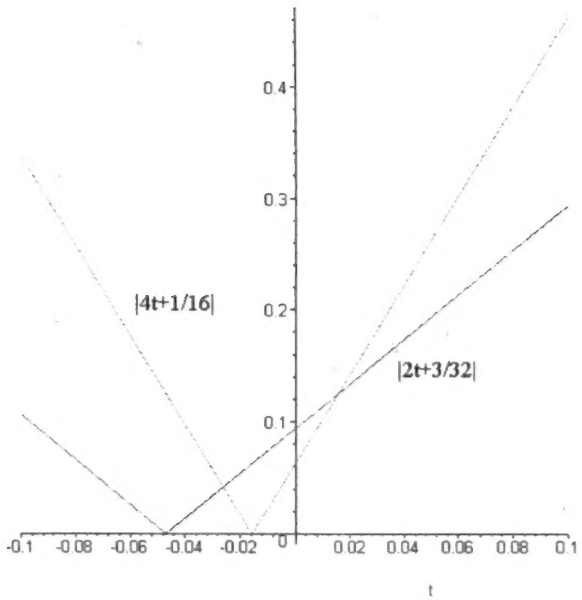

Figure 2.2: The calculation of free parameter "t".

Or, by Theorem 1.4, we have

$$\rho(b,4,\infty,\delta) \leqslant \max_{\alpha\in\mathbb{Z}} \sum_{\beta\in\mathbb{Z}} |b(\alpha+4\beta)| \leqslant \max\{|2t+3/32|, |3t+1/16|+|t|\}.$$

Therefore, we have

$$\begin{aligned} \max\{|2t+3/32|, |4t+1/16|\} &\leqslant \rho(b,4,\infty,\delta) \\ &\leqslant \max\{|2t+3/32|, |3t+1/16|+|t|\}. \end{aligned} \tag{2.11}$$

When $t=-5/192$, the above inequalities yield that $\rho(b,4,\infty,\delta)=1/24$. Therefore, we conclude that $\nu_\infty(a^{best},4) = -\log_4 \rho(b,4,\infty,\delta) = \log_4 24$. □

Therefore, for our one dimensional 4-adic interpolatory subdivision schemes, we have shown that the quantity $\nu_\infty(a,\ 4)$ have a bigger upper bound than that of other dyadic and ternary schemes. That is almost equivalent to saying that 4-adic may generate smoother curves. Moreover, we figured out the best

mask a such that the quantity $\nu_\infty(a,\ 4)$ can achieve its upper bound. That is reason why we call the mask a the best mask.

2.1.2 Smoothness of 4-adic Interpolatory Subdivision Schemes

More precisely, we have the following result on subdivision triplet $(a,\ 4,\ \{-1,\ 1\})$ with two-ring stencils.

Theorem 2.2. *Let $(a, 4, \{-1, 1\})$ be an interpolatory subdivision triplet such that the mask a is supported on $[-7, 7]$ and satisfies the sum rules of order 3. Then the mask a must be given by*

$$\hat{a}(\xi) = e^{5i\xi}(1 + e^{-i\xi} + e^{-2i\xi} + e^{-3i\xi})^3\hat{b}(\xi)$$

with

$$\begin{aligned}\hat{b}(\xi) =& t\, e^{2i\xi} - (3t + 1/16)e^{i\xi} + (2t + 3/32) + (2t + 3/32)e^{-i\xi} \\ & - (3t + 1/16)e^{-2i\xi} + te^{-3i\xi}.\end{aligned}$$

Moreover, we have

$$\nu_\infty(a, 4) = \begin{cases} -\log_4(-4t - 1/16), & \text{if } t \leqslant -5/192, \\ -\log_4(2t + 3/32), & \text{if } -5/192 < t < 1/64, \\ -\log_4(4t + 1/16), & \text{if } t \geqslant 1/64. \end{cases}$$

In particular, the subdivision triplet is C^2 if and only if $-1/32 < t < -1/16$.

Proof. By the proof of Theorem 2.1, we see that (2.11) holds. By a simple

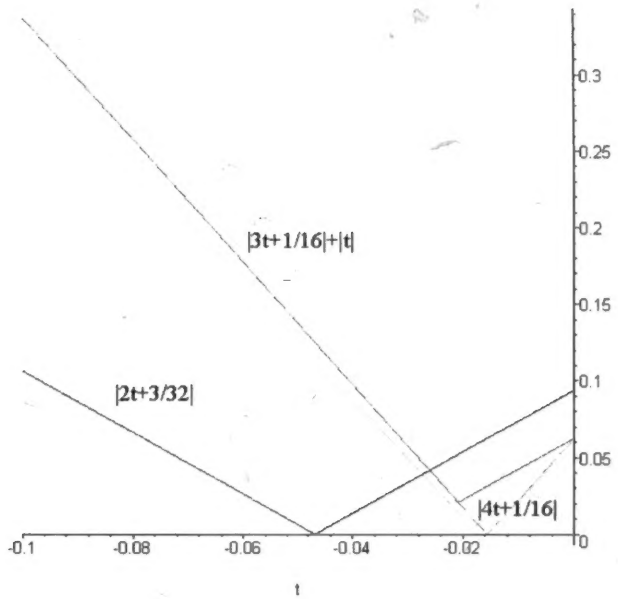

Figure 2.3: Graph of $|2t + 3/32|$, $|4t + 1/16|$ and $|3t + 1/16| + |t|$.

calculation, we observe that

$$\begin{aligned}\max\{|2t + 3/32|, |4t + 1/16|\} &= \max\{|2t + 3/32|, |3t + 1/16| + |t|\} \\ &= \begin{cases} -4t - 1/16, & \text{if } t \leqslant -5/192, \\ 2t + 3/32, & \text{if } -5/192 < t < 1/64, \\ 4t + 1/16, & \text{if } t \geqslant 1/64. \end{cases}\end{aligned}$$

See Figure 2.3 for more details about the above identities.

Therefore, the claim follows directly from (2.11) and

$$\nu_\infty(a, 4) = -\log_4 \rho(b, 4, \infty, \delta).$$

We are done. □

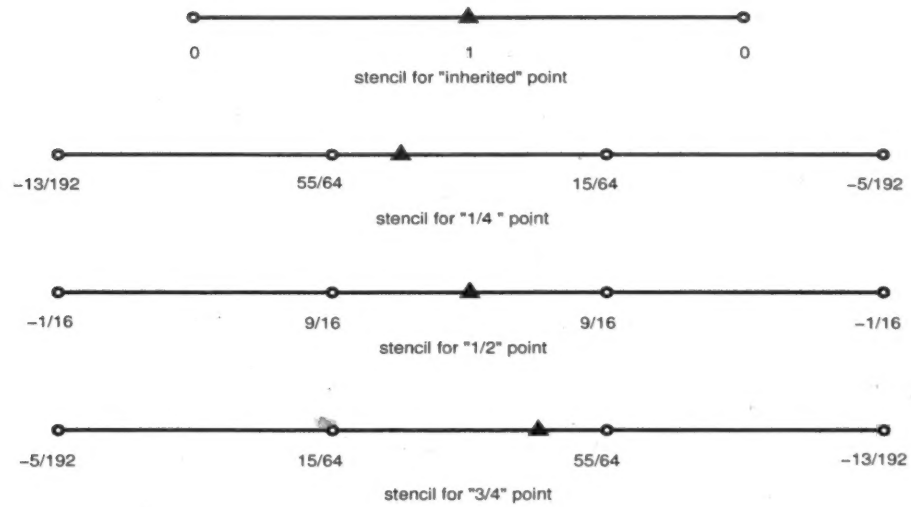

Figure 2.4: Associated subdivision stencils for the best interpolatory 4-adic subdivision scheme. By the symbol "$\triangle$" we denote the new inserted vertex, and the symbol "$\circ$" denotes vertices at the previous level.

2.1.3 Associated Subdivision Stencils

Once we find the optimal mask of the 4-adic interpolatory subdivision scheme, we can start to generate subdivision curves. But the mask cannot be employed directly, we must figure out the stencils from the mask. For one-dimensional case, it is relatively easy to get it. Let $\beta \in \mathbb{Z}/m\mathbb{Z}$, $\{a(\gamma) : \gamma = \beta + m\alpha, \alpha \in \mathbb{Z}\}$ is a stencil for a certain β, where m is the dilation factor. Thus for $\beta = 0, \ldots, m-1$, we have m different stencils.

In our interpolatory 4-adic subdivision scheme case in Section 1, we need insert three new vertices on each edge, we call them "1/4" vertex, "1/2" vertex and "3/4" vertex, respectively. Intuitively, we should figure out three stencils for these three new vertices, and one stencil for the "inherited" vertices. Since this scheme belongs to interpolatory schemes, those "inherited" vertices will definitely remain unchanged. Naturally, the stencil for "inherited" vertices must be $[0, 1, 0]$.

In terms of the symmetric property, we found that, for "1/4 vertex" and "3/4 vertex", the stencils are almost the same, the only difference is the order. Therefore we can treat the stencil for "3/4 vertex" as a flip of that of "1/4 vertex". Thus we actually only need to figure out two subdivision stencils. All the details of the associated subdivision stencils are given in Figure 2.3. It is quite interesting to note that the subdivision stencil for the "1/2 vertex" is the same subdivision stencil derived from the well-known 4-point interpolatory scheme.

2.2 Projection Method for Multi-dimensional Subdivision Triplets

For a sequence a on $\mathbb{Z}^s$, we define a new sequence Pa via the projection operator $P : \ell_0(\mathbb{Z}^s) \mapsto \ell_0(\mathbb{Z})$ as follows:

$$[Pa](j) := \sum_{\beta \in \mathbb{Z}^{s-1}} a(j, \beta), \qquad j \in \mathbb{Z}. \tag{2.12}$$

Now we have the following result on optimal multidimensional interpolatory 4-adic subdivision triplets with two-ring stencils.

Theorem 2.3. *Let $(a, 4I_s, \{I_s, -I_s\})$ be an interpolatory subdivision triplet such that the mask a is supported on $[-7, 7]^s$. Then $\nu_\infty(a, 4) \leqslant \log_4 24$. Moreover, if $\nu_\infty(a, 4I_s) = \log_4 24$, then the projected mask $4^{1-s}Pa$ must be the unique mask a^{best} defined in* (2.1).

Proof. Suppose that $\nu_\infty(a, 4I_s) > \log_4 24$. Then a must satisfy the sum rules of order at least 3. Let Pa be the one-dimensional sequence defined in (2.12). Then by [13, 15], Pa must satisfy the sum rules of order at least 3.

For the convenience of the reader, we provide a proof here for the fact that $4^{1-s}Pa$ is an interpolatory mask and satisfies the sum rules of order 3.

Since a is an interpolatory mask and satisfies the sum rules of order at least 3, we must have

$$a(0) = 1 \qquad \textit{and} \qquad a(4\beta) = 0 \qquad \forall\, \beta \in \mathbb{Z}^s \backslash \{0\}, \tag{2.13}$$

and

$$\sum_{\beta\in\mathbb{Z}^s} a(\alpha+4\beta)(\alpha+4\beta)^\mu = \sum_{\beta\in\mathbb{Z}^s} a(4\beta)(4\beta)^\mu \quad \forall\, \alpha \in \mathbb{Z}^s,\ |\mu| \leqslant 2. \tag{2.14}$$

Obviously, by (2.13), we must have

$$\sum_{\beta\in\mathbb{Z}^s} a(4\beta)(4\beta)^\mu = \delta(\mu) \qquad \forall \mu \in \mathbb{N}_0^s.$$

Therefore, (2.14) becomes

$$\sum_{\beta\in\mathbb{Z}^s} a(\alpha+4\beta)(\alpha+4\beta)^\mu = \delta(\mu) \quad \forall\, \alpha \in \mathbb{Z}^s,\ |\mu| \leqslant 2.$$

That is,

$$\begin{aligned} \sum_{\beta_1\in\mathbb{Z}} \sum_{\beta_2\in\mathbb{Z}^{s-1}} & a(\alpha_1+4\beta_1, \alpha_2+4\beta_2)(\alpha_1+4\beta_1)^{\mu_1}(\alpha_2+4\beta_2)^{\mu_2} \\ & = \delta(\mu_1)\delta(\mu_2) \quad \forall\, \alpha_1 \in \mathbb{Z},\ \alpha_2 \in \mathbb{Z}^{s-1},\ \mu_1 \in \mathbb{N}_0, \mu_2 \in \mathbb{N}_0^{s-1}. \end{aligned} \tag{2.15}$$

On the other hand, by the definition of the projected mask Pa, we have

$$\begin{aligned} \sum_{\beta_1\in\mathbb{Z}} [Pa](\alpha_1+4\beta_1)(\alpha_1+4\beta_1)^{\mu_1} &= \sum_{\beta_1\in\mathbb{Z}} \sum_{\beta_2\in\mathbb{Z}^{s-1}} a(\alpha_1+4\beta_1, \beta_2)(\alpha_1+4\beta_1)^{\mu_1} \\ &= \sum_{\beta_1\in\mathbb{Z}} \sum_{\alpha_2\in\{0,1,2,3\}^{s-1}} \sum_{\beta_2\in\mathbb{Z}^{s-1}} a(\alpha_1+4\beta_1, \alpha_2+4\beta_2)(\alpha_1+4\beta_1)^{\mu_1} \\ &= \sum_{\alpha_2\in\{0,1,2,3\}^{s-1}} \sum_{\beta_1\in\mathbb{Z}} \sum_{\beta_2\in\mathbb{Z}^{s-1}} a(\alpha_1+4\beta_1, \alpha_2+4\beta_2)(\alpha_1+4\beta_1)^{\mu_1} \end{aligned}$$

Now by (2.13), it follows from the above identity that

$$\sum_{\beta_1\in\mathbb{Z}} [Pa](\alpha_1+4\beta_1)(\alpha_1+4\beta_1)^{\mu_1} = \sum_{\alpha_2\in\{0,1,2,3\}^{s-1}} \delta(\mu_1) = 4^{s-1}\delta(\mu_1), \quad \mu_1 = 0, 1, 2.$$

So,

$$\sum_{\beta_1 \in \mathbb{Z}} [4^{1-s}Pa](\alpha_1 + 4\beta_1)(\alpha_1 + 4\beta_1)^{\mu_1} = \delta(\mu_1) \qquad \forall\, \mu_1 = 0, 1, 2. \tag{2.16}$$

Therefore, $4^{1-s}Pa$ satisfies the sum rules of order 3 with respect to the lattice $4\mathbb{Z}$.

Note that the mask a is supported on $[-7,\ 7]^s$. Therefore the mask $4^{1-s}Pa$ must be supported on $[-7,\ 7]$. Taking $\alpha_1 = 0$ in (2.16), we conclude that

$$\sum_{\beta_1=-1}^{1} [4^{1-s}Pa](4\beta_1)(4\beta_1)^{\mu_1} = \delta(\mu_1) \qquad \forall\, \mu_1 = 0, 1, 2.$$

Putting the above equations into a matrix form, we have

$$\begin{bmatrix} 1 & 1 & 1 \\ -4 & 0 & 4 \\ 16 & 0 & 16 \end{bmatrix} \begin{bmatrix} [4^{1-s}P_a](-4) \\ [4^{1-s}P_a](0) \\ [4^{1-s}P_a](4) \end{bmatrix} = \begin{bmatrix} 1 \\ 0 \\ 0 \end{bmatrix}.$$

By solving the above system of linear equations, we must have the following unique solution:

$$[4^{1-s}P_a](-4) = [4^{1-s}P_a](4) = 0 \quad \textit{and} \quad [4^{1-s}P_a](0) = 1.$$

Therefore, $4^{1-s}P_a$ must be an interpolatory mask with respect to the lattice $4\mathbb{Z}$.

Now by [13, Theorem 2.5] and Theorem 2.1, we must have $\nu_\infty(a, 4I_s) \leqslant \nu_\infty(4^{1-s}Pa, 4) \leqslant \log_4 24$. When $\nu_\infty(a, 4I_s) = \log_4 24$, we must have $\nu_\infty(4^{1-s}Pa, 4) = \log_4 24$. Therefore, by the uniqueness of the mask a^{best} in (2.1), we conclude that $4^{1-s}Pa = a^{best}$. □

Chapter 3

Two-dimensional Interpolatory Four-adic Subdivision Schemes with Two-ring Stencils

In this chapter we shall present some examples of two-dimensional interpolatory subdivision triplets $(a, 4I_2, G)$ with two-ring stencils for both the regular triangular mesh ($G = D_6$) and the regular quadrilateral mesh ($G = D_4$). Moreover, for these subdivision triplets, we shall investigate the smoothest subdivision triplets such that the quantity $\nu_\infty(a, 4I_2)$ can achieve its upper bound $\log_4 24 (\approx 2.29248)$, which provides us a better smoothness than C^2 and is the best possible smoothness.

3.1 Subdivision Schemes for the Regular Triangular Mesh

Let us first consider subdivision triplets $(a, 4I_2, D_6)$ for the regular triangular mesh. Since we only discuss the schemes with two-ring stencils, the interpola-

tory mask a must be supported on $[-7,7]^2$. The following subsections describe a way how we figure out the optimal subdivision triplets such that the quantity $\nu_\infty(a, 4I_2)$ can achieve its upper bound.

3.1.1 Computing the b Sequence

For subdivision triplets $(a, 4I_2, D_6)$ with two-ring stencils, since the support of the mask a is $[-7,\ 7]^2$, it is relatively difficult to compute the important quantity $\rho(a, 4I_2, \infty, \nabla^\mu\delta)$, where $\mu = (3,0),\ (2,1),\ (1,2),\ (0,3)$. By Theorem 1.3, we are expecting to figure out another sequence b and compute the quantity of $\rho(b, 4I_2, \infty, \delta)$ instead of $\rho(a, 4I_2, \infty, \nabla^\mu\delta)$, where the support of b is much shorter than that of a. In order to facilitate our analysis, we require that the mask a should take the following form:

$$\begin{aligned}\hat{a}(\xi_1,\xi_2) =&(1+e^{-i\xi_1}+e^{-2i\xi_1}+e^{-3i\xi_1})(1+e^{-i\xi_2}+e^{-2i\xi_2}+e^{-3i\xi_2})\\ &\times(1+e^{i(\xi_1+\xi_2)}+e^{2i(\xi_1+\xi_2)}+e^{3i(\xi_1+\xi_2)})\hat{b}(\xi_1,\xi_2).\end{aligned} \tag{3.1}$$

Since the product of the first three terms on the right-hand side of (3.1) is supported on $[-3,3]^2$, it is easy to see that the support of sequence b is $[-4,4]^2$. The sequence b must be D_6-symmetric, and therefore the sequence b takes the following form:

$$\begin{bmatrix}
0 & 0 & 0 & 0 & C_7 & C_8 & C_9 & C_8 & C_7\\
0 & 0 & 0 & C_8 & C_5 & C_6 & C_6 & C_5 & C_8\\
0 & 0 & C_9 & C_6 & C_3 & C_4 & C_3 & C_6 & C_9\\
0 & C_8 & C_6 & C_4 & C_2 & C_2 & C_4 & C_6 & C_8\\
C_7 & C_5 & C_3 & C_2 & C_1 & C_2 & C_3 & C_5 & C_7\\
C_8 & C_6 & C_4 & C_2 & C_2 & C_4 & C_6 & C_8 & 0\\
C_9 & C_6 & C_3 & C_4 & C_3 & C_6 & C_9 & 0 & 0\\
C_8 & C_5 & C_6 & C_6 & C_5 & C_8 & 0 & 0 & 0\\
C_7 & C_8 & C_9 & C_8 & C_7 & 0 & 0 & 0 & 0
\end{bmatrix}. \tag{3.2}$$

For the subdivision triplet $(a, 4I_2, D_6)$, the interpolatory mask a is required to satisfy the following requirements:

(i) The mask a is an interpolatory mask with respect to the lattice $4\mathbb{Z}^2$:

$$a(\mathbf{0}) = 1 \quad \text{and} \quad a(4\beta) = 0 \qquad \forall\, \beta \in \mathbb{Z}^2 \backslash \{\mathbf{0}\}.$$

(ii) The mask a satisfies the sum rules of order 3 with respect to the lattice $4\mathbb{Z}^2$:

$$\sum_{\beta \in 4\mathbb{Z}^2} a(\alpha+\beta) = \sum_{\beta \in 4\mathbb{Z}^2} a(\beta), \qquad \alpha \in \mathbb{Z}^2, \tag{3.3}$$

$$\sum_{\beta \in 4\mathbb{Z}^2} a(\alpha+\beta)(\alpha+\beta)^\mu = \sum_{\beta \in 4\mathbb{Z}^2} a(\beta)\beta^\mu, \quad \mu = (1,0), (0,1), \alpha \in \mathbb{Z}^2, \tag{3.4}$$

and

$$\sum_{\beta \in 4\mathbb{Z}^2} a(\alpha+\beta)(\alpha+\beta)^\mu = \sum_{\beta \in 4\mathbb{Z}^2} a(\beta)\beta^\mu, \tag{3.5}$$
$$\mu = (2,0), (1,1), (0,2), \alpha \in \mathbb{Z}^2.$$

(iii) The projected mask $4^{-1}Pa$ must be equal to the unique best mask a^{best} given in (2.1), that is:

$$\left[-\frac{5}{192}, -\frac{1}{16}, -\frac{13}{192}, 0, \frac{15}{64}, \frac{9}{16}, \frac{55}{64}, \mathbf{1}, \frac{55}{64}, \frac{9}{16}, \frac{15}{64}, 0, -\frac{13}{192}, -\frac{1}{16}, -\frac{5}{192}\right].$$

Since $\hat{a}$ has the following factor

$$(1 + e^{-i\xi_1} + e^{-2i\xi_1} + e^{-3i\xi_1})(1 + e^{-i\xi_2} + e^{-2i\xi_2} + e^{-3i\xi_2}),$$

the mask a automatically satisfies sum rule of order 1 in (3.3). Consequently, the mask a satisfies the sum rules of order 2 in (3.4) because of the symmetric property of the mask a.

Since $\sum_{\beta \in \mathbb{Z}^2} a(\beta) = 16$, we must have $\sum_{\beta \in \mathbb{Z}^2} b(\beta) = C_1 + 6C_2 + 6C_3 + 6C_4 + 6C_5 + 12C_6 + 6C_7 + 12C_8 + 6C_9 = 1/4$.

For the equations of (3.5), by a simple calculation, we have the following linear independent equations:

$$3C_1 + 2C_2 + 2C_3 - 6C_4 + 2C_5 - 12C_6 + 18C_7 + 4C_8 + 2C_9 = 0;$$
$$C_1 + 2C_2 - 2C_3 - 2C_4 + 2C_5 - 4C_6 + 6C_7 + 4C_8 - 2C_9 = 0;$$
$$C_1 - 2C_2 + 6C_3 - 2C_3 - 2C_4 - 2C_5 - 4C_6 + 6C_7 - 4C_8 + 6C_9 = 0.$$

where $C_9 := -5/192 - 2C_7 - 2C_8$ by the condition of projection.

Once we have set up a system of these linear equations, by solving these equations via Maple, we see that there remain only 4 free parameters in the sequence b. Here, for instant, let's choose C_4, C_5, C_7 and C_8 to be free parameters. In addition to the conditions induced by interpolating in $(i)$and projection (ii), we can set up a system of linear equations. By solving them, we have:

$$\begin{aligned}
&C_1 = \frac{1}{192}(3t_1 - 6t_2 - 6t_3 - 6t_4 - 12), && C_2 = \frac{1}{192}(-t_1 + t_2 + 8),\\
&C_3 = \frac{1}{384}(-t_1 + 2t_2 + 6t_3 + 4t_4 + 18), && C_4 = \frac{t_1}{192},\\
&C_5 = \frac{t_2}{192}, && C_6 = \frac{1}{192}(-t_2 - t_3 - 1),\\
&C_7 = \frac{t_4}{192}, && C_8 = \frac{t_3}{192},\\
&C_9 = \frac{1}{192}(-1 - 2t_3 - 2t_4). &&
\end{aligned} \tag{3.6}$$

By now we have not completed the procedure of finding the best mask a, since there are still 4 free parameters. By finding out the corresponding subdivision stencils and forcing the weights of those vertices which are furthest away from the new inserted vertex to be zero, we may figure out some examples with the best mask a.

3.1.2 Computing the Quantity $\nu_\infty(a, 4I_2)$

Now we have the following result on interpolatory subdivision triplets $(a, 4I_2, D_6)$ with two-ring stencils for the regular triangular meshes.

Theorem 3.1. *Let $(a, 4I_2, D_6)$ be an interpolatory subdivision triplet, where the mask a is given by (3.1) and the sequence b is given in (3.2). Then*

$$\nu_\infty(a, 4I_2) = -\log_4 \max\{1/24, \rho(b, 4I_2, \infty, \delta)\}.$$

In particular, $\nu_\infty(a, 4I_2) = \log_4 24$ if and only if $\rho(b, 4I_2, \infty, \delta) \leqslant 1/24$. For example, in (3.6), if $t_1 = 10/3$, $t_2 = 0$, $t_3 = -5/3$ and $t_4 = 0$, then $\rho(b, 4I_2, \infty, \delta) \leqslant 1/24$ and $\nu_\infty(a, 4I_2) = \log_4 24$; therefore, the subdivision triplet is the smoothest two-dimensional interpolatory 4-adic subdivision scheme with two-ring stencils for the regular triangular mesh.

Proof. Our proof here follows the line developed in [19]. Since the mask a satisfies the sum rules of order 3, in order to calculate $\nu_\infty(a, 4I_2)$, we have to calculate

$$\rho(a, 4I_2, \infty, \nabla^\mu \delta) := \lim_{n\to\infty} \|\nabla^\mu \delta * [S^n_{a,4I_2}\delta]\|_{\ell_\infty(\mathbb{Z}^2)}, \tag{3.7}$$

where $\mu = (3,0), (2,1), (1,2), (0,3)$. Since the mask a is D_6-symmetric, the sequence $S^n_{a,4I_2}\delta$ is also D_6-symmetric and it is easy to see that

$$\rho(a, 4I_2, \infty, \nabla^3_{e_2}\delta) = \rho(a, 4I_2, \infty, \nabla^3_{e_1}\delta),$$

and

$$\rho(a, 4I_2, \infty, \nabla_{e_1}\nabla^2_{e_2}\delta) = \rho(a, 4I_2, \infty, \nabla^2_{e_1}\nabla_{e_2}\delta).$$

where $e_1 := (1,0)^T$ and $e_2 := (0,1)^T$ are unit vectors in two dimension.

So it suffices to calculate $\rho(a, 4I_2, \infty, \nabla^3_{e_1}\delta)$ and $\rho(a, 4I_2, \infty, \nabla^2_{e_1}\nabla_{e_2}\delta)$. Note that

$$\begin{aligned} \nabla_{e_1}\delta = \delta - \delta_{e_1} &= [\delta_{-e_2} - \delta_{e_1}] + [\delta - \delta_{-e_2}] \\ &= [\nabla_{e_1+e_2}\delta](\cdot + e_2) - [\nabla_{e_2}\delta](\cdot + e_2). \end{aligned} \tag{3.8}$$

For any $\beta \in \mathbb{Z}^s$, it is easy to see that $u(\cdot - \beta) * [S^n_{a,4I_2}\delta] = (u * [S^n_{a,4I_2}\delta])(\cdot - \beta)$. Therefore,

$$\rho(a, 4I_2, p, u(\cdot - \beta)) = \rho(a, 4I_2, p, u), \qquad \forall\, \beta \in \mathbb{Z}^s.$$

Consequently, by the definition of $\rho(a, 4I_2, \infty, \nabla^\mu\delta)$ in (3.7), it follows straightforward from (3.8) that

$$\begin{aligned}(3.9)\qquad &\rho(a, 4I_2, \infty, \nabla^3_{e_1}\delta)\\ &\qquad\leqslant \max\{\rho(a, 4I_2, \infty, \nabla^2_{e_1}\nabla_{e_1+e_2}\delta), \rho(a, 4I_2, \infty, \nabla^2_{e_1}\nabla_{e_2}\delta)\}.\end{aligned}$$

Let $E := \begin{bmatrix} 1 & -1 \\ 0 & -1 \end{bmatrix} \in D_6$. It is easy to check that

$$[\nabla^2_{e_1}\nabla_{e_2}\delta](E\cdot) = \nabla^2_{E^{-1}e_1}\nabla_{E^{-1}e_2}\delta = \nabla^2_{e_1}\nabla_{-e_1-e_2}\delta.$$

Since $[S^n_{a,4I_2}\delta](E\cdot) = S^n_{a,4I_2}\delta$ by $E \in D_6$, we must have

$$[(\nabla^2_{e_1}\nabla_{e_2}\delta) * (S^n_{a,4I_2}\delta)](E\cdot) = (\nabla^2_{e_1}\nabla_{-e_1-e_2}\delta) * (S^n_{a,4I_2}\delta).$$

Therefore, it follows that

$$\rho(a, 4I_2, \infty, \nabla^2_{e_1}\nabla_{e_2}\delta) = \rho(a, 4I_2, \infty, \nabla^2_{e_1}\nabla_{-e_1-e_2}\delta) = \rho(a, 4I_2, \infty, \nabla^2_{e_1}\nabla_{e_1+e_2}\delta).$$

Since $\nabla^{(2,1)}\delta = \nabla^2_{e_1}\nabla_{e_2}\delta$, in order to calculate $\rho(a, 4I_2, \infty, \nabla^\mu\delta)$ in (3.7), by (3.9) and the above identity, we see that it suffices to calculate the quantity $\rho(a, 4I_2, \infty, \nabla^2_{e_1}\nabla_{e_1+e_2}\delta)$. Note that

$$\begin{aligned}&\frac{\widehat{\nabla_{e_1}\nabla_{e_1+e_2}\delta}(4\xi_1, 4\xi_2)}{\widehat{\nabla_{e_1}\nabla_{e_1+e_2}\delta}(\xi_1, \xi_2)} = \frac{1-e^{-4i\xi_1}}{1-e^{-i\xi_1}}\,\frac{1-e^{-4i(\xi_1+\xi_2)}}{1-e^{-i(\xi_1+\xi_2)}}\\ &= (1+e^{-i\xi_1}+e^{-2i\xi_1}+e^{-3i\xi_1})(1+e^{-i(\xi_1+\xi_2)}+e^{-2i(\xi_1+\xi_2)}+e^{-3i(\xi_1+\xi_2)}).\end{aligned}$$

By Theorem 1.3, it follows from $\nabla^2_{e_1}\nabla_{e_1+e_2}\delta = [\nabla_{e_1}\delta] * [\nabla_{e_1}\nabla_{e_1+e_2}\delta]$ that

$$(3.10)\qquad \rho(a, 4I_2, \infty, \nabla^2_{e_1}\nabla_{e_1+e_2}\delta) = \rho(h, 4I_2, \infty, \nabla_{e_1}\delta),$$

where the sequence h is defined by

$$(3.11)\qquad \hat{h}(\xi_1, \xi_2) := (e^{-i\xi_2}+1+e^{i\xi_2}+e^{2i\xi_2})\hat{b}(\xi_1, \xi_2).$$

It is easy to check that h satisfies the sum rules of order 1. Define $\Gamma := [-1,2]^2 \cap \mathbb{Z}^2$. Then Γ is a complete set of representatives of the distinct cosets of the quotient group $\mathbb{Z}^2/4\mathbb{Z}^2$. Denote

$$K := \{(j,k) \in \mathbb{Z}^2 \ : \ |j| \leqslant 1, |k| \leqslant 2\} \tag{3.12}$$

and define the linear space U by

$$U := \Big\{ u \in \ell_0(\mathbb{Z}^2) \ : \ u(\beta) = 0 \quad \forall\, \beta \in \mathbb{Z}^s \backslash K \quad \text{and} \quad \sum_{\beta \in \mathbb{Z}^2} u(\beta) = 0 \Big\}. \tag{3.13}$$

Then it is easy to check that $[(\text{supp}h - \Gamma + K)/4] \cap \mathbb{Z}^2 \subseteq K$. Since h satisfies the sum rules of order 1, we see that $T_{h,\gamma} U \subseteq U$ for all $\gamma \in \Gamma$. Set

$$\begin{aligned} &\mathcal{A} := \{\delta_{(0,0)} - \delta_{(-1,0)}, \delta_{(1,0)} - \delta_{(0,0)}\}, \\ &\mathcal{B} := \{\delta_{(j,k+1)} - \delta_{(j,k)} \ : \ j = -1,0,1; k = -2,-1,0,1,2\}. \end{aligned} \tag{3.14}$$

Since $\hat{h}(\xi_1,\xi_2) = (e^{-i\xi_2} + 1 + e^{i\xi_2} + e^{2i\xi_2})\hat{b}(\xi_1,\xi_2)$, we see that $W := \text{span}\mathcal{B}$ is invariant under all the operators $T_{h,\gamma}, \gamma \in \Gamma$. Therefore, by [25], we have

$$\begin{aligned} &\rho_\infty(\{T_{h,\gamma}|_U \ : \gamma \in \Gamma\}) \\ &\qquad = \max\{\rho_\infty(\{T_{h,\gamma}|_W \ : \ \gamma \in \Gamma\}), \ \rho_\infty(\{T_{h,\gamma}|_{U/W} \ : \ \gamma \in \Gamma\})\}. \end{aligned}$$

Since all the elements in $\mathcal{B}$ take the form $[\nabla_{e_2}\delta](\cdot - \beta)$ for some $\beta \in \mathbb{Z}^2$, by Theorem 1.3, we have

$$\rho_\infty(\{T_{h,\gamma}|_W \ : \ \gamma \in \Gamma\}) = \rho_\infty(h, 4I_2, \infty, \nabla_{e_2}\delta) = \rho(b, 4I_2, \infty, \delta). \tag{3.15}$$

For any $u \in U$, we denote $[u]$ its equivalence class in U/W. The representation matrices of $T_{h,\gamma}|_{U/W}$, denoted by H_γ, under the basis $\{[u] \ : \ u \in \mathcal{A}\} =$

$\{[\delta_{(1,0)} - \delta_{(0,0)}], [\delta_{(0,0)} - \delta_{(-1,0)}]\}$, are given by

$$
\begin{aligned}
H_{(-1,2)} = H_{(-1,1)} = H_{(-1,0)} = H_{(-1,-1)} &= \frac{1}{192}\begin{bmatrix} -5 & 3 \\ 0 & 8 \end{bmatrix}, \\
H_{(0,2)} = H_{(0,1)} = H_{(0,0)} = H_{(0,-1)} &= \frac{1}{192}\begin{bmatrix} 3 & -5 \\ -5 & 3 \end{bmatrix}, \\
H_{(1,2)} = H_{(1,1)} = H_{(1,0)} = H_{(1,-1)} &= \frac{1}{192}\begin{bmatrix} 8 & 0 \\ -3 & -5 \end{bmatrix}, \\
H_{(2,2)} = H_{(2,1)} = H_{(2,0)} = H_{(2,-1)} &= \frac{1}{192}\begin{bmatrix} 8 & 0 \\ 8 & 0 \end{bmatrix}.
\end{aligned} \tag{3.16}
$$

By a simple calculation, we have

$$
\begin{aligned}
\rho_\infty(\{T_{h,\gamma}|_{U/W} \ : \ \gamma \in \Gamma\}) &= \rho_\infty(\{H_\gamma \ : \ \gamma \in \Gamma\}) \\
&\leqslant \max\{\|H_\gamma\|_{\ell_{1,\infty}} \ : \ \gamma \in \Gamma\} = 1/24,
\end{aligned} \tag{3.17}
$$

where $\|\cdot\|_{\ell_{1,\infty}}$ is a matrix norm which is defined to be

$$
\|(t_{ij})_{1\leqslant i\leqslant I, 1\leqslant j\leqslant J}\|_{\ell_{1,\infty}} := \max_{1\leqslant i\leqslant I} \sum_{j=1}^{J} |t_{ij}|.
$$

Since $\nabla_{e_1}\delta \in U$, by (3.15), we conclude that:

$$
\begin{aligned}
\max\{\rho(a, 4I_2, \infty, \nabla^\mu\delta) \ : \ |\mu| = 3\} &\leqslant \rho(h, 4I_2, \infty, \nabla_{e_1}\delta) \\
&\leqslant \rho_\infty(\{T_{h,\gamma}|_U \ : \ \gamma \in \Gamma\}) \\
&\leqslant \max\{1/24, \rho(b, 4I_2, \infty, \delta)\}.
\end{aligned}
$$

On the other hand, by (3.8), we have $\nabla_{e_1+e_2}\delta = \nabla_{e_2}\delta + [\nabla_{e_1}\delta](\cdot - e_2)$ and it is not difficult to see that

$$
\begin{aligned}
\rho(b, 4I_2, \infty, \delta) &= \rho(a, 4I_2, \infty, \nabla_{e_1}\nabla_{e_2}\nabla_{e_1+e_2}\delta) \\
&\leqslant \max\{\rho(a, 4I_2, \infty, \nabla_{e_1}^2\nabla_{e_2}\delta), \rho(a, 4I_2, \infty, \nabla_{e_1}\nabla_{e_2}^2\delta)\}.
\end{aligned}
$$

By Theorem 2.1, we conclude that

$$\max\{\rho(a, 4I_2, \infty, \nabla^\mu\delta) \ : \ |\mu| = 3\} = \max\{1/24, \rho(b, 4I_2, \infty, \delta)\}. \tag{3.18}$$

In the following, we estimate $\rho(b, 4I_2, \infty, \delta)$. By Theorem 1.4, we have

$$\begin{aligned}\rho(b, 4I_2, \infty, \delta) &\leqslant \max_{\alpha\in\mathbb{Z}^2} \sum_{\beta\in\mathbb{Z}^2} |b(\alpha + 4\beta)| \\ &= \frac{1}{192} \max\{|3t_1 - 6t_2 - 6t_3 - 6t_4 - 12| + 6|t_4|, \\ &\qquad |t_2| + 2|t_3| + |8 - t_1 + t_2|, \\ &\qquad |18 - t_1 + 2t_2 + 6t_3 + 4t_4| + |10 + 4t_3 + 4t_4|, \\ &\qquad |t_1| + |2 + 2t_2 + 2t_3|\}.\end{aligned}$$

It is easy to verify that, when $t_1 = 10/3,\ t_2 = 0,\ t_3 = -5/3$ and $t_4 = 0$, it follows from the above inequality that $\rho(b, 4I_2, \infty, \delta) \leqslant 1/24$. Therefore, the claim in this theorem follows directly from (3.18). □

Thus, we have figured out the smoothest 4-adic subdivision triplets such that the quantity $\nu_\infty(a, 4I_2)$ is equal to its upper bound $\log_4 24$. Consequently, with this best 4-adic subdivision triplets, we can generate the smoothest subdivision surfaces.

3.1.3 Interpolatory Subdivision Stencils for the Triangular Meshes

In this subsection, we shall give out our interpolatory 4-adic subdivision stencils, which have two-ring neighbourhoods, for the example given in Theorem 3.1. All the stencils shall be used in our C++ programs to generate the refined subdivision surfaces.

For 4-adic subdivision schemes on triangular meshes, we shall insert three new vertices on each edge, thus an edge will consequently be split into four

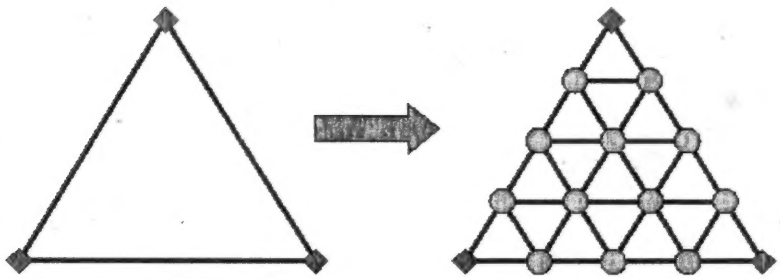

Figure 3.1: The interpolatory 4-adic subdivision scheme for the triangular mesh. By adding 3 new vertices on an edge and 3 new vertices for each face, one edge is split into 4 new edges and one face is split into 16 new faces. "◇" denotes the old vertices and "○" denotes the new inserted vertices.

new edges. Here, we denote "1/4 vertex", "1/2 vertex" and "3/4 vertex" the three new inserted vertices, respectively. Naturally, we need three subdivision stencils for these three new inserted vertices. However, by the property of symmetry, the stencil for "3/4 vertex" is a flip of that of "1/4 vertex". Therefore, we actually need only two stencils, one is for "1/4 vertex", another is for "1/2 vertex".

Similarly, we shall insert three new interior vertices inside a face, which can be regarded as the intersections of the connections between the corresponding new inserted vertices on three edges of a face. Consequently, a face will be split into 16 new faces. Although there are three new vertices, we need only one stencil in implementation because of the symmetry property.

The stencils of the subdivision triplets in Theorem 3.1 are given in Figure 3.2. The weights $u_1, \ldots, u_7$ in Figure 3.2 are given by

$$
\begin{aligned}
u_1 &= \frac{7}{12} - \frac{t_3}{96} - \frac{t_4}{96}, & u_2 &= \frac{59}{192} + \frac{t_3}{192} + \frac{t_4}{192}, \\
u_3 &= -\frac{1}{16} - \frac{t_3}{96} - \frac{t_4}{96}, & u_4 &= -\frac{1}{96} + \frac{t_3}{192} + \frac{t_4}{192}, \\
u_5 &= -\frac{1}{32}, & u_6 &= \frac{t_3}{192} + \frac{t_4}{192}, \\
u_7 &= -\frac{5}{192} - \frac{t_3}{192} - \frac{t_4}{192}.
\end{aligned}
\tag{3.19}
$$

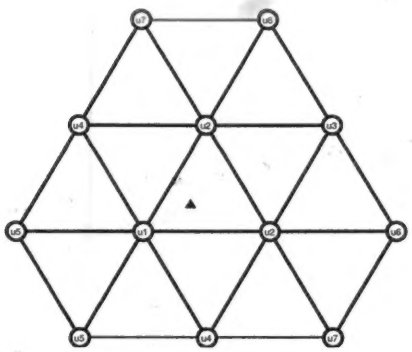

Figure 3.2: Associated subdivision stencils for the best two-dimensional interpolatory 4-adic subdivision scheme for the interior new inserted vertex. By the symbol "$\triangle$" we denote the new inserted vertex, and the symbol "$\bigcirc$" denotes vertex of the previous level, the numbers inside the circles, which are named $u1,\ u2,\ \ldots, u7$, are the weights of the corresponding vertices.

Moreover, if taking $t_1 = 10/3,\ t_2 = 0,\ t_3 = -5/3$ and $t_4 = 0$, we have

$$u_1 = 173/288, \qquad u_2 = 167/576, \qquad u_3 = -13/288,$$
$$u_4 = -11/576, \qquad u_7 = -10/576.$$

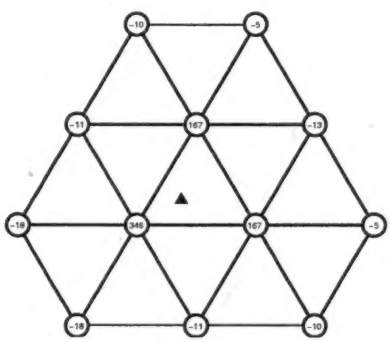

Figure 3.3: The interpolatory subdivision stencil for new inserted *interior vertex* inside a face, with $t_1 = 10/3,\ t_2 = 0,\ t_3 = -5/3$ and $t_4 = 0$. All the numbers in the above stencil should be divided by 576.

The corresponding stencil for the special case $t_1 = 10/3,\ t_2 = 0,\ t_3 =$

$-5/3$ and $t_4 = 0$ is shown in Figure 3.3.

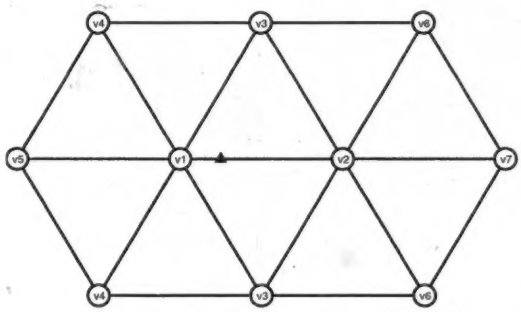

Figure 3.4: Associated subdivision stencils for "1/4 vertex" on an edge.

The followings are the weights of the associated interpolatory subdivision stencils for the new inserted "1/4 vertex" on an edge, which is shown in Figure 3.4:

$$
\begin{aligned}
v_1 &= 5/6 - t_4/64, \\
v_2 &= 35/192 + t_1/384 - t_2/192 - t_3/192 - t_4/192, \\
v_3 &= 5/64 - t_1/384 + t_2/192 + t_3/192 + t_4/96, \\
v_4 &= -5/96 + t_1/384 - t_2/192 - t_3/192 - t_4/192, \\
v_5 &= -1/64 - t_1/384 + t_2/192 + t_3/192 + t_4/192, \\
v_6 &= -5/192 - t_3/192, \\
v_7 &= t_4/192.
\end{aligned} \tag{3.20}
$$

Moreover, if $t_1 = 10/3,\ t_2 = 0,\ t_3 = -5/3$ and $t_4 = 0$, we have

$$
\begin{aligned}
&v_1 = 5/6, \qquad v_2 = 105/576, \qquad v_3 = 35/576, \qquad v_4 = -5/144, \\
&v_5 = -19/576, \qquad v_6 = -5/288, \qquad v_7 = 0.
\end{aligned}
$$

The corresponding stencil for above special case is shown in Figure 3.5.

Similarly, the following are the weights of the associated interpolatory subdivision stencils for the new inserted "1/2 vertex" on an edge, as shown in

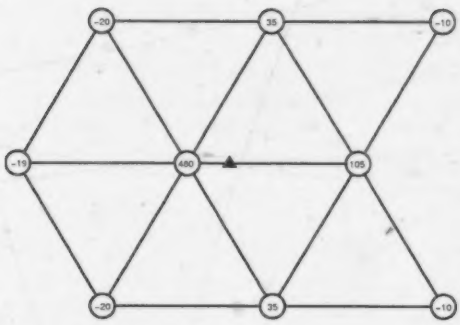

Figure 3.5: The interpolatory subdivision stencil for "1/4 vertex" on an edge, with $t_1 = 10/3,\ t_2 = 0,\ t_3 = -5/3$ and $t_4 = 0$. All the numbers in the above stencil should be divided by 576.

Figure 3.6:

$$
\begin{aligned}
w_1 &= \frac{1}{2} - \frac{t_2}{192} - \frac{t_3}{96} - \frac{t_4}{96}, \\
w_3 &= \frac{1}{8} + \frac{t_2}{96} + \frac{t_3}{48} + \frac{t_4}{48}, \\
w_4 &= -\frac{1}{16} - \frac{t_2}{192} - \frac{t_3}{96} - \frac{t_4}{96}, \\
w_5 &= \frac{t_2}{192} + \frac{t_3}{96} + \frac{t_4}{96}.
\end{aligned}
\tag{3.21}
$$

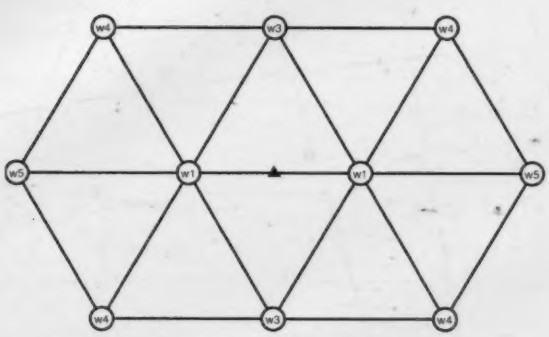

Figure 3.6: Associated subdivision stencil for "1/2 vertex" on an edge.

Moreover, if $t_1 = 10/3,\ t_2 = 0,\ t_3 = -5/3$ and $t_4 = 0$, we have

$$w_1 = \frac{149}{288}, \qquad w_3 = \frac{13}{144}, \qquad w_4 = -\frac{13}{288}, \qquad w_5 = -\frac{5}{288},$$

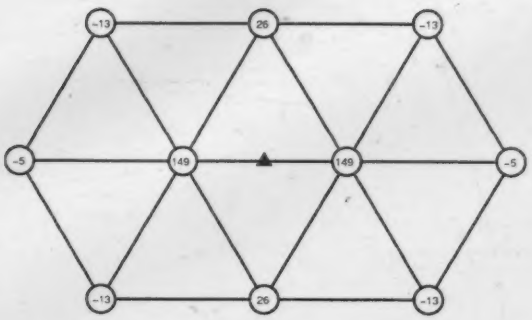

Figure 3.7: The interpolatory subdivision stencil for "1/2 vertex" on an edge, with $t_1 = 10/3,\ t_2 = 0,\ t_3 = -5/3$ and $t_4 = 0$. All the numbers in the above stencil should be divided by 288.

and the corresponding stencil is shown in Figure 3.7.

See Figure 3.8 for the graph of the basis function in the subdivision triplets in Theorem 3.1. Note that the support of the basis function is contained in $[-7/3, 7/3]^2$ while the basis function of the butterfly scheme is supported on $[-3, 3]^2$.

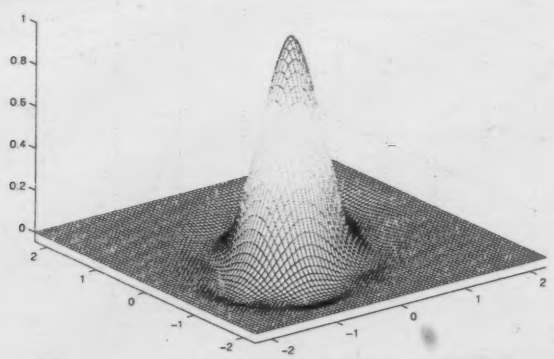

Figure 3.8: The graph of the basis function ϕ for the subdivision triplet in the Theorem 3.1 with $t_1 = 10/3,\ t_2 = 0,\ t_3 = -5/3$ and $t_4 = 0$.

We have implemented the stencils on the regular triangular mesh on com-

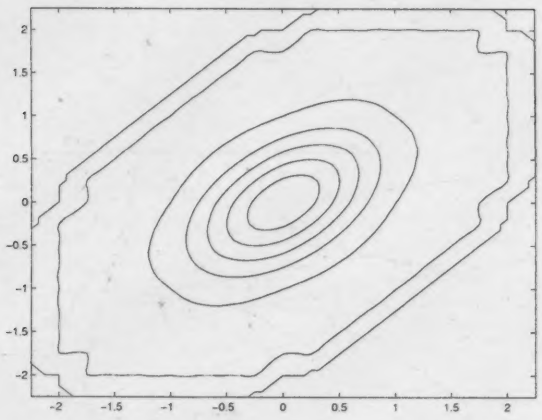

Figure 3.9: The graph of the contour value of the basis function ϕ for the subdivision triplet in the Theorem 3.1 with $t_1 = 10/3$, $t_2 = 0$, $t_3 = -5/3$ and $t_4 = 0$.

puter by C++ programs. The following figures are the initial mesh and refined meshes after one and two subdivision steps, respectively.

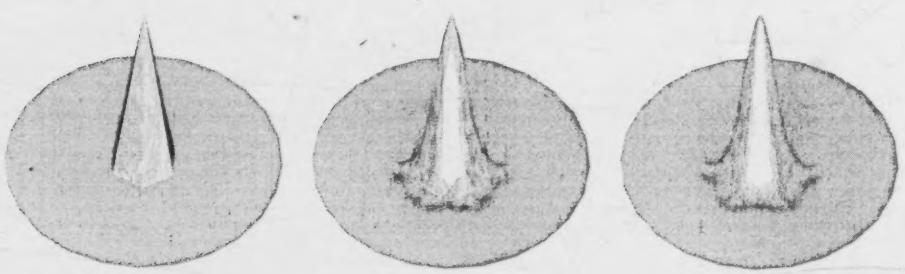

Figure 3.10: An example of subdivision surfaces by applying interpolatory 4-adic subdivision scheme on the regular triangular mesh. They are the initial mesh, the first step subdivision surface and the second step subdivision surface, respectively.

3.2 Subdivision Schemes for the Regular Quadrilateral Mesh

In this section, we shall investigate interpolatory 4-adic subdivision schemes with two-ring stencils for the regular quadrilateral mesh. By computing the quantity of $\nu_\infty(a, 4I_2)$ and finding out its upper bound, we shall figure out the best mask among all the possible subdivision schemes.

3.2.1 Masks of the Two-dimensional Interpolatory Four-adic Subdivision Schemes for the Quadrilateral Meshes

For quadrilateral meshes, we can use the tensor product of the one-dimensional interpolatory subdivision triplet $(a^{best}, 4, \{-1, 1\})$ to get an optimal two-dimensional interpolatory 4-adic subdivision scheme. In the following, let us present some other examples of subdivision triplets $(a, 4I_2, D_4)$ with better time localization of their basis functions for the quadrilateral meshes.

In order to facilitate our analysis, we require that the mask a should take the following form:

$$\begin{aligned}\hat{a}(\xi_1, \xi_2) =& (1 + e^{-i\xi_1} + e^{-2i\xi_1} + e^{-3i\xi_1})^2 \\ & \times (1 + e^{-i\xi_2} + e^{-2i\xi_2} + e^{-3i\xi_2})^2 e^{3i\xi_1} e^{3i\xi_2} \hat{b}(\xi_1, \xi_2).\end{aligned} \tag{3.22}$$

It is easy to check that the support of the product of first four terms on the right-hand side is $[-3, 3]^2$, thus the sequence b should be supported on $[-4, 4]^2$, and must be D_4-symmetric.

Since we are discussing a two-dimensional interpolatory four-adic subdivision schemes with two-ring stencils, the corresponding mask a must satisfy the same three conditions $(i), (ii), (iii)$ as for the symmetry group D_6, where

we discussed the analysis on the regular triangular mesh. In the same way, we can set up a system of linear equations. By solving these equations,we see that the sequence b, which is supported on $[-4,4]^2$ and is D_4-symmetric as well, must take the following form:

$$\frac{1}{768}\begin{bmatrix} t_{15} & t_{14} & t_{13} & t_{12} & t_{11} & t_{12} & t_{13} & t_{14} & t_{15} \\ t_{14} & t_{10} & t_9 & t_8 & t_7 & t_8 & t_9 & t_{10} & t_{14} \\ t_{13} & t_9 & t_6 & t_5 & t_4 & t_5 & t_6 & t_9 & t_{13} \\ t_{12} & t_8 & t_5 & t_3 & t_2 & t_3 & t_5 & t_8 & t_{12} \\ t_{11} & t_7 & t_4 & t_2 & t_1 & t_2 & t_4 & t_7 & t_{11} \\ t_{12} & t_8 & t_5 & t_3 & t_2 & t_3 & t_5 & t_8 & t_{12} \\ t_{13} & t_9 & t_6 & t_5 & t_4 & t_5 & t_6 & t_9 & t_{13} \\ t_{14} & t_{10} & t_9 & t_8 & t_7 & t_8 & t_9 & t_{10} & t_{14} \\ t_{15} & t_{14} & t_{13} & t_{12} & t_{11} & t_{12} & t_{13} & t_{14} & t_{15} \end{bmatrix}. \tag{3.23}$$

Since $\sum_{\beta\in\mathbb{Z}^2} a(\beta) = 16$, we must have $\sum_{\beta\in\mathbb{Z}^2} b(\beta) = t_1 + 4t_2 + 4t_3 + 4t_4 + 8t_5 + 4t_6 + 4t_7 + 8t_8 + 8t_9 + 4t_{10} + 4t_{11} + 8t_{12} + 8t_{13} + 8t_{14} + 4t_{15} = 1/16$.

Since $\hat{a}(\xi)$ has the following factors:

$$(1 + e^{-i\xi_1} + e^{-2i\xi_1} + e^{-3i\xi_1})^2 \times (1 + e^{-i\xi_2} + e^{-2i\xi_2} + e^{-3i\xi_2})^2,$$

the mask a automatically satisfies the sum rule of order 2. By the condition of the sum rules of order 3, we have:

$$\begin{aligned} 6t_1 + 4t_2 - 4t_3 + 4t_4 - 8t_5 - 4t_6 + 4t_7 - 8t_8 \\ - 8t_9 - 4t_{10} + 12t_{11} + 8t_12 + 8t_{13} + 8t_{14} + 12t_{15} = 0, \end{aligned}$$

and

$$4t_2 + 2t_1 + 8t_{12} + 8t_{14} + 8t_{15} - 8t_5 - 8t_6 + 4t_7 - 8t_9 + 8t_{11} = 0.$$

By solving the above equations, we see that $t_1,\ t_2,\ t_3,\ t_4,\ t_7,\ t_{11}$ are given by

(3.24)

$$
\begin{aligned}
t_1 &:= -4 - 8t_5 - 12t_6 - 16t_8 - 40t_9 - 32t_{10} - 24t_{12} - 56t_{13} - 88t_{14} - 60t_{15},\\
t_2 &:= 10 + 6t_5 + 8t_6 + 10t_8 + 24t_9 + 18t_{10} + 14t_{12} + 32t_{13} + 48t_{14} + 32t_{15},\\
t_3 &:= -4t_5 - 4t_6 - 6t_8 - 12t_9 - 9t_{10} - 8t_{12} - 16t_{13} - 24t_{14} - 16t_{15},\\
t_4 &:= 6 - 2t_5 - 2t_6 - 2t_9 - 2t_{13},\\
t_7 &:= -2 - 2t_8 - 2t_9 - 2t_{10} - 2t_{14},\\
t_{11} &:= -5 - 2t_{12} - 2t_{13} - 2t_{14} - 2t_{15},
\end{aligned}
$$

where $t_5,\ t_6,\ t_8,\ t_9,\ t_{10},\ t_{12},\ t_{13},\ t_{14},\ t_{15}$ are chosen as free parameters.

3.2.2 Computing the Smoothness $\nu_\infty(a,\ 4I_2)$

Now we have the following result on interpolatory subdivision triplets $(a, 4I_2, D_4)$ with two-ring stencils for the regular quadrilateral meshes.

Theorem 3.2. *Let $(a, 4I_2, D_4)$ be an interpolatory subdivision triplet, where the mask a is given by* (3.22) *and the sequence b is given in* (3.23). *Then*

$$\nu_\infty(a, 4I_2) = -\log_4 \max\{1/24, \rho(b, 4I_2, \infty, \delta)\}.$$

In particular, $\nu_\infty(a, 4I_2) = \log_4 24$ if and only if $\rho(b, 4I_2, \infty, \delta) \leqslant 1/24$. For example, if $-2 < t_5 < 2$ and $t_6 = t_8 = t_9 = t_{10} = t_{12} = t_{13} = t_{14} = t_{15} = 0$, then $\rho(b, 4I_2, \infty, \delta) \leqslant 1/24$ and $\nu_\infty(a, 4I_2) = \log_4 24$; therefore, the subdivision triplet is the smoothest two-dimensional interpolatory ternary subdivision scheme with two-ring stencils for the regular quadrilateral mesh.

Proof. By symmetry on the mask a, it suffices to compute $\rho(a, 4I_2, \infty, \nabla_{e_1}^3\delta)$ and $\rho(a, 4I_2, \infty, \nabla_{e_1}^2\nabla_{e_2}\delta)$. Note that

$$\frac{\widehat{\nabla_{e_1}^2\delta}(4\xi_1, 4\xi_2)}{\widehat{\nabla_{e_1}^2\delta}(\xi_1, \xi_2)} = \frac{(1 - e^{-4i\xi_1})^2}{(1 - e^{-i\xi_1})^2} = (1 + e^{-i\xi_1} + e^{-2i\xi_1} + e^{-3i\xi_1})^2.$$

By Theorem 1.3, we see that

$$\rho(a, 4I_2, \infty, \nabla_{e_1}^3 \delta) = \rho(h, 4I_2, \infty, \nabla_{e_1} \delta)$$

and

$$\rho(a, 4I_2, \infty, \nabla_{e_1}^2 \nabla_{e_2} \delta) = \rho(h, 4I_2, \infty, \nabla_{e_2} \delta),$$

where

$$\hat{h}(\xi_1, \xi_2) := e^{-3i\xi}(1 + e^{-i\xi_2} + e^{-2i\xi_2} + e^{-3i\xi_2})^2 \hat{b}(\xi_1, \xi_2). \tag{3.25}$$

It is easy to verify that h satisfies the sum rules of order 1. Denote $\Gamma := [-1, 2]^2 \cap \mathbb{Z}^2$. Let K and U be defined in (3.12) and (3.13), respectively. Since h satisfies the sum rules of order 1, we have $T_{h,\gamma} U \subseteq U$ for all $\gamma \in \Gamma$. Set

$$\begin{aligned} \mathcal{A} &:= \{\delta_{(0,0)} - \delta_{(-1,0)}, \delta_{(1,0)} - \delta_{(0,0)}\}, \\ \mathcal{B} &:= \{\delta_{(-1,1)} - \delta_{(-1,0)}, \delta_{(0,1)} - \delta_{(0,0)}, \delta_{(1,1)} - \delta_{(1,0)}\}, \\ \mathcal{C} &:= \{\delta_{(j,k+2)} - 2\delta_{(j,k+1)} + \delta_{(j,k)} \ : \ j = -1, 0, 1; k = -2, -1, 0\}. \end{aligned} \tag{3.26}$$

Define $W := \text{span}(\mathcal{B} \cup \mathcal{C})$ and $V := \text{span}\mathcal{C}$. Since $\hat{h}(\xi_1, \xi_2) = (1 + e^{-i\xi_2} + e^{-2i\xi_2} + e^{-3i\xi_2})(1 + e^{i\xi_2} + e^{2i\xi_2} + e^{3i\xi_2})\hat{b}(\xi_1, \xi_2)$, we see that $T_{h,\gamma} W \subseteq W$ and $T_{h,\gamma} V \subseteq V$ for all $\gamma \in \Gamma$.

For any $u \in U$, we denote $[u]$ its equivalence class in U/W. The representation matrices of $T_{h,\gamma}|_{U/W}$, denoted by H_γ, under the basis $\{[u] \ : \ u \in \mathcal{A}\}$, are given in (3.16). Therefore, by what has been proved, (3.17) holds.

For any $u \in W$, we denote $[u]$ its equivalence class in W/V. The representation matrices of $T_{h,\gamma}|_{W/V}$, denoted by $H_{2,\gamma}$, under the basis $\{[u] \ : \ u \in \mathcal{B}\}$, are given by

$$H_{2,(-1,2)} \doteq H_{2,(-1,1)} = H_{2,(-1,0)} = H_{2,(-1,-1)} = \frac{1}{76032} \cdot \begin{bmatrix} -495 & 2178 & -495 \\ 0 & 1386 & -198 \\ 0 & 594 & 594 \end{bmatrix},$$

$$H_{2,(0,2)} = H_{2,(0,1)} = H_{2,(0,0)} = H_{2,(0,-1)} = \frac{1}{76032}\begin{bmatrix} -198 & 1386 & 0 \\ -495 & 2178 & -495 \\ 0 & 1386 & -198 \end{bmatrix},$$

and

$$H_{2,(1,2)} = H_{2,(1,1)} = H_{2,(1,0)} = H_{2,(1,-1)} = \frac{1}{76032}\begin{bmatrix} 594 & 594 & 0 \\ -198 & 1386 & 0 \\ -495 & 2178 & -495 \end{bmatrix}.$$

Therefore, we have

$$\begin{aligned} \rho_\infty(\{T_{h,\gamma}|_{W/V} \,:\, \gamma \in \Gamma) &= \rho_\infty(\{H_{2,\gamma} \,:\, \gamma \in \Gamma\}) \\ &\leqslant \max\{\|H_{2,\gamma}\|_{\ell_{1,\infty}} \,:\, \gamma \in \Gamma\} = 1/24. \end{aligned} \tag{3.27}$$

Note that every element in $\mathcal{C}$ takes the form $\nabla^2_{e_2}\delta(\cdot - \beta)$ for some $\beta \in \mathbb{Z}^2$, by Theorem 1.3, we have

$$\rho_\infty(\{T_{h,\gamma}|_{\mathcal{C}} \,:\, \gamma \in \Gamma\}) = \rho(h, 4I_2, \infty, \nabla^2_{e_2}\delta) = \rho(b, 4I_2, \infty, \delta). \tag{3.28}$$

Now by Theorem 1.4, we have

$$\begin{aligned} \rho(b, 4I_2, \infty, \delta) &\leqslant \max_{\alpha\in\mathbb{Z}^2} \sum_{\beta\in\mathbb{Z}^2} |b(\alpha + 4\beta)| \\ &\leqslant \frac{1}{768}\max\{|4 + 8t_5 + 12t_6 + 16t_8 + 40t_9 + 32t_{10} + 24t_{12} + 56t_{13} + 88t_{14} + 60t_{15}| \\ &\qquad + 4|5 + 2t_{12} + 2t_{13} + 2t_{14} + 2t_{15}| + 4|t_{15}|, \\ &\qquad |10 + 6t_5 + 8t_6 + 10t_8 + 24t_9 + 18t_{10} + 14t_{12} + 32t_{13} + 48t_{14} + 32t_{15}| \\ &\qquad + 2|1 + t_8 + t_9 + t_{10} + t_{14}| + 2|t_{12}| + 2|t_{14}|, \\ &\qquad |4t_5 + 4t_6 + 6t_8 + 12t_9 + 9t_{10} - 8t_{12} + 16t_{13} + 24t_{14} + 16t_{15}| \\ &\qquad + 2|t_8| + |t_{10}|\}, \end{aligned}$$

where $t_j, j = 6,\ 8,\ 9,\ 10,\ 12,\ 13,\ 14,\ 15$ are defined in (3.23). When $t_6 = t_8 = t_9 = t_{10} = t_{12} = t_{13} = t_{14} = t_{15} = 0$, the above inequality becomes

$$\rho(b, 4I_2, \infty, \delta) \leqslant \frac{1}{768}\max\{20 + 4|1 + 2t_5|, 2 + |10 + 6t_5|, 4|t_5|\}.$$

It follows easily from the above inequality that if $-2 < t_5 < 2$, then $\rho(b, 4I_2, \infty, \delta) \leqslant 1/24$. Moreover, if $t_5 = -1/384$ we have $\rho(b, 4I_2, \infty, \delta) = 1/24$. Since the elements in $\mathcal{A}$ take the form $\nabla_{e_1}\delta(\cdot - \beta)$ and the elements in $\mathcal{B}$ take the form $\nabla_{e_2}\delta(\cdot - \beta)$, by (3.17) and (3.28), we see that

$$\begin{aligned}
&\max\{\rho(a, 4I_2, \infty, \nabla_{e_1}^3\delta), \rho(a, 4I_2, \infty, \nabla_{e_1}^2\nabla_{e_2}\delta)\} \\
&\quad = \max\{\rho(h, 4I_2, \infty, \nabla_{e_1}\delta), \rho(h, 4I_2, \infty, \nabla_{e_2}\delta)\} \\
&\quad = \rho_\infty(\{T_{h,\gamma}|_U \ : \ \gamma \in \Gamma\}) \\
&\quad = \max\{1/24, \rho(b, 4I_2, \infty, \delta)\},
\end{aligned}$$

which completes the proof. □

Therefore, for the quadrilateral meshes, we can also figure out the optimal subdivision triplets $(a, 4I_2, D_4)$ such that the quantity $\nu_\infty(a,\ 4I_2)$ achieves its upper bound $\log_4 24$.

3.2.3 Subdivision Stencils for the Quadrilateral Meshes

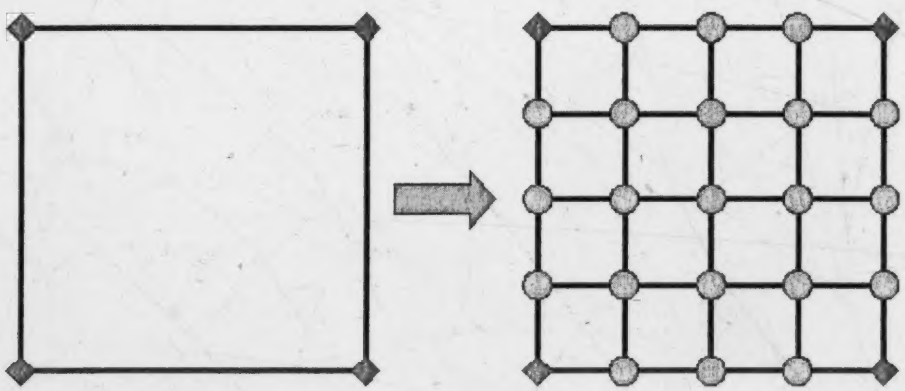

Figure 3.11: The interpolatory 4-adic subdivision scheme for the quadrilateral mesh. By adding 3 new vertices on an edge and 4 new vertices for each face, one edge is split into 4 new edges and one face is split into 16 new faces. "◇" denotes the old vertices and "○" denotes the new inserted vertices.

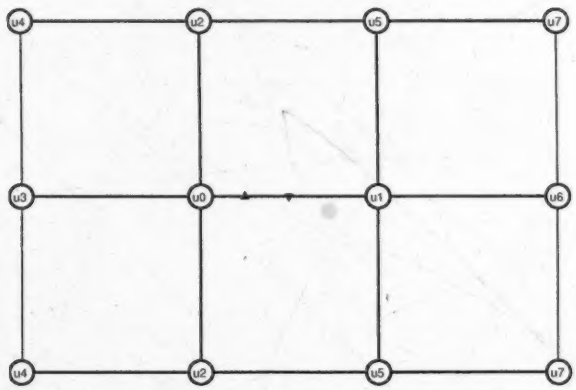

Figure 3.12: Associated subdivision stencils for new inserted vertices on an edge. Up triangle denote the "1/4 vertex" and down triangle denotes the "1/2 vertex".

For 4-adic subdivision schemes on the quadrilateral meshes, we shall insert three new vertices on each edge, thus an edge will be split into four new edges. According to the property of symmetry, we need only two stencils in programming implementation, one is for "1/4 vertex", another is for "1/2 vertex". The stencil for "3/4 vertex" is the flip of that of "1/4 vertex". Similarly, although we shall insert nine new interior vertices inside a face, we need only three stencils because of the symmetric property. Consequently, a face will be split into 16 new faces. The stencils of the subdivision triplets for all new inserted vertices in Theorem 3.2 are shown in Figure 3.12 and Figure 3.13. Here we use the general parameters $u_0, \ldots, u_7$; and $v_0, \ldots, v_{14}$ in Figure 3.12 and Figure 3.13, because for different new inserted vertex, the value of $u_0, \ldots, u_7$; and $v_0, \ldots, v_{14}$ in the stencils are different, we shall discuss them in details in the following.

For the new inserted "1/4 vertex", the parameters $u_0, \ldots, u_7$ in Figure 3.12

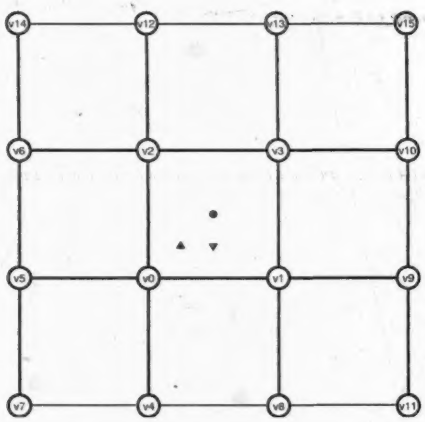

Figure 3.13: Associated subdivision stencils for new inserted interior vertices inside a face. The upper triangle symbol denotes the "(1/4, 1/4) vertex", down triangle symbol denotes the "(1/2, 1/4) vertex" and small circle symbol denotes the "(1/2, 1/2) vertex".

are given by

(3.29)

$$u_0 := 55/64 + 4t_5 + 8t_6 + 8t_8 + 28t_9 + 24t_{10} + 10t_{12} + 36t_{13} + 62t_{14} + 40t_{15},$$

$$u_1 := 15/64 - 2t_5 - 4t_6 - 4t_8 - 14t_9 - 12t_{10} - 2t_{12} - 12t_{13} - 22t_{14} - 8t_{15},$$

$$u_2 := -2t_5 - 4t_6 - 4t_8 - 14t_9 - 12t_{10} - 5t_{12} - 18t_{13} - 31t_{14} - 20t_{15},$$

$$u_3 := -13/192 - 2t_5 - 4t_6 - 4t_8 - 14t_9 - 12t_{10} - 6t_{12} - 20t_{13} - 34t_{14} - 24t_{15},$$

$$u_4 := t_5 + 2t_6 + 2t_8 + 7t_9 + 6t_{10} + 3t_{12} + 10t_{13} + 17t_{14} + 12t_{15},$$

$$u_5 := t_5 + 2t_6 + 2t_8 + 7t_9 + 6t_{10} + t_{12} + 6t_{13} + 11t_{14} + 4t_{15},$$

$$u_6 := -5/192 - 2t_{12} - 4t_{13} - 6t_{14} - 8t_{15},$$

$$u_7 = -t_{12} + 2t_{13} + 3t_{14} + 4t_{15},$$

and for the new inserted "1/2 vertex", the parameters $u_0, \ldots, u_7$ in Figure 3.12

are given by

$$
\begin{aligned}
&u_0 := 9/16 + 2t_8 + 4t_9 + 6t_{10} + 4t_{12} + 8t_{13} + 20t_{14} + 16t_{15} := u_1,\\
&u_2 := -t_8 - 2t_9 - 3t_{10} - 2t_{12} - 4t_{13} - 10t_{14} - 8t_{15} := u_5,\\
&u_3 := -1/16 - 2t_8 - 4t_9 - 6t_{10} - 4t_{12} - 8t_{13} - 20t_{14} - 16t_{15} := u_6,\\
&u_4 := t_8 + 2t_9 + 3t_{10} + 2t_{12} + 4t_{13} + 10t_{14} + 8t_{15} := u_7.
\end{aligned}
\tag{3.30}
$$

For the new inserted interior "(1/2, 1/2) vertex", the parameters $v_0, \ldots, v_{15}$ in Figure 3.13 are given by

$$
\begin{aligned}
&v_0 := v_1 := v_2 := v_3 := 5/16 + t_{10} + 4t_{14} + 4t_{15},\\
&v_4 := v_5 := v_6 := v_8 := v_9 := v_{10}\\
&\qquad\qquad := v_{12} := v_{13} := -1/32 - t_{10} - 4t_{14} - 4t_{15},\\
&v_7 := v_{11} := v_{14} := v_{15} := t_{10} + 4t_{14} + 4t_{15}.
\end{aligned}
\tag{3.31}
$$

For the new inserted interior "(1/4, 1/4) vertex", the parameters $v_0, \ldots, v_{14}$ in Figure 3.13 are given by

$$
\begin{aligned}
&v_0 := 93/192 + 4t_6 + 16t_9 + 16t_{10} + 20t_{13} + 40t_{14} + 25t_{15},\\
&v_1 := v_2 := 13/64 - 2t_6 - 8t_9 - 8t_{10} - 7t_{13} - 14t_{14} - 5t_{15},\\
&v_3 := 7/128 + t_6 + 4t_9 + 4t_{10} + 2t_{13} + 4t_{14} + t_{15},\\
&v_4 := v_5 := -13/256 - 2t_6 - 8t_9 - 8t_{10} - 11t_{13} - 22t_{14} - 15t_{15},\\
&v_6 := v_8 := -13/768 + t_6 + 4t_9 + 4t_{10} + 4t_{13} + 8t_{14} + 3t_{15},\\
&v_7 := t_6 + 4t_9 + 4t_{10} + 6t_{13} + 12t_{14} + 9t_{15},\\
&v_9 := v_{12} := -5/256 - 2t_{13} - 4t_{14} - 5t_{15},\\
&v_{10} := v_{13} := -5/768 + t_{13} + 2t_{14} + t_{15},\\
&v_{14} := v_{11} := t_{13} + 2t_{14} + 3t_{15}, \qquad v_{15} := t_{15}.
\end{aligned}
\tag{3.32}
$$

For the new inserted interior "(1/2, 1/4) vertex", the parameters $v_0, \ldots, v_{15}$

in Figure 3.13 are given by

$$
\begin{aligned}
&v_0 := v_1 := 61/128 + 2t_9 + 4t_{10} + 4t_{13} + 13t_{14} + 10t_{15},\\
&v_2 := v_3 := 17/128 - t_9 - 2t_{10} - 2t_{13} - 5t_{14} - 2t_{15},\\
&v_4 := v_8 := -13/384 - t_9 - 2t_{10} - 2t_{13} - 7t_{14} - 6t_{15},\\
&v_5 := v_9 := -3/64 - 2t_9 - 4t_{10} - 4t_{13} - 13t_{14} - 10t_{15},\\
&v_6 := v_{10} := -1/64 + t_9 + 2t_{10} + 2t_{13} + 5t_{14} + 2t_{15},\\
&v_7 := v_{11} := t_9 + 2t_{10} + 2t_{13} + 7t_{14} + 6t_{15},\\
&v_{12} := v_{13} := -5/384 - t_{14} - 2t_{15}, \qquad v_{14} := v_{15} := t_{14} + t_{15}.
\end{aligned}
\tag{3.33}
$$

When $t_6 = t_8 = t_9 = t_{10} = t_{12} = t_{13} = t_{14} = t_{15} = 0$ and $t_5 = -1/384$, the parameters of all the stencils should be pretty simple, we shall show the details as follows.

The parameters in (3.29) become (all divided by 384), as shown in Figure 3.14.

$$
\begin{aligned}
&u_0 = 326,\ u_1 = 92,\ u_2 = 2,\ u_3 = -24,\\
&u_4 = -1,\ u_5 = -1,\ u_6 = -10,\ u_7 = 0.
\end{aligned}
\tag{3.34}
$$

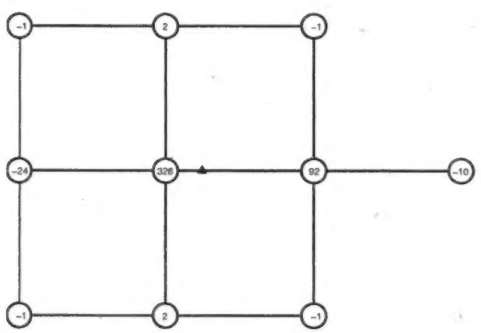

Figure 3.14: Associated subdivision stencils for new inserted vertices on an edge at the "1/4 vertex". All the numbers in the above stencil should be divided by 384.

The parameters in (3.30) become

$$u_0 = u_1 = 9/16,\ u_3 = u_6 = -1/16,\ u_2 = u_4 = u_5 = u_7 = 0. \tag{3.35}$$

We can find that the corresponding stencil (shown in Figure 3.15) is the same as the well-known "4-point" subdivision scheme.

Figure 3.15: Associated subdivision stencils for new inserted vertices on an edge at the "1/2 vertex". This coincides with the stencil of the univariate 4-point interpolatory scheme.

The parameters in (3.31) become

$$\begin{aligned} &v_0 := v_1 := v_2 := v_3 := 5/16, \\ &v_4 := v_5 := v_6 := v_8 := v_9 := v_{10} := v_{12} := v_{13} := -1/32, \\ &v_7 := v_{11} := v_{14} := v_{15} := 0. \end{aligned} \tag{3.36}$$

The corresponding stencil is shown in Figure 3.16.

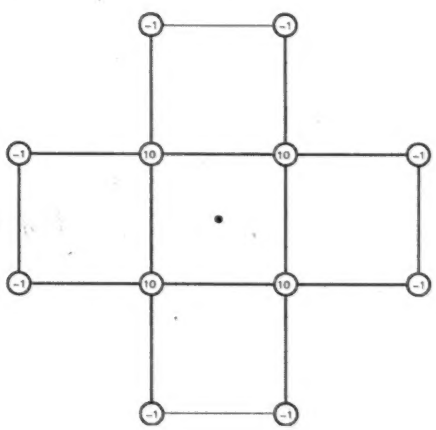

Figure 3.16: Associated subdivision stencils for new inserted vertices interior of a face at the "(1/2, 1/2) vertex". All the numbers in the above stencils should be divided by 32.

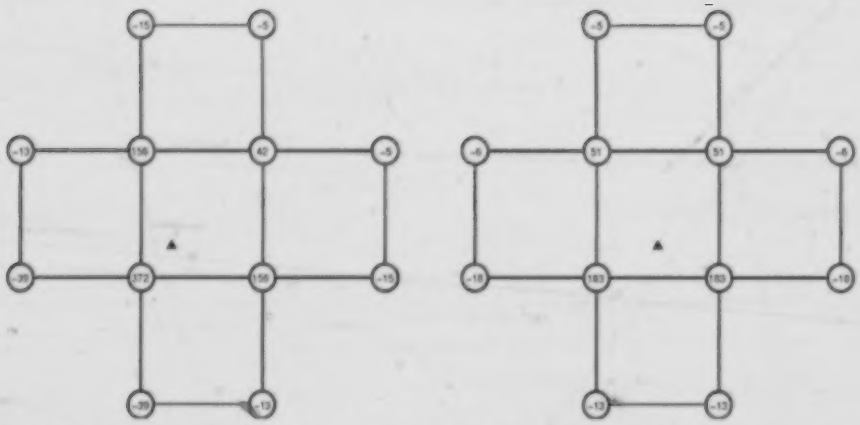

Figure 3.17: Associated subdivision stencils for new inserted vertices interior of a face at the "(1/4, 1/4) vertex" and at "(1/2, 1/4) vertex". All the weights are divided by 768.

The parameters in (3.32) become

$$
\begin{aligned}
&v_0 = 93/192,\ v_1 = v_2 = 13/64,\\
&v_3 = 7/128,\ v_4 = v_5 = -13/256,\\
&v_6 = v_8 = -13/768,\ v_7 = v_{11} = v_{13} = v_{14} = 0,\\
&v_9 = v_{12} = -5/256,\ v_{10} = v_{13} = -5/768.
\end{aligned}
\tag{3.37}
$$

The corresponding stencil is shown in Figure 3.17.

The parameters in (3.33) become

$$
\begin{aligned}
&v_0 = v_1 = 61/128,\ v_2 = v_3 = 17/128,\ v_4 = v_8 = -13/384,\\
&v_5 = v_9 = -3/64,\ \ v_6 = v_{10} = -1/64,\\
&v_7 = v_{11} = v_{14} = v_{14} = 0, v_{12} = v_{13} = -5/384.
\end{aligned}
\tag{3.38}
$$

The corresponding stencil is shown in Figure 3.17.

See Figure 3.18 for the graph of the basis function in the subdivision triplets in Theorem 3.2 with $t_6 = t_8 = t_9 = t_{10} = t_{12} = t_{13} = t_{14} = t_{15} = 0$, Figure 3.19 for the contour of the basis function ϕ for the subdivision triplet in Theorem 3.2, when $t_6 = t_8 = t_9 = t_{10} = t_{12} = t_{13} = t_{14} = t_{15} = 0$.

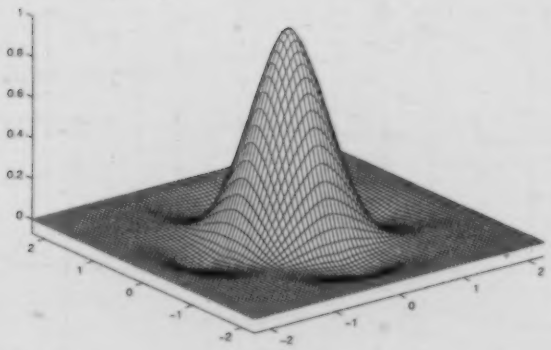

Figure 3.18: The graph of the basis function ϕ for the subdivision triplet in Theorem 3.2, when $t_6 = t_8 = t_9 = t_{10} = t_{12} = t_{13} = t_{14} = t_{15} = 0$ and $t_5 = -1/384$.

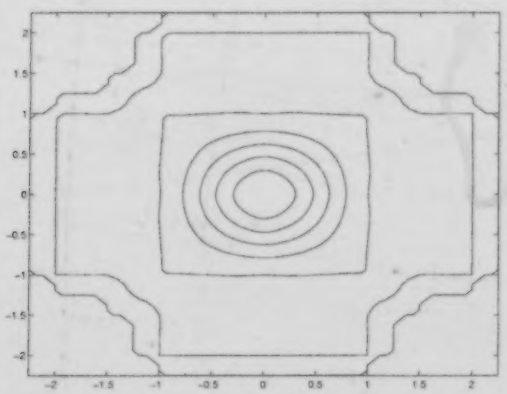

Figure 3.19: The graph of the contour of the basis function ϕ for the subdivision triplet in Theorem 3.2, when $t_6 = t_8 = t_9 = t_{10} = t_{12} = t_{13} = t_{14} = t_{15} = 0$ and $t_5 = -1/384$.

Chapter 4

Smoothness Analysis at Extraordinary Vertices

In this chapter, we shall first review the background techniques discussed and developed in [30, 32, 34]. Then we shall apply the analysis to design special subdivision rules at extraordinary vertices for the ternary subdivision schemes given in [19]. Similar analysis and design can be applied to our 4-adic subdivision schemes in Chapter 3. For simplicity, in this chapter, we shall mainly discuss the special ternary subdivision rules for $k = 3$ and $k = 4$, and special 4-adic subdivision rules for $k = 3$. We shall leave other cases as a future problem.

4.1 Subdivision Matrix and Characteristic Map

So far as we know in CAGD for one dimensional case, once a subdivision triplet is given, all the stencils of the subdivision rules that are needed to generate a curve are completely determined. The structure of the control polygon for curves is always very simple: the vertices are arranged into a

chain, and any two pieces of the chain of the same length always have identical structure. However, the situation is radically different and much more complex for surfaces, since for two-dimensional meshes, the local structure of the mesh may vary. For example, the number of edges emanating from a vertex may be different from vertex to vertex. As a result the rules derived from the a subdivision scheme for a regular mesh may be applied only to parts of the mesh that are locally regular. For regular vertices, we have set up a theory to analyze the smoothness of subdivision surfaces, but we cannot apply the same analysis on extraordinary vertices. The main methods we use are subdivision matrix and its eigenvalues and the associated characteristic map, as developed in [30, 32, 34] and explained in [1].

It is evident that for any arbitrary initial mesh, the number of extraordinary vertices remain the same at every subdivision step. Moreover, for a scheme with 2-ring subdivision stencils, extraordinary vertices will be isolated after the first subdivision step. Here "isolated" means that there is at most one extraordinary vertex within its 2-ring neighbors. Additional special subdivision rules are needed for extraordinary vertices with some desired properties, such as good smoothness and small stencils. Note that these special rules can only influence local behavior of the surface near extraordinary vertices.

4.1.1 Parameterization of Subdivision Surfaces

Definition 4.1. When computing a new inserted vertex, all the neighbouring vertices associated with *mask a* are called *control points* p_i^j, $(i = 0, \ldots, km(m+1)/2)$ at subdivision level j, where k is the valence of the extraordinary vertex, and m is the dilation factor of subdivision scheme.

The subdivision processing produces a sequence of meshes with increasing numbers of faces and vertices. In this thesis we study the relatively simple case: suppose the initial mesh is a simple polyhedron, i.e., it does not have self-

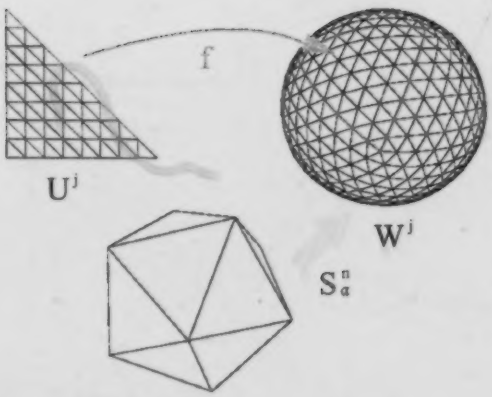

Figure 4.1: Parameterization of the subdivision surface (see [1]).

intersections. Intuitively, the subdivision surface is the limit of this sequence. For the purpose of analysis, it is convenient to represent subdivision surfaces as functions defined on some parametric domain with values in $\mathbb{R}^3$. Thus we can treat subdivision surfaces as functions from the planar plane $\mathbb{R}^2$ to the $\mathbb{R}^3$ space $f : U^j \mapsto W^j$, where U^j denotes the planar plane domain and W^j denotes the $\mathbb{R}^3$ domain. U^j is also called topology of the corresponding subdivision surface parts, the points with topology are called control points. We define this procedure the parameterization of subdivision surfaces.

Suppose each time we apply the subdivision scheme to surfaces to compute the finer control mesh, we also apply the same subdivision scheme to the topology of the polyhedron. Intuitively, the control points, edges and faces on U^j have one to one correspondence to vertices, edges and faces on W^j .

Definition 4.2. A surface $f : U^j \mapsto W^j$ is tangent plane continuous at $x \in U^j$ if and only if surface normals are defined in a neighborhood around x and there exists a limit of normals at x, where $U^j \in \mathbb{R}^2$ and $W^j \in \mathbb{R}^3$.

This is a useful definition, since it is easier to show the tangent plane continuity (all that is required is to show the existence of a limit). Additionally the definition is very intuitive since it captures the notion that a surface is

smooth if there exists a tangent plane. Tangent plane continuity, however, is actually weaker than C^1-continuity [1].

4.1.2 Subdivision Matrix and Eigenvalue Analysis

Consider an extraordinary vertex B, after sufficient number of subdivision steps, we will get a 1-neighborhood U^j of B, such that all control points defining $f(U^j)$ are regular, except B itself. For example, we need only one subdivision step for ternary or higher dilation subdivision schemes. This demonstrates that it is sufficient to determine if the scheme generates C^1-continuous surfaces for a very specific type of domains K: triangulations of the plane which have a single extraordinary vertex in their center, surrounded by regular vertices. We can assume all triangles of these triangulations to be identical and call such triangulations k-regular.

Let $\mathbf{p}^j$ be the vector at subdivision level j of the control points $p_i^j, i = 1, \ldots, km(m+1)/2$, corresponding to an extraordinary vertex B. Note that U^j and U^{j+1} are similar: thus we can establish a one-to-one correspondence between the vertices simply by shrinking U^j by a factor of m (for ternary subdivision schemes $m = 3$). Enumerate the vertices in the rings; there is total of $km(m+1)/2$ vertices, plus the extraordinary vertex in the center.

By definition of the control set, we can compute all values p_i^{j+1} in the set $\mathbf{p}^{j+1}$ from the values p_i^j in the set $\mathbf{p}^j$. Since we only consider subdivision which computes finer levels by linear combination of points from the coarser level, we see that the subdivision matrix S is given by:

$$\begin{bmatrix} p_0^{j+1} \\ p_1^{j+1} \\ \cdots \\ p_{N-1}^{j+1} \\ p_N^{j+1} \end{bmatrix} = S \begin{bmatrix} p_0^j \\ p_1^j \\ \cdots \\ p_{N-1}^j \\ p_N^{j+1} \end{bmatrix}$$

where $N = km(m+1)/2+1$ is the number of control points, S is the subdivision matrix and is a $N \times N$ matrix. Each component p_i^j of $\mathbf{p}^j$ is a point in the three-dimensional space. Since we consider only stationary schemes, the subdivision matrix S will be the same at all levels.

We can now rewrite each of the coordinate vectors in terms of the eigenvectors of the matrix S. Thus,

$$\mathbf{p}^0 = \sum_i a_i x_i$$

and

$$\mathbf{p}^j = (S)^j \mathbf{p}^0 = \sum_i a_i \lambda_i^j x_i$$

where the x_i are the eigenvectors of S, and the λ_i are the corresponding eigenvalues, arranged in non-increasing order in modulus. By a simple argument, λ_0 has to be 1 for all subdivision schemes, in order to guarantee invariance with respect to translations and rotations. Furthermore, all stable, converging subdivision schemes will have all the remaining λ_i less than 1 in modulus.

Subdominant eigenvalues and eigenvectors It is clear that as we subdivide, the behavior of $\mathbf{p}^j$, which determines the behavior of the surface in the immediate vicinity of our point of interest, will depend only on the eigenvectors corresponding to the largest eigenvalues of S.

To proceed with the derivation, we will assume for simplicity that $\lambda_0 = 1$ and $\lambda = \lambda_1 = \lambda_2 > \lambda_3 > \cdots$. We will call λ_1 and λ_2 subdominant eigenvalues. Furthermore, we let $a_0 = 0$; this corresponds to choosing the origin of our coordinate system in the limit position of the vertex of interest. Then we can write

$$\frac{p^j}{\lambda^j} = a_1 x_1 + a_2 x_2 + (\frac{\lambda_3}{\lambda})^j x_3 + \cdots,$$

where the higher-order terms disappear in the limit as $j \to \infty$.

This formula is very important, and deserves careful consideration. Recall that $\mathbf{p}^j$ is a vector of $km(m+1)/2+1$ 3D points, while x_i are vectors of

$km(m+1)/2+1$ numbers. Hence the coefficients a_i in the decomposition above have to be 3D points.

This means that, up to a scaling by λ^j , the control set for $f(U^j)$ approaches a fixed configuration. This configuration is determined by the two eigenvectors x_1 and x_2, which depend only on the subdivision scheme, and on a_1 and a_2 which depend on the initial control mesh.

Each vertex in $\mathbf{p}^j$ for sufficiently large j is a linear combination of a_1 and a_2, up to a vanishing term. This indicates that a_1 and a_2 span the tangent plane. Also note that if we apply an affine transform A, taking a_1 and a_2 to coordinate vectors e_1 and e_2 in the plane, then, up to a vanishing term, the scaled configuration will be independent of the initial control mesh. The transformed configuration consists of 2D points with coordinates $(x_{1,i},\ x_{2,i})$, $i=0,\ldots,km(m+1)/2$, which depend on the subdivision matrix.

4.1.3 Characteristic Map

In order to have a further detailed analysis, we shall employ the characteristic map which has been introduced by Reif, in [32] and further developed by Prautzsch [30] and Zorin [34] and many other people. Informally speaking, any subdivision surface generated by a scheme looks near an extraordinary vertex of valence k like the characteristic map of that scheme for valence k.

Note that when we described subdivision as a function from the plane to $\mathbb{R}^3$, we may use control vertices not from $\mathbb{R}^3$, but from $\mathbb{R}^2$; clearly, subdivision rules can be applied in the plane rather than in space. Then in the limit we obtain a map from the plane to the plane. The characteristic map is a map of this type.

As we have seen, the configuration of control points near an extraordinary vertex approaches $a_1x_1+a_2x_2$, up to a scaling transformation. This means

that the part of the surface defined on the k-gon U^j as $j \to \infty$, and scaled by the factor $1/\lambda^j$, approaches the surface defined by the vector of control points $a_1x_1 + a_2x_2$. Let $f[\mathbf{p}] : U \mapsto \mathbb{R}^3$ be the limit surface generated by subdivision on U from the control set $\mathbf{p}$.

Definition 4.3. The characteristic map of a subdivision scheme for a valence k is the map $\Phi : U \mapsto \mathbb{R}^2$ generated by the vector of 2D control points $e_1x_1+e_2x_2$: $\Phi = f[e_1x_1 + e_2x_2]$, where e_1 and e_2 are the unit coordinate vectors, and x_1 and x_2 are the subdominant eigenvectors of the subdominant eigenvalues λ_1 and λ_2.

Regularity of the characteristic map inside each sector of the k-gon U, is C^1: since we can identify each sector with a sector in a regular mesh and we assumed that our subdivision scheme for a regular mesh in at least C^1. Figure 4.2 shows this process. Moreover, the map has one-sided derivatives on the boundaries of the triangles, except at the extraordinary vertex, so we can define one-sided Jacobians on the boundaries of triangles too. We will say that the characteristic map is regular if its Jacobian is not zero anywhere on U excluding the extraordinary vertex but including the boundaries between triangles.

The regularity of the characteristic map has a geometric meaning: any subdivision surface can be written, up to a scale factor λ^j, as the following form:

$$f[\mathbf{p}^j](t) = T\Phi(t) + v(t)O((\frac{\lambda_3}{\lambda})^j), t \in U^j,$$

where $v(t)$ is a bounded function $v : U^j \mapsto \mathbb{R}^3$, and T is a linear transformation taking the unit coordinate vectors in the plane to a_1 and a_2. Differentiating along the two coordinate directions t_1 and t_2 in the parametric domain U^j, and taking a cross product, after some calculations, we get the expression for the normal of the surface:

$$(a_1 \times a_2)J[\Phi(t)] + O\big((\frac{\lambda_3}{\lambda})^{2j}\big)\tilde{v}(t),$$

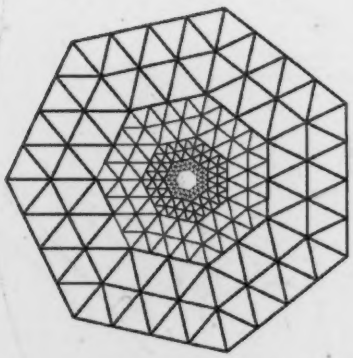

Figure 4.2: The k-gon without origin extraordinary vertex can be decomposed into similar rings. Taking dyadic subdivision schemes into account, each two times smaller than the previous ring. The size of the ring is chosen in such a way that the control set of any ring does not contain the extraordinary vertex. In this figure the control set is assumed to consist of the vertices of the triangles of the ring itself, and of a single layer of vertices outside the ring.

where $J[\Phi(t)]$ is the Jacobian, and $\tilde{v}(t)$ is some bounded vector function on U^j. So the normalized normal is given by

$$\mathbf{n}(t) = \frac{a_1 \times a_2}{\|a_1 \times a_2\|} \frac{J[\Phi(t)]}{|J[\Phi(t)]|}.$$

The fact that the Jacobian does not vanish for Φ means that the normalized normal is guaranteed to converge to $\pm\frac{a_1 \times a_2}{\|a_1 \times a_2\|}$; therefore, the surface is tangent plane continuous.

Now we need to take only one more step. If, in addition to regularity, we assume that Φ is injective, we can invert it and parameterize any surface as $f(\Phi^{-1}(s))$, where $s \in \Phi(U)$. Intuitively, it is clear that up to a vanishing term this map is just an affine map, and is differentiable. See the work [32, 34] for more detail.

We arrive at the following condition, which is the basis of smoothness analysis of all subdivision schemes considered in the work.

Reif's sufficient condition for smoothness. Suppose the eigenvectors of a subdivision matrix form a basis, the largest three eigenvalues are real and satisfy

$$\lambda_0 = 1 > \lambda_1 = \lambda_2 > |\lambda_3| > \cdots,$$

if the characteristic map is regular, then almost all surfaces generated by subdivision are tangent plane continuous; if the characteristic map is also injective, then almost all surfaces generated by subdivision are C^1-continuous.

4.1.4 Diagonalizing the Subdivision Matrix

The subdivision matrix will have a convenient block form if we arrange the vertices "by symmetry class". With this ordering of vertices, the subdivision matrix has the form (see [34]):

$$S = \begin{bmatrix} a_{00} & \mathbf{b}_0^T & \cdots & \mathbf{b}_{N-1}^T \\ \mathbf{c}_0 & \mathbf{A}_{00} & \cdots & \mathbf{A}_{0N-1} \\ \vdots & \vdots & \ddots & \vdots \\ \mathbf{c}_{N-1} & \mathbf{A}_{N-10} & \cdots & \mathbf{A}_{N-1N-1} \end{bmatrix}, \tag{4.1}$$

where $\mathbf{A}_{ij}$ are $k \times k$ matrices with entries and $\mathbf{b}_j$ denotes the vector $[b_j, \ldots, b_j]^T$ of size k with equal entries. For interpolatory subdivision schemes, $b_j = 0$. Similarly, $\mathbf{c}_j$ is the vector $[b_j, \ldots, b_j]^T$ of size k with equal entries.

For the convenience of analysis, each matrix block $\mathbf{A}_{ij}$ can be reduced to a diagonal form by using the DFT (Discrete Fourier Transform). Let $\mathcal{D} = diag(1, \frac{1}{k}D_k, \ldots, \frac{1}{k}D_k)$, where D_k is the DFT matrix of size k. The number of DFT blocks in $\mathcal{D}$ is N. Applying the transform to the subdivision matrix S, we obtain

$$\mathcal{D}S\mathcal{D}^{-1} = \begin{bmatrix} a_{00} & \mathbf{b}_0^T\overline{D_k} & \cdots & \mathbf{b}_{N-1}^T\overline{D_k} \\ \frac{1}{k}D_k\mathbf{c}_0 & \frac{1}{k}D_k\mathbf{A}_{00}\overline{D_k} & \cdots & \frac{1}{k}D_k\mathbf{A}_{0N-1}\overline{D_k} \\ \vdots & \vdots & \ddots & \vdots \\ \frac{1}{k}D_k\mathbf{c}_{N-1} & \frac{1}{k}D_k\mathbf{A}_{N-10}\overline{D_k} & \cdots & \frac{1}{k}D_k\mathbf{A}_{N-1N-1}\overline{D_k} \end{bmatrix}. \tag{4.2}$$

The matrices $\frac{1}{k} D_k \mathbf{A} \overline{D_k}$ are diagonal with entries on the diagonal.

Finally, the subdivision matrix can be reduced to block diagonal form by applying a permutation. Let P be the permutation that rearranges the entries of a vector of length $kN+1$ as follows: $[0, 1, 2, 3, \ldots, Nk] \mapsto [0, 1, k+1, \ldots, (N-1)k+1, k+2, \ldots, (N-1)k+2, \ldots, Nk]$. Applying this permutation, we have

$$P\mathcal{D}S\mathcal{D}^{-1}P^{-1} = \operatorname{diag}\big(Z, B(e^{\frac{2\pi i}{k}}), \ldots, B(e^{\frac{2(k-1)\pi i}{k}})\big). \tag{4.3}$$

where Z is a $k \times k$ block and $B(\omega)$ is an $N \times N$ block, $\omega = e^{2\pi i/k}, \ldots, e^{2(k-1)\pi i/k}$. See the work of Zorin [34] for more detail.

4.2 Special Subdivision Rules for Ternary Subdivision Schemes

4.2.1 Stencils of Ternary Subdivision Scheme for Regular Meshes

A C^2 interpolatory ternary subdivision scheme with 2-ring stencils has been proposed in Han and Jia [19] for the regular triangular meshes. The associated stencils are given in Figure 4.3. In order to apply the interpolatory ternary subdivision schemes in computer graphics, one has to design special subdivision rules at extraordinary vertices, we shall discuss this issue for special cases in this section.

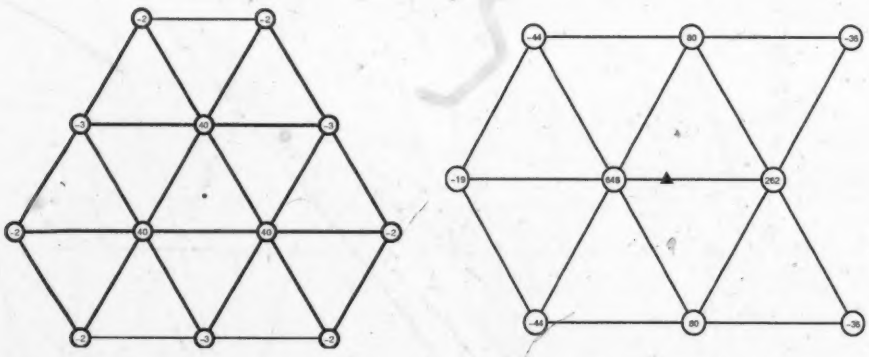

Figure 4.3: The stencils of the ternary subdivision schemes for regular meshes. The numbers at left shall be divided by 99; the numbers at right shall be divided by 891 [19].

In the following two subsections, we shall give two examples of interpolatory ternary subdivision schemes for triangular meshes to demonstrate the analysis at the extraordinary vertex.

4.2.2 Subdivision Rule for $k = 3$ case

The stencils are given in Figure 4.5, and 4.6.

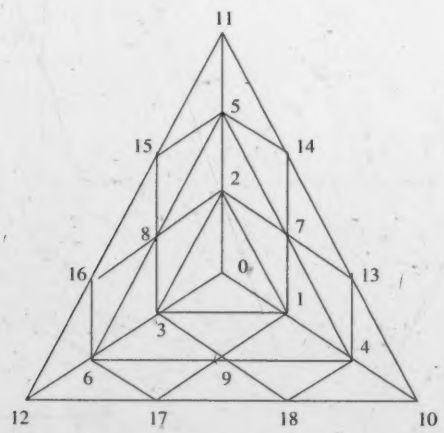

Figure 4.4: Numbering of the k-gon for the order as in the subdivision matrix.

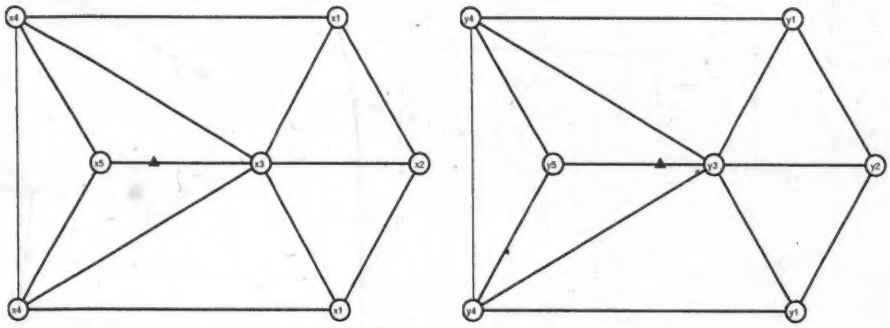

Figure 4.5: The stencil at left is for a new inserted "1/3 vertex", and at right is for a new inserted "2/3 vertex" on an edge associated with a $k = 3$ extraordinary vertex.

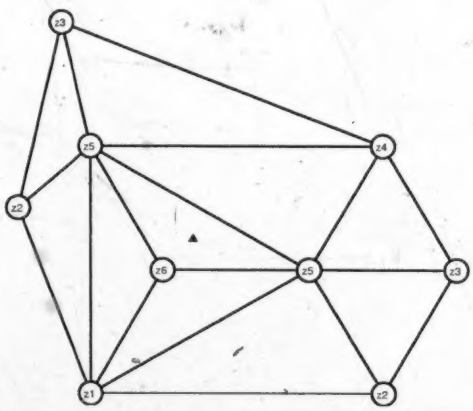

Figure 4.6: The stencil for a new inserted interior vertex inside a face which contains an extraordinary vertex with the valence $k = 3$.

In order to facilitate the analysis, we consider the following stencils. Here $N = 3$. Since the valence of extraordinary vertex is equal to 3, the corresponding subdivision matrix with 2-ring invariant vertices has the following

form:

$$S = \begin{bmatrix}
1 & 0 & 0 & 0 & 0 & 0 & 0 & 0 & 0 & 0 \\
x_5 & x_3 & x_4 & x_4 & 0 & 0 & x_2 & x_1 & 0 & x_1 \\
x_5 & x_4 & x_3 & x_4 & x_2 & 0 & 0 & x_1 & x_1 & 0 \\
x_5 & x_4 & x_4 & x_3 & 0 & x_2 & 0 & 0 & x_1 & x_1 \\
y_5 & y_4 & y_3 & y_4 & y_2 & 0 & 0 & y_1 & y_1 & 0 \\
y_5 & y_4 & y_4 & y_3 & 0 & y_2 & 0 & 0 & y_1 & y_1 \\
y_5 & y_3 & y_4 & y_4 & 0 & 0 & y_2 & y_1 & 0 & y_1 \\
z_6 & z_5 & z_5 & z_1 & z_3 & 0 & z_3 & z_4 & z_2 & z_2 \\
z_6 & z_1 & z_5 & z_5 & z_3 & z_3 & 0 & z_2 & z_4 & z_2 \\
z_6 & z_5 & z_1 & z_5 & 0 & z_3 & z_3 & z_2 & z_2 & z_4
\end{bmatrix}. \tag{4.4}$$

By a simple calculation, the DFT matrix of size 3 is as follows:

$$\begin{bmatrix}
1/3 & 1/3 & 1/3 \\
1/3 & -1/6 + i\sqrt{3}/6 & -1/6 - i\sqrt{3}/6 \\
1/3 & -1/6 - i\sqrt{3}/6 & -1/6 + i\sqrt{3}/6
\end{bmatrix}.$$

Applying the permutation on subdivision matrix S, by (4.3) we have:

$$\begin{bmatrix}
Z & \mathbf{0} & \mathbf{0} \\
\mathbf{0} & B\big(e^{2\pi i/3}\big) & \mathbf{0} \\
\mathbf{0} & \mathbf{0} & B\big(e^{4\pi i/3}\big)
\end{bmatrix},$$

where

$$Z = \begin{bmatrix}
1 & 0 & 0 & 0 \\
x_5 & x_3 + 2x_4 & x_2 & 2x_1 \\
y_5 & y_3 + 2y_4 & y_2 & 2y_1 \\
z_6 & zz_1 + 2z_5 & 2z_3 & z_4 + 2z_2
\end{bmatrix},$$

and

$$B(\omega) = \frac{1}{\omega(\omega - 1)} \begin{bmatrix}
\omega(\omega - 1)(x_3 - x_4) & (\omega + 2)x_2 & (\omega^2 + 2)x_1 \\
(\omega^2 + 2)(y_4 - y_3) & \omega(\omega - 1)y_2 & -(\omega + 2)y_1 \\
(\omega + 2)x(z_1 - z_5) & (\omega^2 + 2)z_3 & \omega(\omega - 1)(z_4 - z_2)
\end{bmatrix},$$

where $\omega = e^{2\pi i/3},\ e^{4\pi i/3}$.

Recall from linear algebra that an eigenvector $\mathbf{x}$ of the matrix S is a nonzero vector such that $S\mathbf{x} = \lambda\mathbf{x}$. Let

$$x_1 := 0,\ x_2 := 0,\ x_3 := 1/4,\ x_4 := -1/12,\ x_5 := 11/12;$$
$$y_1 := 0,\ y_2 := 0,\ y_3 := 72/12,\ y_4 := -1/12,\ y_5 := 7/12;$$
$$z_1 := -1/6,\ z_2 := 0,\ z_3 := 0,\ z_4 := 0,\ z_5 := 1/,\ z_6 := 5/6.$$

then we have

$$Z\begin{bmatrix} 0 & 0 & 0 & 1 \\ 0 & 0 & 1 & 0 \\ 0 & 1 & 5 & 2 \\ 1 & 1 & 1 & 1 \end{bmatrix} = \begin{bmatrix} 0 & 0 & 0 & 0 \\ 0 & 0 & 0 & 0 \\ 0 & 0 & 1/12 & 0 \\ 0 & 0 & 0 & 1 \end{bmatrix} \begin{bmatrix} 0 & 0 & 0 & 1 \\ 0 & 0 & 1 & 0 \\ 0 & 1 & 5 & 2 \\ 1 & 1 & 1 & 1 \end{bmatrix}, \tag{4.5}$$

(4.6)

$$B\big(e^{2\pi i/3}\big)\begin{bmatrix} (-1+i\sqrt{3})/4 & 0 & 0 \\ 1 & 0 & 1 \\ (1+i\sqrt{3})/4 & 1 & 0 \end{bmatrix} = \begin{bmatrix} 1/3 & 0 & 0 \\ 0 & 0 & 0 \\ 0 & 0 & 0 \end{bmatrix} \begin{bmatrix} (-1+i\sqrt{3})/4 & 0 & 0 \\ 1 & 0 & 1 \\ (1+i\sqrt{3})/4 & 1 & 0 \end{bmatrix},$$

and

$$B\big(e^{4\pi i/3}\big)\begin{bmatrix} 1 & 0 & 0 \\ -1+i\sqrt{3} & 1 & 0 \\ (1+i\sqrt{3})/2 & 0 & 1 \end{bmatrix} = \begin{bmatrix} 1/3 & 0 & 0 \\ 0 & 0 & 0 \\ 0 & 0 & 0 \end{bmatrix} \begin{bmatrix} 1 & 0 & 0 \\ -1+i\sqrt{3} & 1 & 0 \\ (1+i\sqrt{3})/2 & 0 & 1 \end{bmatrix}. \tag{4.7}$$

That is, Z, $B\big(e^{2\pi i/3}\big)$ and $B\big(e^{4\pi i/3}\big)$ have eigenvalues $\{0, 0, 1/12, 1\}$, $\{1/3, 0, 0\}$, $\{1/3, 0, 0\}$.

Theoretically, the size of subdivision matrix is bigger than the one we used in our previous analysis. By $\mathcal{S}$ we denote the real subdivision matrix with 3-ring invariant vertices (see Figure 4.4), which is $(6k+1) \times (6k+1)$ and given by

$$\mathcal{S} = \begin{bmatrix} S & 0 \\ * & S' \end{bmatrix},$$

where S is a $(3k+1) \times (3k+1)$ matrix block given in (4.4) and really useful in eigen-analysis; The block S' is a $3k \times 3k$ block, and the eigenvalues of S' are all constants and determined by the regular subdivision stencils. Figure 4.4 shows all the vertices contained in our subdivision matrix (19×19).

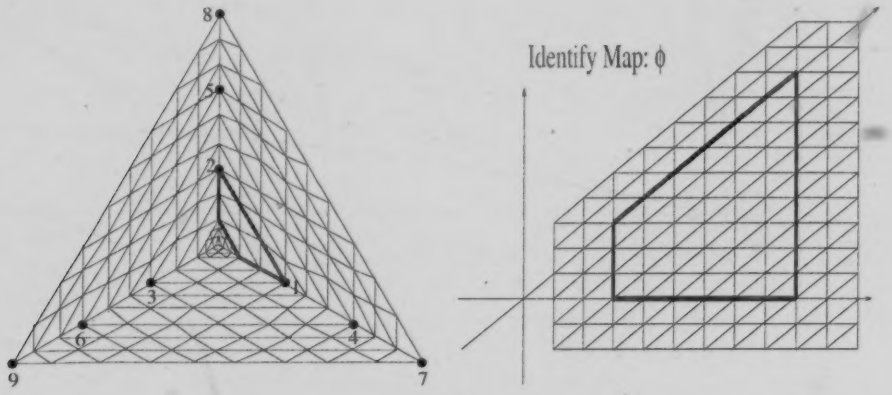

Figure 4.7: Identify a section around extraordinary vertex with a sector in the regular triangular mesh. All the vertices inside this bold area can be computed by the vertices within two rings outside this bold area.

In the following, let us shortly describe how to comput ethe Jacobian of the characteristic map using a method in [34].

Inside the area bounded by bold lines (see Figure 4.7), all the new inserted vertices are independent from the extraordinary vertex in the center of the topology. Moreover, these new vertices will be computed within two-ring around this bold area. By characteristic map, for each vertex, with which there is a vector (u, v) attached to it, we can map it into a corresponding vertex in a sector of two regular triangular meshes. One can attach the first component u to one of the regular meshes and attach the second component v to the other of the regular meshes. Let ϕ be the basis function of the subdivision scheme in the regular mesh. Now up to an affine transform the characteristic map

Figure 4.8: Applying the special interpolatory ternary subdivision scheme on an example mesh with an unique extraordinary vertex ($k = 3$). From left to right are the initial, first level and second level subdivision surfaces, respectively.

$\Phi = (\psi_1,\ \psi_2)$ restricted on one section of a ring can be obtained as a linear combination of the functions $\phi(\cdot - k),\ k \in \mathbb{Z}^2$. In particular

$$\psi_1 = \sum_{k \in \mathbb{Z}^2} u(k)\phi(\cdot - k)$$

and

$$\psi_2 = \sum_{k \in \mathbb{Z}^2} v(k)\phi(\cdot - k).$$

To check the Jacobian of the associated characteristic map, we have

$$J(\Phi) = \det \begin{bmatrix} \frac{\partial \psi_1}{\partial x} & \frac{\partial \psi_1}{\partial y} \\ \frac{\partial \psi_2}{\partial x} & \frac{\partial \psi_2}{\partial y} \end{bmatrix}.$$

with

$$\frac{\partial \psi_1}{\partial x} = \sum_{k \in \mathbb{Z}^2} u(k)\frac{\partial \phi}{\partial x}(\cdot - k), \quad \frac{\partial \psi_1}{\partial y} = \sum_{k \in \mathbb{Z}^2} u(k)\frac{\partial \phi}{\partial y}(\cdot - k),$$

$$\frac{\partial \psi_2}{\partial x} = \sum_{k \in \mathbb{Z}^2} v(k)\frac{\partial \phi}{\partial x}(\cdot - k), \quad \frac{\partial \psi_2}{\partial y} = \sum_{k \in \mathbb{Z}^2} v(k)\frac{\partial \phi}{\partial y}(\cdot - k).$$

Since $\frac{\partial \phi}{\partial x}$ and $\frac{\partial \phi}{\partial y}$ can be numerically computed using the cascade algorithm or the refinement equation, we can now numerically estimate the sign of $J(\Phi)$ on one section of a ring, which is the area bounded by the bold

lines in Figure 4.7. By symmetry of the characteristic map and the relation $J[\Phi](t/3) = 9\lambda_1\lambda_2[\Phi](t)$, if the sign of $J(\Phi)$ inside this section of a ring is the same, then the sign of $J(\Phi)$ inside U_1, which is defined as the interior triangular region given by the vertices of "1, 2, 3" in Figure 4.7, excluding the extraordinary vertex is the same as the sign of $J(\Phi)$ on this particular section of a ring.

4.2.3 Subdivision Rule for $k = 4$ case

The stencils for the case $k = 4$ are shown as Figure 4.9, and 4.10.

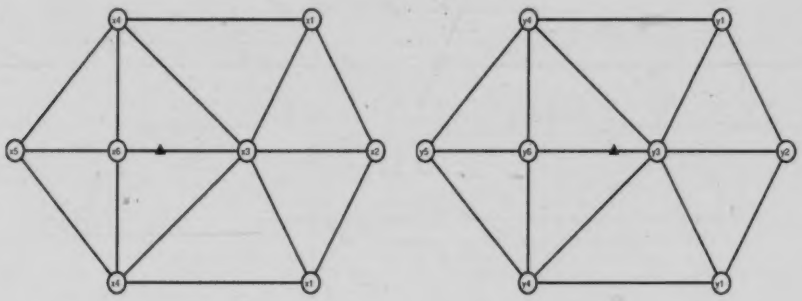

Figure 4.9: The stencils for the new inserted "1/3 vertex" and "2/3 vertex" on an edge associated with a $k = 4$ extraordinary vertex.

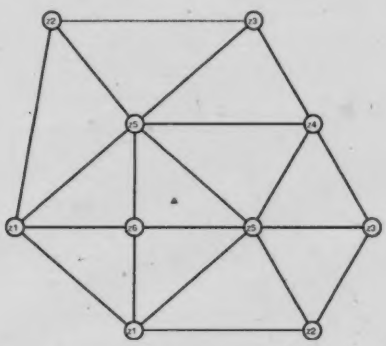

Figure 4.10: The stencil for a new inserted interior vertex inside a face which contains a $k = 4$ extraordinary vertex.

Similarly, we can figure out some stencils for $k = 4$. The subdivision matrix with 2-ring invariant vertices should be:

$$S = \begin{bmatrix}
1 & 0 & 0 & 0 & 0 & 0 & 0 & 0 & 0 & 0 & 0 & 0 & 0 \\
x_6 & x_3 & x_4 & x_5 & x_4 & 0 & 0 & 0 & x_2 & x_1 & 0 & 0 & x_1 \\
x_6 & x_4 & x_3 & x_4 & x_5 & x_2 & 0 & 0 & 0 & x_1 & x_1 & 0 & 0 \\
x_6 & x_5 & x_4 & x_3 & x_4 & 0 & x_2 & 0 & 0 & 0 & x_1 & x_1 & 0 \\
x_6 & x_4 & x_5 & x_4 & x_3 & 0 & 0 & x_2 & 0 & 0 & 0 & x_1 & x_1 \\
y_6 & y_4 & y_3 & y_4 & y_5 & y_2 & 0 & 0 & 0 & y_1 & y_1 & 0 & 0 \\
y_6 & y_5 & y_4 & y_3 & y_4 & 0 & y_2 & 0 & 0 & 0 & y_1 & y_1 & 0 \\
y_6 & y_4 & y_5 & y_4 & y_3 & 0 & 0 & y_2 & 0 & 0 & 0 & y_1 & y_1 \\
y_6 & y_3 & y_4 & y_5 & y_4 & 0 & 0 & 0 & y_2 & y_1 & 0 & 0 & y_1 \\
z_6 & z_5 & z_5 & z_1 & z_1 & z_3 & 0 & 0 & z_3 & z_4 & z_2 & 0 & z_2 \\
z_6 & z_1 & z_5 & z_5 & z_1 & z_3 & z_3 & 0 & 0 & z_2 & z_4 & z_2 & 0 \\
z_6 & z_1 & z_1 & z_5 & z_5 & 0 & z_3 & z_3 & 0 & 0 & z_2 & z_4 & z_2 \\
z_6 & z_5 & z_1 & z_1 & z_5 & 0 & 0 & z_3 & z_3 & z_2 & 0 & z_2 & z_4
\end{bmatrix}. \tag{4.8}$$

By a simple calculation, the DFT matrix of size 4 is as follows:

$$\begin{bmatrix}
1/4 & 1/4 & 1/4 & 1/4 \\
1/4 & i/4 & -1/4 & -i/4 \\
1/4 & -1/4 & 1/4 & -1/4 \\
1/4 & -i/4 & -1/4 & i/4
\end{bmatrix}.$$

Applying the permutation on subdivision matrix S, by (4.3) we have:

$$\begin{bmatrix}
Z & \mathbf{0} & \mathbf{0} & \mathbf{0} \\
\mathbf{0} & B\left(e^{2\pi i/4}\right) & \mathbf{0} & \mathbf{0} \\
\mathbf{0} & \mathbf{0} & B\left(e^{4\pi i/4}\right) & \mathbf{0} \\
\mathbf{0} & \mathbf{0} & \mathbf{0} & B\left(e^{6\pi i/4}\right)
\end{bmatrix},$$

where

$$Z = \begin{bmatrix} 1 & 0 & 0 & 0 \\ x_6 & x_3+2x_4+x_5 & x_2 & 2x_1 \\ y_6 & y_3+2y_4+y_5 & y_2 & 2y_1 \\ z_6 & 2z_1+2z_5 & 2z_3 & 2z_2+z_4 \end{bmatrix},$$

$$B\big(e^{2\pi i/k}\big) = \begin{bmatrix} x_3-x_5 & ix_2 & (1+i)x_1 \\ i(y_5-y_3) & y_2 & (1-i)y_1 \\ (z_5-z_1)+i(z_5-z1) & (1+i)z_3 & z_4 \end{bmatrix},$$

$$B\big(e^{4\pi i/k}\big) = \begin{bmatrix} x_3-2x_4+x_5 & -x_2 & 0 \\ 2y_4-y_3-y_5 & y_2 & 0 \\ 0 & 0 & z_4-2z_2 \end{bmatrix},$$

and

$$B\big(e^{6\pi i/k}\big) = \begin{bmatrix} x_3-x_5 & -ix_2 & (1-i)x_1 \\ i(y_3-y_5) & y_2 & (1+i)y_1 \\ (z_5-z_1)+i(z_5-z_1) & (1-i)z_3 & z_4 \end{bmatrix}.$$

Let

$$\begin{aligned} &x_1 := 0, \quad x_2 := 0, \quad x_3 := 1/3 + x_5, \quad x_4 := 0, \quad x_5 := -1/12, \\ &x_6 := 1 - 2x_1 - x_2 - x_3 - 2x_4 - x_5, \\ &y_1 := 0, \quad y_2 := 0, \quad y_3 := 2/3 + y_5, \quad y_4 := 0, \quad y_5 := -1/12, \\ &y_6 := 1 - 2y_1 - y_2 - y_3 - 2y_4 - y_5, \\ &z_1 := -1/12, \quad z_2 = 0, \quad z_3 = 0, \quad z_4 = 0, \quad z_5 := 1/3 + z_1, \\ &z_6 := 1 - 2z_1 - 2z_2 - 2z_3 - z_4 - 2z_5, \end{aligned}$$

we have

$$Z \begin{bmatrix} 0 & 0 & 0 & 1 \\ 1 & 0 & 0 & 1 \\ 3 & 1 & 0 & 1 \\ 2 & 0 & 1 & 1 \end{bmatrix} = \begin{bmatrix} 1/6 & 0 & 0 & 0 \\ 0 & 0 & 0 & 0 \\ 0 & 0 & 0 & 0 \\ 0 & 0 & 0 & 1 \end{bmatrix} \begin{bmatrix} 0 & 0 & 0 & 1 \\ 1 & 0 & 0 & 1 \\ 3 & 1 & 0 & 1 \\ 2 & 0 & 1 & 1 \end{bmatrix}, \tag{4.9}$$

$$B\left(e^{2\pi i/4}\right)\begin{bmatrix} 1 & 0 & 0 \\ -2i & 1 & 0 \\ 1-i & 0 & 1 \end{bmatrix} = \begin{bmatrix} 1/3 & 0 & 0 \\ 0 & 0 & 0 \\ 0 & 0 & 0 \end{bmatrix}\begin{bmatrix} 1 & 0 & 0 \\ -2i & 1 & 0 \\ 1-i & 0 & 1 \end{bmatrix}, \tag{4.10}$$

$$B\left(e^{4\pi i/4}\right)\begin{bmatrix} 1 & 0 & 0 \\ -3 & 1 & 0 \\ 0 & 0 & 1 \end{bmatrix} = \begin{bmatrix} 1/6 & 0 & 0 \\ 0 & 0 & 0 \\ 0 & 0 & 0 \end{bmatrix}\begin{bmatrix} 1 & 0 & 0 \\ -3 & 1 & 0 \\ 0 & 0 & 1 \end{bmatrix}. \tag{4.11}$$

and

$$B\left(e^{6\pi i/4}\right)\begin{bmatrix} 1 & 0 & 0 \\ 2i & 1 & 0 \\ 1+i & 0 & 1 \end{bmatrix} = \begin{bmatrix} 1/3 & 0 & 0 \\ 0 & 0 & 0 \\ 0 & 0 & 0 \end{bmatrix}\begin{bmatrix} 1 & 0 & 0 \\ 2i & 1 & 0 \\ 1+i & 0 & 1 \end{bmatrix}, \tag{4.12}$$

That is, Z, $B\left(e^{2\pi i/4}\right)$, $B\left(e^{4\pi i/4}\right)$ and $B\left(e^{6\pi i/4}\right)$ have eigenvalues $\{1/6, 0, 0, 1\}$, $\{1/3, 0, 0\}$,$\{1/6, 0, 0\}$ and $\{1/3, 0, 0\}$, respectively.

Similarly, the real subdivision matrix $\mathcal{S}$ with 3-ring invariant vertices has a 25×25 size and is given by

$$\mathcal{S} = \begin{bmatrix} S & 0 \\ * & S' \end{bmatrix},$$

where S is the above 13×13 matrix block given in (4.13); and block S' is a 12×12 block, which has constant eigenvalues determined by regular subdivision stencils.

Using the technique as discussing before, we can numerically verify that the associated characteristic map indeed has nonzero Jacobian, and therefore the subdivision surface must be tangent plane continuous.

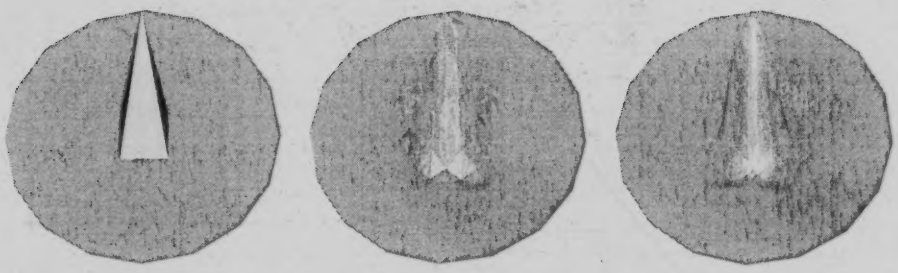

Figure 4.11: Applying the special interpolatory ternary subdivision scheme on an example mesh with an unique extraordinary vertex ($k = 4$). From left to right are the initial, first level and second level subdivision surfaces, respectively.

4.3 Four-adic Subdivision Rule for $k = 3$ case

The stencils for the case $k = 3$ are shown as Figure 4.11 and 4.12.

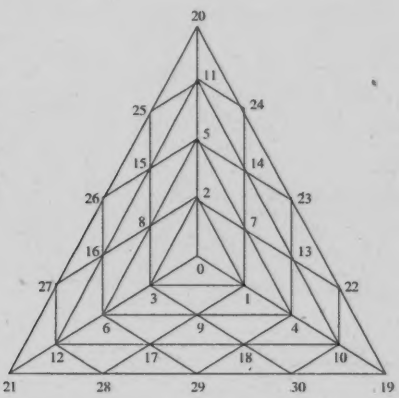

Figure 4.12: Numbering of the k-gon for the order as subdivision matrix .

By the property of symmetry, the stencil for the new inserted "(1/4, 1/2)" is a flip of the stencil of "(1/2, 1/4)" vertex. Thus we need only two stencils for the new inserted interior vertices inside a face. Similarly, we can figure out some stencils for $k = 4$. The subdivision matrix with 2-ring invariant vertices

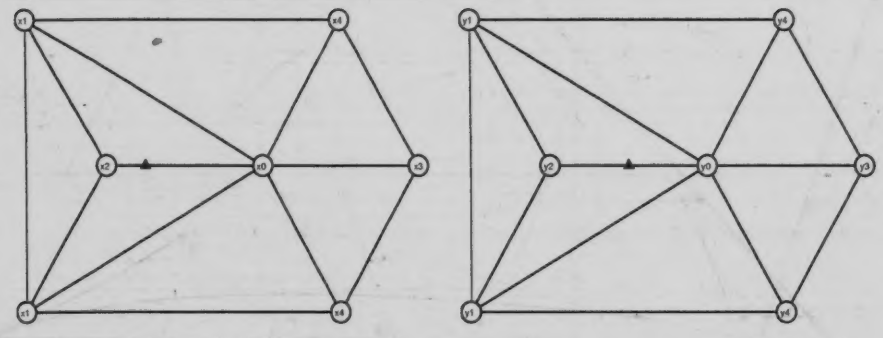

Figure 4.13: The stencil for a new inserted "1/4 vertex" and "1/2 vertex" on an edge associated with a $k = 4$ extraordinary vertex.

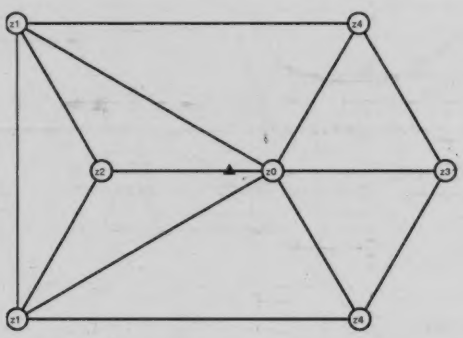

Figure 4.14: The stencil for a new inserted "3/4 vertex" on an edge associated with a $k = 3$ extraordinary vertex.

should be:

$$S = \begin{bmatrix} 1 & 0 & 0 & 0 & 0 & 0 & 0 & 0 & 0 & 0 \\ x_2 & x_0 & x_1 & x_1 & 0 & 0 & x_3 & x_4 & 0 & x_4 \\ x_2 & x_1 & x_0 & x_1 & x_3 & 0 & 0 & x_4 & x_4 & 0 \\ x_2 & x_1 & x_1 & x_0 & 0 & x_3 & 0 & 0 & x_4 & x_4 \\ y_2 & y_1 & y_0 & y_1 & y_3 & 0 & 0 & y_4 & y_4 & 0 \\ y_2 & y_1 & y_1 & y_0 & 0 & y_3 & 0 & 0 & y_4 & y_4 \\ y_2 & y_0 & y_1 & y_1 & 0 & 0 & y_3 & y_4 & 0 & y_4 \\ u_2 & u_0 & u_0 & u_1 & u_4 & 0 & u_4 & u_5 & u_3 & u_3 \\ u_2 & u_1 & u_0 & u_0 & u_4 & u_4 & 0 & u_3 & u_5 & u_3 \\ u_2 & u_0 & u_1 & u_0 & 0 & u_4 & u_4 & u_3 & u_3 & u_5 \end{bmatrix} \tag{4.13}$$

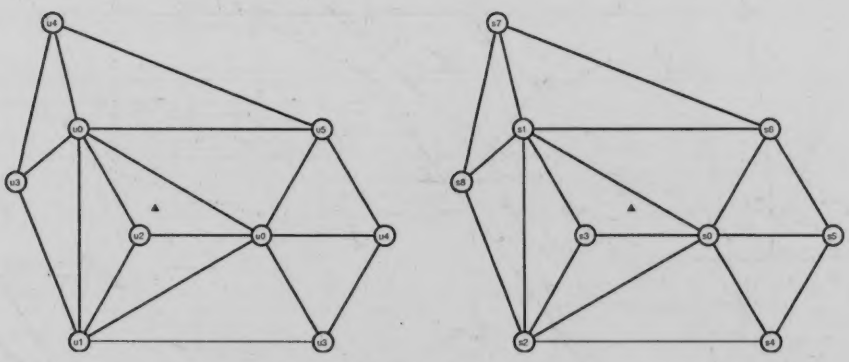

Figure 4.15: The stencil at left is for a new inserted interior "(1/4,1/4)" vertex, and at right is for a new inserted interior "(1/2, 1/4)" vertex inside a face which contains a $k = 3$ extraordinary vertex.

By a simple calculation, the DFT matrix of size 3 is as follows:

$$\begin{bmatrix} 1/3 & 1/3 & 1/3 \\ 1/3 & -1/6+i\sqrt{3}/6 & -1/6-i\sqrt{3}/6 \\ 1/3 & -1/6-i\sqrt{3}/6 & -1/6+i\sqrt{3}/6 \end{bmatrix}.$$

Applying the permutation on subdivision matrix S, by (4.3) we have:

$$\begin{bmatrix} Z & \mathbf{0} & \mathbf{0} \\ \mathbf{0} & B\big(e^{2\pi i/3}\big) & \mathbf{0} \\ \mathbf{0} & \mathbf{0} & B\big(e^{4\pi i/3}\big) \end{bmatrix},$$

where

$$Z = \begin{bmatrix} 1 & 0 & 0 & 0 \\ x_2 & x_0+2x_1 & x_3 & 2x_4 \\ y_2 & y_0+2y_1 & y_3 & 2y_4 \\ z_2 & u_1+2u_0 & 2u_4 & u_5+2u_3 \end{bmatrix},$$

and

$$B(\omega) = \frac{1}{\omega(\omega-1)} \begin{bmatrix} \omega(\omega-1)(1-3x_1-x_2-x_3-2x_4) & (\omega^3+\omega+1)x_3 & (\omega^3+\omega^2+1)x_4 \\ (\omega^3+\omega^2+1)(3y_1+y_2+y_3+y_4-1) & \omega(\omega-1)y_3 & -(\omega^3+\omega+1)y_4 \\ (\omega^3+\omega+1)x(u_1-z_0) & (\omega^3+\omega^2+1)u_4 & \omega(\omega-1)(u_5-u_3) \end{bmatrix},$$

where $\omega = e^{2\pi i/3},\ e^{4\pi i/3}$.

Let

$$x_0 := 1 - 2x_1 - x_2 - x_3 - 2x_4,$$
$$x_1 := -9/128,\ x_2 := 3/4 - 3x_1,\ x_3 := 0,\ x_4 := 0,\ x_5 := 0,\ x_6 := 0,$$
$$y_0 := 1 - 2y_1 - y_2 - y_3 - 2y_4,$$
$$y_1 := -1/8,\ y_2 := 6/8,\ y_3 := 0,\ y_4 := 0,\ y_5 := 0,\ y_6 := 0,$$
$$z_0 := 1 - 2z_1 - z_2 - z_3 - 2z_4,$$
$$z_1 := -1/16,\ z_2 := 0,\ z_3 := 0,\ z_4 := 0,\ z_5 := 0,\ z_6 := 0,$$
$$u_0 := (1 - u_1 - u_2 - 2u_3 - 2u_4 - u_5)/2,$$
$$u_1 := -1/6,\ u_2 = 3/4,\ u_3 := 0,\ u_4 := 0,\ u_5 := 0,$$
$$s_0 := 1 - s_1 - s_2 - s_3 - s_4 - s_5 - s_6 - s_7 - s_8,$$
$$s_1 := 1/4,\ s_2 := -1/6,\ s_3 = 3/8,\ s_4 := 0,\ s_5 := 0,\ s_6 := 0,\ s_7 := 0,\ s_8 := 0.$$

then we have

$$Z \begin{bmatrix} 1 & 0 & 0 & 0 \\ 1 & 0 & 0 & 1 \\ 1 & 1 & 0 & 32/5 \\ 1 & 0 & 1 & 32/5 \end{bmatrix} = \begin{bmatrix} 1 & 0 & 0 & 0 \\ 0 & 0 & 0 & 0 \\ 0 & 0 & 0 & 0 \\ 0 & 0 & 0 & 5/128 \end{bmatrix} \begin{bmatrix} 1 & 0 & 0 & 0 \\ 1 & 0 & 0 & 1 \\ 1 & 1 & 0 & 32/5 \\ 1 & 0 & 1 & 32/5 \end{bmatrix}, \tag{4.14}$$

$$B\big(e^{2\pi i/3}\big) \begin{bmatrix} (1+i\sqrt{3})/3 & 0 & 0 \\ (5-i\sqrt{3})/6 & 0 & 1 \\ 1 & 1 & 0 \end{bmatrix} = \begin{bmatrix} 1/4 & 0 & 0 \\ 0 & 0 & 0 \\ 0 & 0 & 0 \end{bmatrix} \begin{bmatrix} (1+i\sqrt{3})/3 & 0 & 0 \\ (5-i\sqrt{3})/6 & 0 & 1 \\ 1 & 1 & 0 \end{bmatrix}, \tag{4.15}$$

and

$$B\big(e^{4\pi i/3}\big) \begin{bmatrix} 1 & 0 & 0 \\ (-1+i\sqrt{3})5/4 & 1 & 0 \\ (1+i\sqrt{3})3/4 & 0 & 1 \end{bmatrix} = \begin{bmatrix} 1/4 & 0 & 0 \\ 0 & 0 & 0 \\ 0 & 0 & 0 \end{bmatrix} \begin{bmatrix} 1 & 0 & 0 \\ (-1+i\sqrt{3})5/4 & 1 & 0 \\ (1+i\sqrt{3})3/4 & 0 & 1 \end{bmatrix}. \tag{4.16}$$

That is, Z, $B\big(e^{2\pi i/3}\big)$ and $B\big(e^{4\pi i/3}\big)$ have eigenvalues $\{1, 0, 0, 5/128\}$, $\{1/4, 0, 0\}$ and $\{1/4, 0, 0\}$, respectively.

Theoretically, the size of subdivision matrix is bigger than the one we used in our previous analysis. By $\mathcal{S}$ we denote the real subdivision matrix with 3-ring invariant vertices (see Figure 4.11), which is $(10k+1) \times (10k+1)$ and given by

$$\mathcal{S} = \begin{bmatrix} S & 0 \\ * & S' \end{bmatrix},$$

where S is a $(3k+1) \times (3k+1)$ matrix block given in (4.13) and really useful in eigen-analysis; The block S' is a $3k \times 3k$ block, and the eigenvalues of S' are all constants and determined by the regular subdivision stencils. Figure 4.11 shows all the vertices contained in our subdivision matrix (31×31).

By the same technique as we discussed before, we can numerically verify that the associated characteristic map indeed has nonzero Jacobian, and therefore the subdivision surface must be tangent plane continuous.

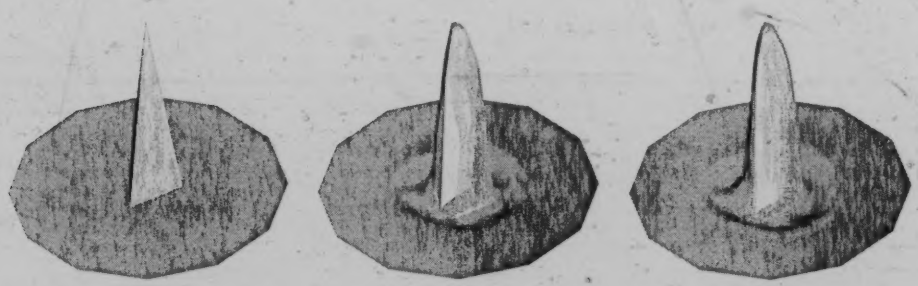

Figure 4.16: Applying the special interpolatory 4-adic subdivision scheme on an example mesh with an unique extraordinary vertex ($k = 3$). From left to right are the initial, first level and second level subdivision surfaces, respectively.

Bibliography

[1] Subdivision for Modeling and Animation, course notes by T. DeRose, D. R. Forsey, L. Kobebelt, M. Lounsbery, J. Peters, P. Schröder, and D. Zorin, (1998).

[2] A. A. Ball, and D. J. T. STORRY, Conditions for tangent plane continuity over recursively generated B-spline surfaces. *ACM Trans. Gr.* **7, 2** (1988), 83–102.

[3] A. S. Cavaretta, W. Dahmen, and C.A. Micchelli, Stationary subdivision, *Mem. Amer. Math. Soc.* **453** (1991), American Math. Soc, Providence.

[4] E.Catmull, and J. Clark, Recursively generated B-Spline surfaces on arbitrary topological meshes. *Computer Aided Design* **10** (1978), 350-355.

[5] R. P. Darwyn, Solid texturing of complex surfaces. In B. A. Barsky, editor, *Computer Graphics (SIGGRAPH 85 Proceedings)*, **19** (1985), 279-286.

[6] N. A. Dodgson, M. A. Sabin, L. Barthe, M. F. Hassan, Towards a ternary interpolatory subdivision scheme for the triangular mesh, *preprint.*

[7] D. Doo, and M. Sabin, Analysis of the Behaviour of Recursive Division Surfaces near Extraordinary Points. *Computer Aided Design* **10** (1978), 356-360.

[8] S. Dubuc, Interpolation through an iterative scheme, *J. Math. Anal. Appl.* **114** (1986) 185–204.

[9] N. Dyn and D. Levin, Subdivision schemes in geometric modeling, *Acta Numerica*, **11** (2002), 73–144.

[10] N. Dyn, D. Levin and J. A. Gregory, A butterfly subdivision scheme for surface interpolation with tension control, *ACM Transactions on Graphics*, **9** (1990), 160–169.

[11] L. Kobbelt, Interpolatory subdivision on open quadrilateral nets with arbitrary topology. In Proceedings of Eurographics 96, *Computer Graphics Forum*, (1996), 409-420.

[12] B. Han, Analysis and construction of optimal multidimensional biorthogonal wavelets with compact support, *SIAM J. Math. Anal.* **31** (2000), 274–304.

[13] B. Han, Projectable multidimensional refinable functions and biorthogonal wavelets, *Appl. Comput. Harmon. Anal.* **13** (2002), 89–102.

[14] B. Han, Computing the smoothness exponent of a symmetric multidimensional refinable function, *SIAM J. Matrix Anal. Appl.* **24** (2003), no. 3, 693–714.

[15] B. Han, Symmetry property and construction of wavelets with a general dialtion matrix, *Linear Algerbria Appl.* **353** (2002), 207–225.

[16] B. Han, Vector cascade algorithms and refinable function vectors in Sobolev spaces, *J. Approx. Theory.* **124** (2003), 44–88.

[17] B. Han, Classification and construction of two-dimensional subdivision schemes, *Proceedings on Curves and Surfaces Fitting: Saint-Malo 2002*, (A. Cohen, J.-L. Merrien, and L. L. Schumaker eds.), (2003), 187–197.

[18] B. Han and R. Q. Jia, Multivariate refinement equations and convergence of subdivision schemes, *SIAM J. Math. Anal.* **29** (1998), 1177–1199.

[19] B. Han and R. Q. Jia, Optimal C^2 two-dimensional interpolatory ternary subdivision schemes with two-ring stencils. Preprint, 2004.

[20] B. Han and R. Q. Jia, Optimal interpolatory subdivision schemes in multidimensional spaces, *SIAM J. Numer. Anal.* **36**, (1998), 105–124.

[21] M. F. Hassan, I. P. Ivrissimitzis, N. A. Dodgson, and M. A. Sabin, An interpolatory 4-point C^2 ternary stationary subdivision scheme, *Comput. Aided Geom. Design* **19** (2002), 1–18.

[22] H. Hoppe, T. DeRose, T. Duchamp, M. Halstead, H. Jin, J. McDonald, J. Schweitzer, and W. Stuetzle, Piecewise smooth surface reconstruction. *Computer Graphics*, **28**, (July 1994), 295-302.

[23] R. Q. Jia, Subdivision schemes in L_p spaces, *Adv. Comput. Math.* **3** (1995), 309–341.

[24] R. Q. Jia, Approximation properties of multidimensional wavelets, *Math. Comp.* **67** (1998), 647–665.

[25] R. Q. Jia, S. D. Riemenschneider, and D.X. Zhou, Smoothness of multiple refinable functions and multiple wavelets. *SIAM J. Matrix Anal. Appl.* **21** (1999), 1–28.

[26] C. Loop, T. Charles, Smooth subdivision surfaces based on triangles. Masters thesis, Department of Mathematics, University of Utah, August 1987.

[27] C. Loop, Smooth ternary subdivision of triangle meshes, *Proceedings on Curves and Surfaces Fitting: Saint-Malo 2002*, (A. Cohen, J.-L. Merrien, and L. L. Schumaker eds.), (2003), 295–302.

[28] A.H. Nasri, Polyhedral subdivision methods for free-form surfaces. *ACM Trans. Gr.* **6** (1987), 29-73.

[29] J. Peters, U. Reif, Analysis of algorithms generalizing B-spline subdivision. *SIAM J. Numer. Anal.* **35** (1998), 728–748.

[30] H. Prautzsch, Smoothness of subdivision surfaces at extraordinary points. *Advances in Computational Mathematics.* **9** (1998), 377–389.

[31] J. Peters, and U. Reif, Analysis of generalized B-spline subdivision algorithms. *SIAM J. Numer. Anal.* **35** (1998), 728–748.

[32] U. Rief, A Unified approach to subdivision algorithms near extraordinary points. *Comput. Aided Geom. Des.* **12** (1995), 153-174.

[33] D. Zorin, Subdivision and multiresolution surface representations. PhD thesis, Caltech, Pasadena, 1997.

[34] D. Zorin, A method for analysis of C^1-continuity of subdivision surfaces. *SIAM J. Numer. Anal.* **37**, (2000), 1677–1708.

[35] D. Zorin, P. SchrÖder, and W. Sweldens, Interpolating Subdivision for meshes with arbitrary topology. *Computer Graphics Proceedings (SIGGRAPH 96)* (1996), 189-192.